Heatline Visualization of Thermal Transport in Anisotropic Porous Media using a Generalized Non – Darcy Formulation

A Dissertation
Submitted in partial fulfillment of the requirements for
the award of the degree of

DOCTOR OF PHILOSOPHY

in

MECHANICAL ENGINEERING

by

Narasimha Suri Tinnaluri
(Roll No: 714130)

Supervisor:

Dr. D. Jaya Krishna
Associate Professor

DEPARTEMENT OF MECHANICAL ENGINEERING
NATIONAL INSTITUTE OF TECHNOLOGY,
WARANGAL (TS) - 506004, INDIA.
NOVEMBER-2019

DEPARTEMENT OF MECHANICAL ENGINEERING

NATIONAL INSTITUTE OF TECHNOLOGY,

WARANGAL, TS, INDIA – 506004

CERTIFICATE

This is to certify that the dissertation work entitled "**Heatline Visualization of Thermal Transport in Anisotropic Porous Media using a Generalized Non – Darcy Formulation"** which is being submitted by **Mr. Narasimha Suri Tinnaluri (Roll No. 714130)**, is a bonafide work submitted to the Department of Mechanical Engineering, National Institute of Technology, Warangal in partial fulfillment of the requirement for the award of the degree of **Doctor of Philosophy** in **Mechanical Engineering.**

To the best of our knowledge, the work incorporated in this thesis has not been submitted elsewhere for the award of any degree.

Dr. D. Jaya Krishna
(Associate Professor)
(Supervisor)
Department of Mechanical Engineering
National Institute of Technology
Warangal- 506004

Prof. N. Selvaraj
Head, Department of Mechanical Engineering
National Institute of Technology
Warangal-506004

Dedicated to

My parents Sri Narahari Tinnaluri and
Smt Venkata Ramana

My beloved wife Prasanthi Tinnaluri and
My son Vijayendra Suri Tinnaluri

&

All my teachers

APPROVAL SHEET

This Thesis entitled "**Heatline Visualization of Thermal Transport in Anisotropic Porous Media using a Generalized Non – Darcy Formulation"** by **Narasimha Suri Tinnaluri (Roll No. 714130)** is approved for the Degree of **Doctor of Philosophy** in **Mechanical Engineering.**

Examiners

Supervisor

Dr. D. Jaya Krishna
Associate Professor
Department of Mechanical Engineering
National Institute of Technology (NIT)
Warangal

Chairman

Prof. N. Selvaraj
Head of the Department
Department of Mechanical Engineering
National Institute of Technology (NIT),
Warangal

Date: 14/11/2019
Place: NIT Warangal

DECLARATION

This is to certify that the work presented in the thesis entitled **"Heatline Visualization of Thermal Transport in Anisotropic Porous Media using a Generalized Non – Darcy Formulation"** is a bonafide work done by me under the supervision of **Dr. D. Jaya Krishna,** and was not submitted elsewhere for the award of any degree. I declare that this written submission represents my ideas in my own words and where others ideas or words have been included, I have adequately cited and referenced the original sources. I also declare that I have adhered to all principles of academic honesty and integrity and have not misrepresented or fabricated or falsified any idea / data / fact / source in my submission. I understand that any violation of the above will be a cause for disciplinary action by the Institute and can also evoke penal action from the sources which have thus not been properly cited or from whom proper permission has not been taken when needed.

Date: (**Narasimha Suri Tinnaluri**)

(Roll No.: 714130)

ACKNOWLEDGMENT

I would like to express my sincere thanks and gratitude for my supervisor, **Dr. D. Jaya Krishna,** Mechanical Engineering Department, National Institute of Technology, Warangal, for his continuous guidance, support, enthusiasm and motivation in my PhD research work.

I am grateful to **Prof. N.V. Ramana Rao,** Director NIT Warangal who has been constant source of inspiration for me. I thank **Prof. N. Selvaraj,** Head of the Department of Mechanical Engineering for his help and continuous encouragement to complete this work. I would like to express my sincere thanks to **Prof. S. Srinivasa Rao** and **Dr. V.R.K. Raju** (Mechanical Engineering Department), and **Dr. P.V. Suresh** (Chemical Engineering Department), learned members of my Doctoral Scrutiny Committee for being helpful and generous during the entire course of this work.

My sincere thanks also go to **Prof. C.S.P Rao, Prof. S. Srinivasa Rao** and **Prof. P. Bangarubabu** former HoDs, Mechanical Engineering Department, National Institute of Technology, Warangal, for their encouragement, for providing access to the laboratory and research facilities. Without their precious support it would not be possible to conduct this research.

I sincerely express my deepest gratitude to my fellow scholars **Mr. G. Uma Maheswara Rao**, **Mr. T. Markandeyulu**, **Mr. K. Lokesh** and **Mr. K. Sandeep** for their help and extreme support.

I would like to thank my family my wife **Prasanthi Tinnaluri,** my son **Vijayendra Suri Tinnaluri,** my parents (**Sri. Narahari Tinnaluri** and **Smt. Venkata Ramana**), my brother **Hari Suri Babu Tinnaluri,** sister in law **Sravani Tinnaluri** and sisters (**Dhana Lakshmi** and **Venkata Lakshmi**) for supporting me throughout writing this thesis and my life in general.

Last but not the least, I sincerely thanks to my M Tech friends (**Mr. B. Srinivasa Reddy**, **Mr. M. Ramesh** and **Mr. K. Raja Sekhar**) and co- scholars for their help and constant encouragement.

Narasimha Suri Tinnaluri

(Roll No: 714130)
Research Scholar
Department of Mechanical Engineering
National Institute of Technology Warangal- 506004

ABSTRACT

The understanding of hydrodynamics and thermal transport in enclosures filled with fluid saturated porous media is of great importance due to its extensive applications. Some of the applications such as heat exchangers, nuclear fuel rod bundle, food processing, solar thermal systems etc. involve intricate geometries which are isotropic and anisotropic in nature. For the efficient design of these systems a thorough understanding of thermal transport is required. Visualization of thermal transport in terms of heatlines was observed to provide a better insight.

In the present study, initially a numerical code has been developed for the visualization of isotherms and heatlines in two-dimensional domains viz. square, trapezoidal, skewed, S-curve and H-curve. The developed code is used to read the mesh of various shapes from commercial meshing software (GAMBIT). Here, the data pertaining to mesh has been given as input to the numerical code developed for the visualization of thermal transport in these domains. The integral form of the governing equations are discretized using collocated grid based Finite Volume Method (FVM). The resulting governing equations are solved using the Gauss-Seidel iterative method. The present numerical scheme is rigorously validated for temperature distribution with commercial CFD code ANSYS – Fluent. Later, it is extended to the Bejan's heatline visualization for the considered geometries provided with and without discrete heat sources. The developed generalized code is validated with earlier numerical works pertaining to heatline visualization. Numerical results are presented in terms of temperature distribution and heatlines for analyzing the thermal transport in 2D solid geometries.

Further, the study is extended to investigate the hydrodynamics for a lid-driven flow saturated with non-Darcy anisotropic porous media. The applications include float glass production, food processing, soil liquefaction etc. The Reynolds numbers (Re) considered for the study are 10, 100 and 1000. The effect of Darcy number ($10^{-5} \leq Da \leq 10^{-2}$) and porosity ($\varepsilon$ = 0.3 and 0.6) have been varied to analyze the permeability ratio (K^* = 0.1, 1 and 10), Forchheimer constants ratio (F^*=1, 10 and 100) and principal axes inclination ($\theta = 0^o$, 45^o and 90^o) on flow behavior. A SIMPLE algorithm based finite volume method has been employed to solve the governing equations. The quadrilateral cells in a collocated grid arrangement have

been considered. Initially, the consistency check for the numerical scheme has been carried out by setting porosity equal to unity and Darcy number to a very high value. This is the limiting case for porous media, where the porous media tends to behave as a single-phase fluid. Further, the validation of pertinent problem is carried with available literature. The flow physics has been interpreted by plotting the results in terms of streamlines and maximum stream function values. The study could reveal that with the increase in Reynolds number the influence of non-linear drag forces become significant. Also, it is observed that the anisotropic parameters of the non-Darcy porous media profoundly modulate the flow.

Finally, thermal hydraulics for anisotropic porous media is analyzed to study the influence of anisotropic parameters by varying Rayleigh number ($Ra = 10^3 - 10^6$), Darcy number ($Da = 10^{-6} - 10^{-2}$), porosity ($\varepsilon = 0.3, 0.6$) and Prandtl number ($Pr = 0.1$,1 and 10). The anisotropic parameters investigated are permeability ratio: K^* (0.1, 1 and 10), principal axes inclination: θ ($0^o - 90^o$), Forchheimer constant ratio: F^* (1, 10 and 100) and thermal conductivity ratio: k^* (0.1, 1 and 10). The results are presented in terms of streamlines, isotherms, heatlines and average Nusselt number. The heatlines are plotted to visualize the path of thermal transport. The anisotropic behavior of the porous matrix is observed to significantly influence the thermal hydraulics. Heatlines along with isotherms are observed to help in great detail for the understanding of thermal hydraulics in these geometries.

KEYWORDS: Non- orthogonal; Collocated grid; Isotherms; Heatlines, Visualization; Finite Volume Method; Various geometries; Thermal transport; Discrete heat source; Anisotropy; natural convection; Porous Media; Generalized Non-Darcy Formulation.

CONTENTS

LIST OF FIGURES

LIST OF TABLES

NOMENCLATURE

A	projected area, m^2
AR	Aspect ratio
BEM	Boundary element method
b_{no}	non orthogonality of the grid
C*	Forchheimer coefficients ratio
C	Forchheimer coefficient (m^{-1})
CSCM	Chebyshev spectral collocation method
C_p	Specific heat (J Kg^{-1} K^{-1})
Da	Darcy number
Da_m	Modified Darcy number
d^1	orthogonal part of diffusive flux
d^2	non-orthogonal part of diffusive flux
E,N,W,S	east, north, west, south nodes
e,n,w,s	east, north, west, south faces
F	Forchheimer constant
FDM	Finite Difference Method
FVM	Finite Volume Method
F*	Forchheimer constants ratio
g	Acceleration due to gravity (m s^{-2})
H	Dimensional heat function / height in vertical direction, m
ISPH	Incompressible Smoothed Particle Hydrodynamics
J_D	diffusive flux
J_{De}	east face diffusive flux
K	Permeability (m^2)
K*	Permeability ratio
k	Thermal conductivity,($W.m^{-1}.K^{-1}$)
k*	Thermal conductivity ratio
L	length in horizontal direction, m
L1	length in vertical direction, m
LB	Lattice Boltzmann

MRT	Multiple Relaxation Time
NE	north east node
ne	north east corner
Nu	Nusselt number
$\overline{Nu}$	Average Nusselt number
NW	north west node
P	Pressure ($N.m^{-2}$)
Pr	Prandtl number
QUICK	Quadratic Upstream Interpolation for Convective Kinematics
q_1''	left heater, W/m^2
q_2''	right heater, W/m^2
Ra	Rayleigh number
REV	Representative Elementary Volume
Re	Reynolds number
SE	south east node
se	south east corner
SIMPLE	Semi Implicit Pressure Linked Equations
SW	south west node
sw	south west corner
T	temperature, K
t	time (s)
U	moving lid velocity ($m.s^{-1}$)
u	x-direction volume averaged velocity ($m.s^{-1}$)
v	y-direction volume averaged velocity ($m.s^{-1}$)
$\lvert v \rvert$	magnitude of velocity vector ($= \sqrt{u^2 + v^2}$) ($m.s^{-1}$)
X_a	distance of left bottom adiabatic surface, m
X_b	distance of bottom center heater, m
x_a	distance between left adiabatic, m
x_b	distance between left heater, m
x_c	distance between center adiabatic, m
x_d	distance between right heater, m
x_e	distance between right adiabatic, m
X	distance along x coordinate, m

x, y	coordinate axis
Y	distance along y coordinate, m

Greek Symbols

ε	Porosity
β	Coefficient of thermal expansion (K^{-1})
μ	Dynamic viscosity ($N.s.m^{-2}$)
$\tilde{\mu}$	Effective viscosity ($N.s.m^{-2}$)
θ	Principal axes inclination(degree)
ρ	Density ($kg.m^{-3}$)
ψ	Stream function
σ	Ratio of heat capacities
Π	Non dimensional heat function,
d∀	control volume, m^3

Subscripts

1,2	Principal axes direction
avg	average
c	Cold
f	Fluid
h	Hot
max	Maximum
0	reference

Superscripts

*	Anisotropic properties ratio
═	Tensor

CHAPTER 1

INTRODUCTION

1.1 BACKGROUND

The understanding of hydrodynamics and thermal transport in various equipments viz. heat exchangers, nuclear fuel rod bundle, food processing, solar thermal systems etc. is very much necessary for their efficient design. These equipment involve intricate geometries which need approaches like porous media and heatline visualization for the insight of flow physics. Some of the applications for porous media is provided in Fig. 1.1. These applications involve intricate geometries which are isotropic and anisotropic in nature for which the heat transport analysis is very complex. For the efficient design of these equipment a thorough analysis of heat transport characteristics is needed.

Complex structure of the medium involved in the above mentioned applications makes it difficult to perform experimental investigations. Analytical solutions are available only for the simplified situations and obtaining the accurate analytical solution for the actual problem is a herculean task. The availability of higher computational facilities in the recent days makes it viable to adapt numerical techniques to obtain the solutions for complex phenomenon.

The formulation for porous media can be carried out either by microscopic or macroscopic approach. In microscopic approach the properties are taken at pore level and in the case of macroscopic approach a control volume as shown in Fig. 1.2 is considered. In the present thesis macroscopic approach has been considered for porous media formulation. Throughout the study it is considered that the solid matrix of the porous matrix does not undergo deformation and is saturated with fluid. Table 1.1 shows some of the examples for porous media.

Heat exchangers
(https://www.hvac.com/blog/heat-exchangers-need-know/)

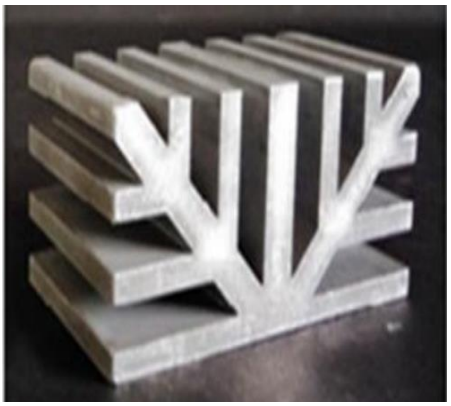

Branched heat sink
(https://www.gdrectifiers.co.uk/products/aluminium_heatsinks)

Porous filters
(http://nytribunal24.com/2019/10/22/metal-porous-filters-market-growth-rate-2019-entegris-usa-mott-usa-gkn-uk-purolator-usa/)

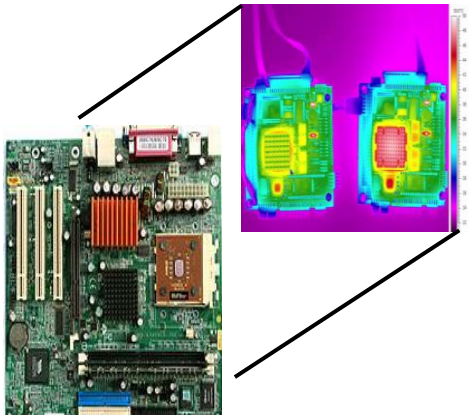

Mother board
(https://www.computerhope.com/jargon/m/mothboar.htm)

Food grains
(http://www.indspices.com/food_grains.php)

Fuel rod bundle
(http://mccabism.blogspot.com/2014/08/cfd-lessons-from-nuclear-reactors.html)

Fig. 1.1. Applications of porous media

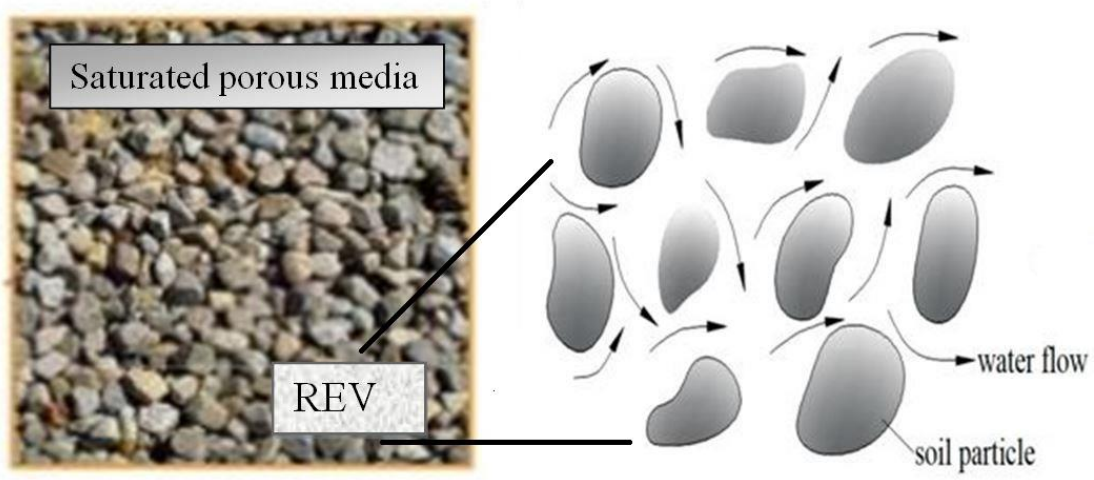

Fig. 1.2. Control volume for porous media

Porosity (ε)

The porosity of a porous medium is defined as the ratio of void volume to total volume, in other words it is the fraction of total volume that is occupied by voids.

$$\varepsilon = \frac{\text{void volume}}{\text{total volume}} \tag{1.1}$$

Permeability (K)

Permeability can be defined as hydraulic conductivity of the porous media. It gives a measure of the ease with which the fluid flows through the porous matrix.

Depending on the nature of the porous media and flow conditions, formulations such as Darcy model, Forchheimer extended Darcy model, Brinkmen extended Darcy model and modified Navier-stokes model were employed. Though non – Darcian effects are not significant for tightly packed porous media it becomes very much necessary to consider for the porous media with high porosity (loosely packed). It becomes necessary to study a generalized model which can predict the thermal hydraulics for wide range of porous media.

Table 1.1 Some of the porous materials

Material	Porosity, ε	Permeability, K (cm^2)	Picture	Reference
Soil	0.37 – 0.50	2×10^{-7} – 1.8×10^{-6}		https://www.toppr.com/guides/science/soil/types-of-soil-and-suitable-crops/
Tube bundle	0.214 – 0.9	1.64×10^{-6} – 2.06×10^{-2}	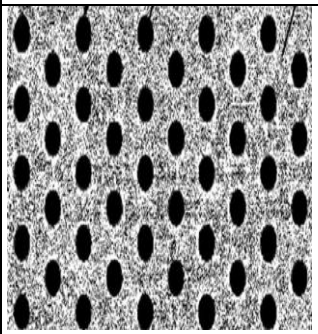	https://www.researchgate.net/figure/Schematic-of-a-staggered-tube-bundle-with-a-porous-material-insert_fig2_239401750
Metal foam	0.88 – 0.93	10^{-5} – 10^{-3}	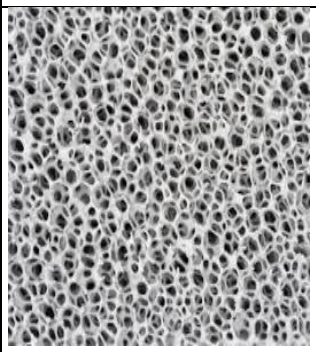	https://porter36.en.made-in-china.com/product/hsuEFNoAEcWp/China-High-Porosity-Battery-Nickel-Foam-Sheet.html
Heat sink	≈ 0.6 – 0.8	----	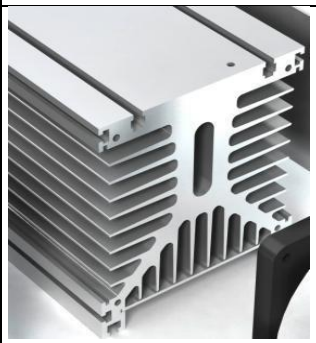	https://www.telerex-europe.com/en-gb/heat-sinks

1.1.1 Darcy Law

The Darcy's model (1856) was the only available model for about fifty years. The Darcy's experimental set up is shown in Fig. 1.3. Darcy model sufficiently describes the momentum and thermal energy transport in fluid saturated porous media with lower porosities which include the flow in rocks, soil, sand and other media. The well known form of equation can be given as

$$v = -\frac{K}{\mu_f}.\nabla P \tag{1.2}$$

In Eqn. (1.2) $v = \varepsilon v_f$ (volume average velocity component), K: permeability, μ_f: viscosity of the fluid and ∇P: pressure gradient for isotropic porous media.

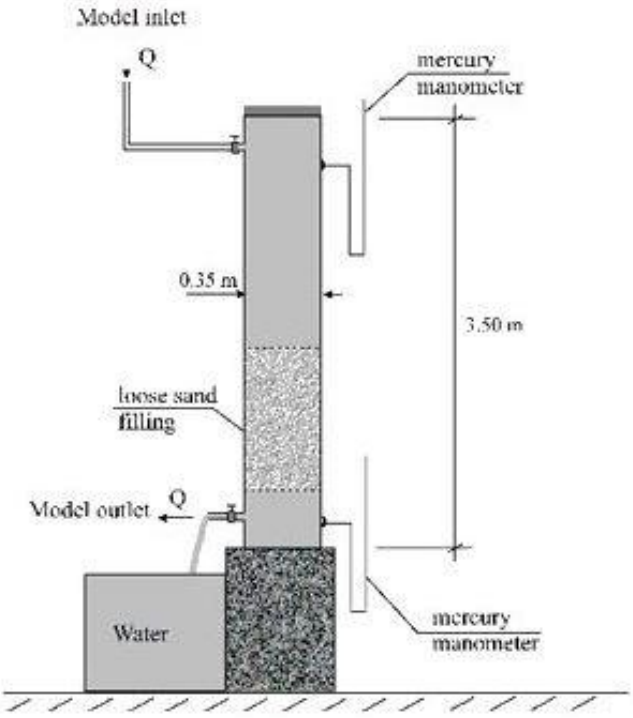

Fig. 1.3. Darcy's apparatus

(Reproduced from http://echo2.epfl.ch/VICAIRE/mod_3/chapt_5/main.htm)

As the number of porous media applications increase, Darcy relation may not give adequate results for all types of porous media flows. In particular this is true when the velocity of

the fluid increases in the porous medium with higher porosities. For example, Darcy formulation becomes invalid for porous materials like rod bundle and metal form as shown in Table 1.1 due to its higher porosities and permeabilities.

1.1.2 Forchheimer Model

Forchheimer (1901) proposed the role of nonlinear terms taking into account the drag on the fluid due to solid matrix, which could be neglected for lower fluid velocities. Ward (1964) proposed the dependence of Forchheimer term on the square root of the permeability, which is still being widely used. It is assumed that the limit of validity for Darcy's law should be considered on the basis of a Reynolds number (Re) given in terms of particle size of the porous medium, and in particular, as this number is greater than one, Darcy's law is no longer adequate.

$$\nabla P = -\frac{\mu_f}{K} v - \frac{F}{\sqrt{K}} \rho_f v|v| \tag{1.3}$$

In Eqn. (1.3) K: permeability, v: volume average velocity component, μ_f: viscosity of the fluid, ∇P: pressure gradient for porous media and F: Forchheimer constant. Ward (1964) assumed F to be an universal constant, with an approximate value of 0.55 because of its validity for wide range of porous media, but later F was found to be varying with the nature of porous media.

1.1.3 Brinkman Model

Brinkman (1947) furnished a modification for Darcy's equation which is generally given as Brinkman's equation. In this equation a viscous term in the momentum conservation equation has been introduced besides the Darcy term, similar to the diffusion term in the classical Navier Stokes equations.

$$\nabla P = -\frac{\mu_f}{K} v + \tilde{\mu} \nabla^2 v \tag{1.4}$$

In Eqn. (1.4) $\tilde{\mu}$ is an effective viscosity, v: volume average velocity component, K: permeability, μ_f: viscosity of the fluid, ∇P: pressure gradient for isotropic porous media.

Some of the researchers have made use of both Forchheimer's and Brinkman's terms along with Darcy formulation to account no slip wall effect at the walls and inertial forces for flow with pore diameter based Reynolds number more than one.

$$\nabla P = -\frac{\mu_f}{K} v + \tilde{\mu} \nabla^2 v - \frac{F}{\sqrt{K}} \rho_f v|v| \tag{1.5}$$

In Eqn. (1.5) $\tilde{\mu}$: effective viscosity, v: volume average velocity component, K: permeability, F: Forchheimer constant, ρ_f: fluid density, μ_f: viscosity of the fluid and ∇P: pressure gradient for isotropic porous media.

1.1.4 Modified Navier Stokes Equation Model

Wooding (1957) seems to have been the first to introduce convective term in the macroscopic momentum equation for fluid flow through porous media. One particularly interesting approach is the usage of equations in the form of modified Navier Stokes equations. Some of the researchers used linear drag term while some others used both linear and non-linear drag terms for the solid resistance. The modified Navier Stokes equation which incorporates both linear and nonlinear drag is named 'generalized non-Darcy model'. The validity of generalized non-Darcy formulation for a variety of physical problems made this formulation to be most reliable when compared to other modified formulations.

$$\frac{\rho_f}{\varepsilon}\left[\frac{\partial v}{\partial t} + \left(\frac{v}{\varepsilon}\right).\nabla v\right] = -\nabla P + \frac{\mu_f}{\varepsilon}\nabla^2 v - \frac{\mu_f}{K} v - \frac{F}{\sqrt{K}} \rho_f v|v| \tag{1.6}$$

In Eqn. (1.6) v: volume average velocity component, K: permeability, μ_f: viscosity of the fluid, ∇P: pressure gradient, F: Forchheimer constant for isotropic porous media.

1.1.5 Heatline Visualization

Kimura and Bejan (1983) introduced the concept of heatlines. The concept was observed to play a very important role in the visualization and analysis of convective heat transport. Heatlines and heat function are analogous to the streamline and stream function. This visualization and analyzing tool has become the very useful and necessary due to its application in various field, viz. geothermal reservoirs, solidification of casting, solar energy collectors, sterilization, food separation processes, molten metal applications, molten salt applications etc.

When encountering problem of the fluid flow streamlines are well established as the most adequate and very useful tool to visualize and analyze the flow behavior. Analogous to streamlines there are heat flux lines for pure conduction problem which are normal to the isotherms. When dealing with the convection heat transfer the isotherm and heat flux line are not necessarily normal to each other. In convection problem it is important to study the flow of energy and flow of fluid. For any such a field, Kimura and Bejan (1983) defined the heat function as given in Eqn. (1.7) such that the net flow of energy is zero across each heatline. For solid domains where $u = v = 0$ the heatlines become identical to the heat flux lines which is used to visualize conduction heat phenomena.

$$\frac{\partial}{\partial x}\left[\rho_f u c_p (T - T_0) - \left(k\frac{\partial T}{\partial x}\right)\right] + \frac{\partial}{\partial y}\left[\rho_f v c_p (T - T_0) - \left(k\frac{\partial T}{\partial y}\right)\right] = 0 \qquad (1.7)$$

In Eqn. (1.7) u, v: volume average velocity component in x and y directions, ρ_f: fluid density ($kg.m^{-3}$), c_p: specific heat ($J.kg^{-1}.K^{-1}$), k: thermal conductivity ($W.m^{-1}.K^{-1}$), T_0: reference temperature (K), T: temperature (K).

In this thesis initially an in-house code has been developed to read the mesh data of different geometries from commercial meshing software. Later, the data pertaining to mesh has been given as input to the developed code for the visualization of heat transport. Further, it is extended to the Bejan's heatline visualization for the considered geometries. After extensive validation, the study is extended to a problem of discrete heat sources and analyzed in terms of isotherms and heatline profiles for various solid geometries. The study is also extended to a problem of hydrodynamics for non-Darcy shear driven flows with anisotropic porous media. Later, thermal hydraulics of steady-state buoyancy induced flows for a square cavity impregnated with anisotropic porous media is investigated. As the concept of heatline visualization can help in great detail for the understanding of thermal transport in various structures, the energy transport in a cavity filled with anisotropic non-Darcy porous media is analyzed with the concept of heatline visualization.

1.2. ORGANIZATION OF THE THESIS

The present thesis is organized into 8 chapters including the introduction. The review of literature pertaining to all the research problems considered in the present work is presented in

chapter 2. It also includes the objectives and scope of the work. Chapter 3 provides mathematical formulation and method of solution. Validation for each problem considered is provided for chapters 4 to 7. Chapter 4 is based on the problem of heat transport for various solid geometries through heatline visualization. Chapter 5 illustrates hot spots through isotherms and heatline profiles for various solid geometries with discrete heat source(s). Chapter 6 is based on hydrodynamics for non-Darcy shear driven flows with anisotropic porous media. Chapter 7 provides thermal hydraulics using heatline visualization approach for non-Darcy anisotropic porous media. The conclusions from the present study and suggestions for future work are outlined in chapter 8.

1.3. CLOSURE

In this chapter, a brief background and motivation for the research work considered in the present study has been provided. The salient features of the respective chapters of the thesis are also briefly highlighted.

CHAPTER 2

REVIEW OF LITERATURE

2.1. INTRODUCTION

The understanding of thermal transport in complex solid geometries with discrete heat sources and porous media is of major importance. Some of the important applications include geothermal systems (Vafai and Tien (1981)), nuclear reactor safety (Ettefagh et al. (1991)), ground water flow modeling (Lage (1993)), solar power collectors (Saeid and Pop (2005)), food processing (Krishna et al. (2008b)), compact heat exchangers (Swamy et al. (2013) and Sheremet et al. (2015)), heating and cooling of buildings (Chandran et al. (2019)) etc. Due to the arrangement of the solid structure these systems can be anisotropic in nature. Hence, it is necessary to investigate the effect of anisotropic parameters of the porous medium on the fluid flow and heat transport behavior. In addition to these the concept of heatline approach which is introduced by Kimura and Bejan (1983) can be used to analyze the performance of thermal systems by visualizing the magnitude and direction of heat flow. In this section, the review of literature is initiated with thermal transport in various shapes followed by shear driven flows in porous media and buoyancy induced flows in isotropic and anisotropic porous media. In each of the above sections the thermal transport has been analyzed by using the concept of heat line visualization. For convenience and a structured representation, the literature is classified as follows.

2.2. THERMAL TRANSPORT IN VARIOUS GEOMETRIES

Various thermal equipment like solar energy systems, nuclear reactors, cooling of electronic devices, etc., involve intricate geometries for which the analysis is very complex. For the efficient design of these equipment a thorough analysis of heat transport characteristics is needed. In this section literature pertaining to relevant numerical formulation for non – orthogonal geometries is discussed. Harlow and Welch (1965) proposed the staggered grid formulation which involves storing of scalar quantities at cell centers and velocity components at cell faces. Thompson et al. (1982) made use of non-orthogonal curvilinear grid and developed new computational techniques to analyze fluid flow and heat transfer characteristics. The

complex domain is mapped to a simple computational domain and the governing equations are written in terms of generalized curvilinear coordinates.

Maliska and Raithy (1984) and Shyy et al. (1985) made use of staggered grid in which the velocity components are stored at the faces of control volume. Later, Shyy (1994) mentioned that for staggered grid to avoid inconsistencies in interpolation for the cell - face velocities, covariant components of velocity were employed. A collocated grid reduces the geometric and algebraic complexity of the solution for non – orthogonal cells by allowing the velocity components and all scalar quantities to store at the same grid nodes. Because of its simplicity in programming, the non – staggered (collocated) grid has gained popularity and Perić et al. (1988) reported that the collocated grid gave more accurate results than the staggered arrangement. Similar observation was also made by Miller and Schmidt (1988); Melaaen (1992a); Melaaen (1992b); Choi et al. (1994a); Choi et al. (1994b).

Roychowdhury et al. (1999) employed non orthogonal collocated grid to solve incompressible N – S equations. Finite volume method is employed to discretize the governing equations. The convective formulation was carried out using QUICK scheme. The proposed scheme was validated with bench mark solutions. Krishna et al. (2008b) studied lid driven flow in a skewed porous cavity. Governing equations were solved by using FVM. Semi-staggered grid arrangement was employed and coordinate transformation was carried out to transform into a square domain.

Based on the above mentioned works, it can be noted that various numerical methodologies were developed to analyse the flow and heat transport in various domains. Generation of grid for various domains is a tedious task. In order to overcome the difficulty in grid generation, in the present work a generalized code is developed to read the mesh that is generated using a meshing software GAMBIT. A collocated grid based FVM for the analysis of thermal transport in complex domains.

2.3. LID DRIVEN POROUS CAVITY FLOWS

The study of lid/shear driven flow in a porous cavity is not only of academic interest; several other applications comprise float glass production (Pilkington (1969)), analysis of

groundwater flows (Osinov (2003); Krishna et al. (2008b)), packed-bed catalytic reactors (Oztop (2006)), geophysics, chemical engineering and binary alloy solidification (Haddad (2017); Nield and Bejan (2013)) etc.

Generally, earthquakes are associated with soil liquefaction and ground failures. Liquefaction can be referred to the decrease in strength of the saturated cohesion less soil due to the increase in pore water pressure due the application of shear stress. Lid driven flows for fluid can also be treated as a limiting case of porous media with porosity equal to unity and permeability value approaching infinity. The literature on lid driven flow in single phase fluid is very vast. Therefore, the benchmark study for orthogonal geometry is presented.

The lid driven cavity flows with single phase fluid is a commonly used test case for new computational scheme because of the complexity of the flow field. Researchers used a variety of formulations, numerical schemes and grids to tackle the problem. The pioneering work of Ghia et al. (1982) can be considered as a yard stick to test the validity of new numerical approaches for orthogonal square cavity.

Osinov (2003) investigated the distortion of soil under non-uniform cyclic loading with shear conditions. This problem can be correlated to shear/lid driven flows in a porous cavity. Bourchtein et al. (2002) developed a FDM based semi-implicit scheme and implemented to lid-driven porous granular flows. The numerical scheme was examined and suggestions were made for applying boundary conditions. Guo and Zhao (2002) considered lattice Boltzmann approach to investigate the hydrodynamics for non-Darcy porous media. The results were compared with analytical and FDM. The investigation was based on generalized non-Darcy formulation. The study could reveal that non-linear forces play a vital role on flow behavior. Krishna et al. (2008b) investigated the flow behavior for the lid-driven cavity impregnated with isotropic porous media. The Reynolds number was varied and the influence of Darcy number (Da), aspect ratio (AR) and porosity (ε) on flow was studied. It was observed that the non-linear drag forces play a significant role for loosely packed porous media.

Al-Amiri (2000) investigated the heat transport for a porous cavity with a moving top lid. By varying the parameters of the porous media the thermal hydraulics was examined. It was

observed that the heat transport got improved due to the presence of porous media. Jue (2002) examined the thermal hydraulics for a cavity which is impregnated with porous media. A torsional oscillatory lid was considered and the behavior of convective flow was studied. The oscillatory frequency was observed to seriously influence the heat flux variation, especially at the resonant frequency. Vishnuvardhanarao and Das (2008) examined the mixed convection in a porous cavity where the left and right walls were considered to move upwards with the same velocity. In their study, a Darcy number of 10^{-4} was taken.

Oztop (2006) performed numerical analysis for energy transport in a porous cavity with its partially heated moving lid. Several locations for finite heat source were considered to understand the optimum heat transport for the domain. Based on the study the optimum location was observed to be at the middle portion of the left wall. In the above studies, Ergun correlation (1952) was considered to account the inertial and viscous terms. Basak et al. (2010) investigated the thermal hydraulics for a lid driven porous cavity which is provided with a heated bottom wall, linearly heated side walls and cold right wall. At Re=100 for higher Darcy and Prandtl numbers the inertial effect was observed to be dominant. Kumari and Nath (2011) studied thermal transport for a heat generating non-Darcy porous medium with moving top lid. Richardson number was observed to significantly influence the energy transport.

Khanafer and Vafai (2002) studied thermal and species transport in a lid driven porous cavity. A fluid saturated non-Darcy porous medium was considered for the study. It was observed that buoyancy ratio, Lewis number, and Richardson number significantly influence the double-diffusive phenomenon. Nayak et al. (2014) investigated thermal and species transport in a porous cavity with moving top and bottom lids. Mohan and Satheesh (2016) considered magneto hydrodynamic effect and investigated the behavior of thermal and species transport for a porous cavity with the movement of two lids. It was observed that for higher Hartmann number the magnetic field on was significantly influenced. Nithyadevi and Rajarathinam (2017) investigated the influence of magnetic field on double diffusive mixed convection in a porous cavity saturated with copper-water nanofluid. In their study, the flow was assisted by the movement of two lids. Nithyadev et al. (2017) performed transient analysis of thermal and species transport for a lid driven porous cavity saturated with water at its maximum density condition. An increase in thermal and species transport was observed with the increase in Darcy number and decreased

trend was noted with the increase in buoyancy ratio and density inversion parameter. Rahman et al. (2018) studied heat and mass transport in the porous cavity with two side lids moving upward with horizontal insulated walls. The study was performed with two fluids viz. water and water – copper nanofluid. The thermal and mass transport in the cavity was noted to improve with the usage of water – copper nanofluid. Before analyzing the behavior of shear driven flows for anisotropic porous media the earlier studies related to lid driven flows in porous media and hydrodynamics in anisotropic porous cavities need to be addressed.

It can be noted from the above discussion that the studies pertaining to shear driven porous cavity flows were limited to either isotropic porous media in Darcy/non-Darcy regime or anisotropic porous media in Darcy (tightly packed) regime. Also, the earlier studies could reveal that the anisotropy of the porous matrix could significantly influence transport phenomena (Krishna et al. (2008a); Krishna et al. (2009b); Hu et al. (2017)). From the literature it is also observe that the influence of anisotropic parameters of the porous matrix with the variation of lid velocity (Reynolds number), permeability (Darcy number) and porosity on hydrodynamics is yet to be investigated. The objectives and scope of the work carried out on lid driven anisotropic porous cavity flows are presented later, at the end of the chapter.

2.4. NATURAL CONVECTION IN ISOTROPIC DARCY POROUS MEDIA

Due to highly compact nature of naturally available porous media, the Darcy flow model has been extensively used for the analysis of porous media flows. Because of wide range of applications in diversified fields, the literature on natural convection in porous media is very vast. Therefore, the studies related to enclosures filled with Darcy porous medium are highlighted here. When a fluid flows through a porous medium, a resistance is offered by the medium to the flow. This resistance to flow depends on the viscosity of the fluid, porosity of the medium and pore size. This combined effect may be described through a property called permeability of the medium.

Chan et al. (1970) reported numerical results based on finite difference technique for a rectangular porous cavity. They reported that the heat transfer rate was a function of the three dimensionless parameters: (i) Darcy number (Da), (ii) Rayleigh number (Ra) and (iii) aspect ratio

(A). Holst and Aziz (1972a) numerically studied natural convection in a confined porous media. Three dimensional transient simulation was carried out using finite difference technique. It was reported that the three-dimensional motion results in a significantly higher heat transfer across the porous medium than for two-dimensional motion, at a given Rayleigh number. Holst and Aziz (1972b) also studied natural convection in a two dimensional rectangular enclosure experimentally and analyzed the problem with a numerical model, which could handle temperature dependent properties.

By applying the modified Oseen's linearization technique, Weber (1975) developed an analytical solution for the boundary layer regime in a tall vertical porous layer. The obtained solution for average Nusselt number along the hot wall of the cavity was over predicted at higher Rayleigh number. Walker and Homsy (1978) proposed an approximate analytical solution based on the technique of matched asymptotic expansion for natural convective heat transfer in a porous cavity saturated with fluid. Bejan and Tien (1978) studied the natural convection in a horizontal porous cavity subjected to end to end temperature difference, with and without permeable end walls. They concluded that the end wall permeability significantly increases the heat transfer. Bejan (1979) reconsidered the same problem and obtained good agreement with experimental results. An alternative theory was proposed by Simpkins and Blythe (1980) for the boundary layer regime for vertical rectangular cavity based on integral boundary layer solution. Blythe and Simpkins (1981) extended their solution to the more general case where the fluid viscosity is sensitive to changes in temperature. Havstad and Burns (1982) used a finite difference method (FDM), to analyze the free convection in a porous annulus, whose inner and outer walls were maintained at constant but different temperatures. Philip (1982a) developed exact solution for various shapes of the porous cavity for free convection at low Rayleigh number. In another work, the exact solution for axi-symmetric small Rayleigh number convection has also been established (Philip (1982b)).

Haajizadeh and Tien (1983) studied natural convection in a rectangular porous cavity with a permeable end wall experimentally and theoretically. The assumptions of constant pressure and temperature conditions at the permeable wall were found to predict the experimental data satisfactorily. Prasad and Kulacki (1984a) analyzed the natural convective heat transfer in a rectangular enclosure. One vertical wall was maintained at a constant temperature while the other

was subjected to a constant heat flux. It was observed that any increase in the applied heat flux increase the convective effects, but the temperatures were not observed to increase proportionately. The average Nusselt number was higher than that for the case with two isothermal walls. Correlation for Nusselt number in terms of Rayleigh number and aspect ratio was presented. Prasad and Kulacki (1984b) studied the effect of aspect ratio on heat transfer and flow field in a rectangular cavity bounded by isothermal vertical walls at different temperatures. They observed that for a cavity with fixed height, the heat transfer rate increases as the aspect ratio is increased, except when the flow exhibits boundary layer on the vertical walls. The authors clearly delineated the conduction, asymptotic and boundary layer flow regimes in natural convection inside enclosures.

Hickox and Gartling (1985) considered a case in which the side walls are maintained at constant temperatures, top and bottom walls are treated as adiabatic. The inner wall is maintained at a higher temperature and outer wall is maintained at a lower temperature. Using finite element approach, they carried out heat transport analysis for lower Rayleigh numbers (<100) and tall annulus (A>2). They also developed an analytical method applicable to those scenarios using the approach used by Burns et al. (1977). Prasad and Kulacki (1985) and Prasad et al. (1985) conducted a series of experiments in an annular cavity, with isothermal vertical walls for various solid-fluid combinations, such as glass-water, glass-heptane, glass-glycol and steel-water. They have brought out the necessity for non-Darcy models based on their comprehensive experiments and numerical work. They concluded that porous media with smaller L_{ref} /d_p deviate more from the Darcian flow regime. Since agreement between the theory and Darcy model is not satisfactory with static thermal conductivity, they proposed a new method of calculating the effective thermal conductivity. Prasad et al. (1986) experimentally studied a similar geometry with constant heat flux on the inner wall, with two sets of radius ratios and aspect ratios and with several solid-fluid combinations. It was observed that with the increase in ratio of thermal conductivities of solid and fluid, Nusselt number decreased at a given Rayleigh number. Prasad (1986) carried out an exhaustive numerical study of natural convection in annular geometry with constant heat flux on inner wall and isothermal cooling on outer wall. Correlations for average Nusselt number were reported in terms of Rayleigh number and aspect ratio.

Pop and Na (1994); Pop and Na (1995) solved numerically the boundary layer equations for natural convection along an isothermal wavy cone embedded in a fluid saturated porous media using Keller-box method. The wavy nature of the cone was observed to decrease the heat transfer rate when compared to that of a smooth truncated cone. Baytas and Pop (1999) carried out simulations for natural convection in oblique porous enclosures. The heat transfer rate was observed to decrease with the increase in skewness. Tsybulin et al. (2006) carried out steady state analysis with temperature perturbations on the boundary. A selection map was introduced to analyze the selection of steady state from a continuous family of equilibrium which exits under zero boundary condition. Varol et al. (2006) investigated natural convection numerically for a right angle triangular enclosure filled with fluid saturated porous media. They observed that the heat transfer rate increases with the decrease in aspect ratio and increase in Rayleigh number. Shalini and Kumar (2007) investigated the influence of variable heat flux on natural convection along a corrugated wall in porous media. The wavy nature of surface temperature plots were observed to decrease with the increase in Grashof number. Saeid (2007) studied conjugate natural convection numerically for a porous enclosure with finite wall. The influence of Rayleigh number, thermal conductivity ratio and ratio of wall thickness to height on flow behavior was carried out. Ouarhlent and Soudani (2019) consider cubic shaped enclosure filled with homogeneous isotropic porous media. For the considered enclosure left and right wall maintained at hot and cold respectively, and top and bottom boundaries are adiabatic. It was conclude that, as Rayleigh number increases with the increase in Nusselt number. Das et al. (2019) studied free convection in a square and triangular cavities with discreate heat sources. It was observed that, the average Nusselt number is higher for triangular cavity when compared to that of square cavity.

The above mentioned literature have used either Darcy's equation for analysis or conducted model experiments in porous media. If the flow with higher velocities is considered, it is observed that based on the pore size, the matrix drag non-linearities will be exhibited by the system. If the porous media is bounded by impermeable walls as in the case of insulating materials, there will be a need to satisfy no slip boundary conditions. Since Darcy's equation is one order less than the Navier-Stokes equation, it will not satisfy no slip condition at the walls. The inadequate accuracy of Darcy's law at higher porosities and permeabilities drew the attention

of researchers towards suitable non-Darcy models. The following section reviews the available non-Darcy models which are extensions or modified form of the Darcy model.

2.5. NATURAL CONVECTION IN ISOTROPIC NON DARCY POROUS MEDIA

Depending on the nature of the porous media and flow conditions, formulations such as Darcy model, Forchheimer extended Darcy model, Brinkman extended Darcy model and modified Navier-stokes model were employed. Though non – Darcian effects are not significant for tightly packed porous media it becomes very much necessary to consider for the porous media which is loosely packed. Also, it is necessary to contemplate a generalized model which can predict the thermal hydraulics for wide range of porous media. In this section, the non-Darcy models for natural convection in porous media are reviewed.

2.5.1. Forchheimer Extended Darcy Model

In order to account for the non-linear kinetic energy loss, Forchheimer (1901) proposed an extension to the Darcy's law. Later, researchers used this extension to model flow through porous media and found a considerable contribution of the non-linear drag term at higher Reynolds numbers or Rayleigh numbers and higher permeabilities.

Plumb and Huenefeld (1981) employed Ergun's correlation (1952) for the study of natural convection from a heated surface in a saturated porous medium. The effects of non-Darcian flow and non uniform permeability have been studied by Tien and Hong (1985). They used Ergun's correlation to account for the solid matrix drag. Poulikakos and Bejan (1985) studied analytically as well as numerically, the departure from Darcy flow in natural convection in a vertical porous layer heated from side. A cavity with an aspect ratio of two was considered. They found that the average Nusselt number is proportional to $Ra^{1/4}$. Prasad and Tuntomo (1987) studied the inertial effects in natural convection in a vertical cavity. Nakayama et al. (1990) solved free convection over a non-isothermal body of arbitrary shape in a porous medium using Forchheimer extension to Darcy model. They used similarity transformation to solve the equations. Saeid and Pop (2005) investigated natural convection in a square cavity numerically with Darcy-Forchheimer model.

The results were presented to show the effect of inertial parameter on the average Nusselt number and the fluid flow. It was found that for constant Rayleigh number with the increase in inertial parameter the average Nusselt number reduces.

Vafai (1984) analyzed the effects of variable porosity and inertial effects on convective flow and heat transfer in porous media. In this study, a method of matched asymptotic expansions was used to show the qualitative aspects of variable porosity in producing the channeling effect. The numerical data was found to be in excellent agreement with the experimental data. Georgiadis and Catton (1985) studied free convective boundary layer flows in vertical fluid saturated porous slots of high aspects ratio. Hong et al. (1987) examined analytically the effects of non Darcian and non uniform permeability conditions on natural convection for a vertical plate in porous media. In their study, Ergun's correlations have been employed for linear and nonlinear drag forces. It was observed that inertial effect decreases the heat transfer while the dispersion effect increases it. Beckermann et al. (1987) carried out experimental and numerical investigation of natural convection in a rectangular enclosure that is partially filled with porous media. A good agreement was observed between the flow visualization and numerical results.

Mbaye et al. (1993) developed analytical solution and also carried out numerical analysis on natural convection in an inclined porous layer confined by a wall with finite thickness. Hung and Chen (1997) studied free convection in a thermally stratified porous media along a vertical plate with variable heat flux. The non similar transformed equations are solved with Keller's box method. The non-Darcian and thermal dispersion effects were found to have significant influence on heat transfer. Later, Hung et al. (1999) carried out a similar study with non-isothermal vertical surface. In these studies the non linear drag was considered from Ergun's correlations.

2.5.2. Brinkman Extended Darcy Model

The Brinkman extended Darcy model (1947) is another extension to the traditional form of Darcy's model. Flow for many practical applications of porous media involves impermeable solid boundaries which confine flow geometry. In such cases, wall effect is to be accounted. The Brinkman extended Darcy model was proposed to account the viscous effects, considering the effective viscosity of the porous medium. In addition to Darcy's term, viscous term was

employed by Chan et al. (1970) for flow equation. They gave the criteria for the onset of convection in a cavity heated from below as $Ra^*=4\Pi^2$.

Neale and Nader (1974) examined the importance of Brinkman extended Darcy model. They concluded that for the flow outside the boundary layer region, the Brinkman's equation reduces to Darcy's law. Nield (1983) in his study concluded that the Brinkman's term is useful in the treatment of flow past a very sparse collection of obstacles.

Lundgren (1972) investigated slow flow through stationary random beds and suspensions of spheres using Brinkman's equation. He suggested an effective viscosity of $\mu/(1-2.5\varepsilon)$ for suspensions. Durlofsky and Brady (1987) have shown that the Brinkman equation actually describes the flow in porous media with porosity smaller than 0.8.

Tong and Subramanian (1985) carried out boundary layer analysis for natural convection in vertical enclosures with Brinkman extended Darcy model. They used modified-Queen technique to solve the problem and obtained the limit for Darcy model in terms of Rayleigh number (Ra), Darcy number (Da) and the aspect ratio (AR). It was found that the Darcy model is applicable for $Ra^*Da/AR < 10^{-4}$. The authors also confirmed the accuracy of earlier results of Weber (1975).

Vasseur and Robillard (1987) studied buoyancy induced flows in a porous cavity subjected to uniform heat fluxes along the vertical boundaries. The boundary layer equations were solved using Oseen linearization method. It was found that the boundary effects have a non-negligible influence on fluid flow and heat transfer. Vasseur et al. (1989) investigated natural convection in shallow cavities with uniform heat flux by employing Brinkman model. The study considers horizontal boundaries of rigid-rigid, rigid-free and free-free type. Heating is through the bottom or the sidewall. The overall heat transfer rate was noted to reduce drastically with the increase in permeability. It was also observed that the reduction was larger at higher Darcy and Rayleigh numbers. Moreover, as Darcy number tends to zero, the flow field is similar to that given by the Darcy analysis, except in the thin region next to the boundary where the viscous effects are confined.

Vasseur et al. (1990) investigated buoyancy induced flows in an inclined porous slot using Brinkman extended Darcy model. They observed that as the value of Da increased, the magnitude of the peak velocity reduced and the position of the peak velocity got shifted away from the wall. At higher Da, viscous effects become dominant and hence buoyancy-induced convection within the cavity is reduced.

Elsharkawy and Guedouar (2001) studied hydrodynamic lubrication of finite porous journal bearing. The Brinkman extended Darcy and Stokes equations were utilized to model the flow in porous region and clear fluid region. The model was found to have good agreement with experimental results.

Both the Brinkman and Forchheimer models for flow through porous media have found acceptance in the literature at different flow limits. Some of the researchers have made use of both Forchheimer's and Brinkman's terms along with Darcy formulation due to the following reasons. To account i) no slip wall effect, Brinkman's extension was used and ii) inertial forces for flow with Reynolds number based on mean pore diameter of the order more than one.

2.5.3. Modified Navier-Stokes Equation Model

The modified Navier Stokes equation model has been proposed in order to provide a comprehensive theoretical formulation which reduces to each of the earlier models in the appropriate limit depending on the flow rates and permeability of the porous media. Vafai and Tien (1981) developed a generalized model using volume averaging technique. The flow equations contain the fluid inertial terms and the non linear drag terms along with usual Darcy and viscous terms. Nithiarasu et al. (1997) also derived generalized variable porosity model by employing Ergun's correlation for Forchheimer constant. In the above literature the macroscopic generalized equations for incompressible flow were obtained based on volume averaging.

Vafai and Tien (1981) investigated the influence of solid boundary and the nonlinear drag forces on thermal hydraulics of porous media. They concluded that the boundary has more influence on heat transfer at high Prandtl numbers and large pressure difference. They also observed that the inertial effect increased with the increase in permeability and the reduction in fluid viscosity. Hong et al. (1985) investigative natural convective heat transfer from vertical

plate embedded in a high porosity medium under non-Darcian effects. Inline to Vafai and Tien (1981), they also observed that the boundary and inertial effects have a noteworthy influence on the velocity profile and surface heat transfer rate.

Prasad et al. (1985) carried out experiments with an annulus saturated with porous media. The experimental results were found to be in good agreement with numerical simulations. Lauriat and Prasad (1987) employed the Navier Stokes equations with linear solid matrix drag, for handling the flow equations to analyze natural convection heat transfer and flow in porous media. Lauriat and Prasad (1989) examined numerically the non-Darcian effects on natural convection in a vertical porous enclosure. They made a comparative study of Darcy-Brinkman-Forchheimer solutions for a differentially heated vertical cavity. This work considers fluid Rayleigh number and Darcy number as two separate parameters. It was concluded that a) an asymptotic convection regime exits where the heat transfer rate is independent of the permeability of the porous matrix. b) The presence of Forchheimer term leads to the reduction of heat transfer. c) Validity of Darcy model increases with the reduction in both Darcy and Forchheimer term.

Ettefagh et al. (1991) analyzed the importance and relevance of non – Darcian effects associated with natural convection in open ended cavities filled with fluid saturated porous media. It was observed that for higher modified Rayleigh number (Ra_m) the deviation from Darcian formulation appears at $Da > 10^{-4}$. Lage (1992)used the generalized model to study the convective effects on bernard convection in porous media. This numerical study shows that convective term has a negligible effect on the overall heat transfer for most cases. It was observed that the inertial terms can be neglected for lower permeability media while the general equation was intended to bridge the entire domain between low and high permeability.

By scale analysis, Lage (1993) obtained a correlation valid for the entire spectrum covered by the generalized equation. Misra and Sarkar (1995) applied generalized non Darcy model to investigate different models due to Darcy, Brinkman, Forchheimer and combined Darcy-Brinkman-Forchheimer. Hsiao (1995) applied studied transient natural convection from a corrugated plate embedded in a porous medium by generalized model.

Vafai and Kim (1995) provided detailed explanation and the validity of each term in generalized non-Darcy model. Sai et al. (1993) employed finite element method to numerically investigate Darcy and non-Darcy regimes for buoyancy flows in vertical porous annulus. Nithiarasu et al. (1997) provided derivation for generalized non Darcy variable porosity model from fundamental principles. In this model the Forchheimer constant was considered from the experiments carried by Ergun (1952) for flow through packed beds. For fixed porosity and modified Rayleigh number comparison was carried out in Darcy and non-Darcy regimes for a differentially heated porous cavity and porous cavity with single phase fluid at the center. A significant difference for average Nusselt number is observed between Darcy and non-Darcy regimes. The influence of porosity on natural convective flow and heat transfer has been investigated by Nithiarasu et al. (1998) using a generalized porous medium model. Later, Nithiarasu et al. (1999) carried out parametric study for buoyancy driven flow in fluid saturated porous media for different Darcy/ Rayleigh and Biot numbers and aspect ratios. The fluid flow and heat transfer aspects were carried out by explaining the behavior of vortex with the variation of pertinent parameters.

Merrikh and Mohamad (2002) investigated numerically the natural convection in a rectangular enclosure filled with two layers of porous media. Constant heat flux was supplied on the left wall, and the right wall was maintained at a lower temperature. It was found that the boundary effects have significant importance at higher modified Rayleigh numbers.

Pakdee and Rattanadecho (2006) investigated unsteady natural convection for porous cavity with a convection condition at the top surface. FDM has been adopted to solve the governing equations. The influence of Ra and Da has been studied on flow and heat transfer aspects. Basak et al. (2006) investigated the buoyancy driven flow in a square cavity under various boundary conditions. Sathiyamoorthy et al. (2007) studied natural convective flow in a square cavity filled with porous media for linearly heated side walls. Later, Basak et al. (2008) simulated natural convective flow in a porous isosceles triangular enclosure with various thermal boundary conditions. In the above studies penalty finite element method with bi-quadratic rectangular elements were used to solve the governing equations. Krishna et al. (2008) analyzed the influence of Rayleigh number, Prandtl number, Darcy number and porosity on heat transport for isotropic porous media. The formulation was based on the generalized non-Darcy model.

ACFD technique was implemented to generate a correlation for the average Nusselt number. The non-Darcian effects are insignificant in low porosity media which is not the case for high porosity media. Furthermore, for low porosity media the entry region is very small, and the convective term in the governing equations can be neglected. This may not be the case for high porosity media. The boundary and inertial effects on the transport of momentum and thermal energy for natural convection flow play significant roles in the prediction of overall heat transfer.

2.6. NATURAL CONVECTION IN ANISOTROPIC POROUS MEDIA

It can be noted that most of the real life problems such as extraction of metal alloys from ores, nuclear fuel rod bundle, heat exchanger tubes, geothermal processes etc. are anisotropic in nature. Hence, it is necessary to study the effect of anisotropic properties of the porous medium on the fluid flow and heat transport behavior.

Neale (1977) considered clusters of parallel cylindrical fibers of circular/elliptical cross section and obtained relations for the permeability and diffusivity ratios. The anisotropic permeability and conductivity ratio range between 0.5 and 2 for circular cylindrical fibers. These ratios depend on the relative magnitude of the minor and major axes also for elliptical fibers.

Burns et al. (1977) examined analytically the natural convective heat transfer in a vertical slot filled with a porous medium. The results illustrate that the Nusselt number was dependent on Rayleigh number, aspect ratio and anisotropic permeabilities. Hickox and Gartling (1985) mentioned that the anisotropic permeabilities could reduce the heat transfer rate by 2 to 3% for the Darcy-Rayleigh number of 100.

Ni and Beckermann (1991) analyzed the effect of permeability ratio and thermal conductivity ratio on fluid flow and heat transfer behavior in a square enclosure filled with anisotropic porous medium. The anisotropy of the porous medium was found to influence the heat and fluid flow significantly.

Chang and Hsiao (1993) studied the effects of anisotropy on natural convection in a vertical cylindrical enclosure filled with anisotropic porous medium, using primitive variable method. Numerical results showed that the heat transfer rate increased with the increase in

permeability ratio and decrease in thermal conductivity ratio. It was also observed that the average Nusselt number on the side wall increased with the reduction in aspect ratio. Slimi and Nasrallah (1998) carried out two dimensional transient numerical simulations of fluid flow and heat transfer in a vertical cylindrical enclosure. The cylinder is filled with saturated porous medium and a uniform lateral heat flux was supplied. This work provided the validity of Darcy flow model and thermal boundary layer approximations.

Degan et al. (1995) carried out numerical study on free convection in a rectangular porous cavity filled with anisotropic porous medium. The porous medium was assumed to be hydrodynamically as well as thermally anisotropic. The principal axes of the thermal conductivity were taken to be coinciding with coordinate axes. On the other hand, directions of the permeability were varied with respect to gravity vector. Later, Degan and Vasseur (1997) extended the above formulation for Brinkman extended Darcy model to study buoyancy effects. By employing the above formulation for anisotropy in permeability, Vasseur and Degan (1998) studied natural convective heat transfer from a vertical plate embedded in a fluid saturated Darcy porous medium. They concluded that higher heat transfer rate can be obtained if the permeability is higher in the vertical direction. Also, the results indicate that heat transfer is minimum if the thermal conductivity ratio is higher.

Srivastava et al. (2011) investigated the thermal hydraulics for electrically conducting porous media. A non-thermal equilibrium model was considered for their study. The porous media was taken to be in Darcy regime with anisotropy in terms of permeability. The influence of Rayleigh number and wave number on thermal transport was discussed. Gaikwad and Dhanraj (2013) considered anisotropic porous media saturated with Maxwell fluid. The double diffusive convective studies were performed by employing modified Darcy-Maxwell model. The influence of mechanical and thermal anisotropy parameters on convection was studied. Swamy et al. (2013) investigated thermal hydraulics for an anisotropic porous layer saturated with viscoelastic fluid. By providing periodic harmonic vibrations the gravity term was varied. A densely packed porous media with anisotropy in the vertical direction for both thermal and mechanical properties were considered.

Chang and Lin (1994) numerically studied the effect of wall conduction on buoyancy driven flow and heat transfer in a suare cavity filled with anisotropic porous medium. SIMPLE algorithm was used to obtain the solution of governing equations. They observed a critical value of anisotropic thermal diffusivity ratio at which the Nusselt number was minimum. The critical value was observed to be depending upon anisotropic permeability ratio. Moreover, it was observed that wall conductance could lead to significant changes in heat transfer rate.

Keyhani and Polehn (1995) reported an improved finite difference scheme for modeling anisotropic conduction and they showed that it approached the accuracy of the Galerkin weak statement finite element formulation. Chevalier et al. (1999) carried out numerical and experimental investigation for free convection in an inclined porous layer by considering temperature gradient along the vertical direction.

Nithiarasu et al. (2000) extended the formulation of anisotropic permeability and thermal conductivity to generalized non-Darcy model. Ergun's correlations have been employed to account non linear drag forces. In this study the influence of anisotropic properties on heat transfer with the variation of Ra and Da has been clearly brought out.

Lee and Yang (1997) and Yang and Lee (1999) treated bank of cylinders as an anisotropic porous medium and provided correlations for permeability, Forchheimer coefficient and effective thermal conductivity. They mentioned that the permeability approached a value of zero at the particular porosity of 0.2146 which means that fluid flow across the cylinders became impossible. Knupp and Lage (1995) mentioned that inertial coefficient and permeability are independent parameters and is possible to think of cases in which a porous medium presents different amounts of anisotropy for permeability and inertia (Forchheimer) coefficients. Mamou et al. (1998) investigated the natural convection phenomenon in a cavity filled with anisotropic porous medium. It was reported that permeability ratio and principal axes orientation have more influence on the system stability.

Nakayama et al. (2002); Nakayama et al. (2004) investigated thermal hydraulics through a collection of square rods placed in an infinite two-dimensional space. The degree of anisotropy was varied by changing the transverse center to center distance with the longitudinal center to

center distance being fixed. It was found that the principal axes of the permeability tensor differ significantly to that of Forchheimer tensor.

Krishna et al. (2008a) analyzed natural convection in an anisotropic porous medium confined in a square cavity with volumetric heat generation. It was observed that the thermal hydraulics of fluid was largely influenced by anisotropic properties of the porous matrix. Similar conclusions were also given by Krishna et al. (2009a) who analyzed the problem of natural convection in a square cavity packed with anisotropic porous medium using generalized non-Darcy approach. In their study heat source was located at the bottom wall.

Krishna et al. (2010) considered partially heated rod bundle was orthotropic porous media and modeled using non-Darcy formulation. It was observed that when the porosity increases from 0.3 to 0.9 the temperature gradients were reduced, due to decrease of convective strength.

Chandra and Satyamurty (2011) analyzed thermal transport in anisotropic porous media using extended non-Darcy Brinkman model. Their study revealed that the hydrodynamics and thermal anisotropy are governed by Da, Ra, K^*, and k^*. It was found that the increase in permeability ratio (K^*) caused an increase in average Nusselt number ($\overline{Nu}$) and reduction in $\overline{Nu}$ with increase in thermal conductivity ratio (k^*).

Aly and Ahmed (2014) investigated natural and mixed convection for an anisotropic porous media by using ISPH method in non-Darcy region. It was observed that, the results were mainly affected with the variation in Rayleigh number, porosity, Darcy number, permeability ratio and inclination angle of principal axes. It was concluded that velocity magnitude increased with the increase of the Rayleigh number and higher rate of fluid flow was obtained at an inclination angle of 45°. It was also observed that directions of heat and fluid flow depend upon permeability ratio. Mohamad et al. (2015) studied thermal hydraulics for flow through porous conduits. It was mentioned that the understanding of limitation for Darcy's law is necessary for the proper insight of thermal transport in porous media. The above studies have highlighted that the generalized non-Darcy formulation can be employed to predict transport phenomena from tightly to loosely packed porous media.

Mishra et al. (2016) numerically studied the effect of different parameters on the heat transfer rate in a three-dimensional rectangular box filled with porous medium by using non-Darcy formulation. It is observed that, effect of Darcy number was significant at higher Rayleigh number and higher aspect ratio.

Ahmed and Rashad (2016) investigated the problem of natural convection in a square cavity filled with micro fluids using anisotropic porous media formulations. It was mentioned that, with the increase in volume fraction of nanoparticles (Al_2O_3/water) the heat transfer rate increased and with the increase in permeability ratio the vortex strength decreased.

Hu et al. (2017) developed MRT LB model to simulate flow in anisotropic porous media. They considered natural convection problem in a square cavity filled with anisotropic porous medium with/without heat generation. It was observed that thermally anisotropic porous medium layer enhanced heat transfer rate when compared to isotropic porous layer.

Srivastava and Singh (2018) analyzed the thermal and species transport in an anisotropic porous medium with internal heat source saturated with viscoelastic fluid. It was mentioned that, the thermo physical properties have more influence on the heat and fluid flow characteristics. In non-Darcy region, heat transfer rate was more when compared to Darcy region. Based on the above details it can be understood that the thermal hydraulics in anisotropic porous media is complex and thorough insight is necessary for efficient design of thermal equipment. Chandran et al. (2018) investigated free convection in a porous trapezoidal cavity filled with anisotropy permeable material. Numerical analysis were performed to analyze the influence of various parameters such as aspect ratio, angle of inclination, buoyancy ratio and internal heating. Results were analyzed by using steamlines and isotherms contours. Kozelkov et al. (2018) proposed an implicit algorithm for modified Navier-Stokes equations to simulate the flow in anisotropic porous media. The comparison was made with various benchmark problems and observed to predict accurately. Safi and Benissaad (2018) studied natural convection in a anisotropic porous medium. Governing equations are solved using FVM. Darcy- Brinkman – Forchhemier model was considered for the formulation of problem geometry and it is validated with Boussinesq approximation. It was observed that, the rate of heat transfer depends upon permeability ratio.

When permeability ratio increases rate of heat transfer increases. It is also observed that, increase in Rayleigh number with the increase in Nusselt number.

2.7. HEATLINE VISUALIZATION OF THERMAL TRANSPORT IN POROUS MEDIA

The heatline approach can be used to analyze the performance of thermal systems by visualizing the direction and intensity of heat flow. Visualization of heat flow using heatlines was introduced by Kimura and Bejan (1983). Costa (2000) presented the heat functions for the laminar natural convection near a vertical wall with isothermal and constant heat flux conditions. The boundary layer problem was solved using the similarity method.

Deng and Tang (2002) studied the numerical visualization of convective heat transfer by streamlines and heatlines. It was mentioned that the visualization of transport phenomena by means of streamlines and heatlines was observed to provide a more practical and efficient means than the customary ways.

Natarajan et al. (2007) studied two-dimensional heat function within a trapezoidal cavity which is differentially heated in the vertical direction. Finite element method was used to obtain isotherms, streamlines and heatlines. They observed that when Ra (Rayleigh number) $=10^3$, the heat transfer was uniform from hot wall to the cold wall. But for Ra $=10^6$, the lower left and upper right portion of the cavity were observed with higher heat transfer rates.

Dalal and Das (2008) studied two-dimensional cavity with a wavy right vertical wall. Governing equations were solved by using the finite - volume method. Results were presented by means of streamlines, heatlines, isotherms, local and average Nusselt number distribution for a selected range of Rayleigh number (10^0–10^6). Basak and Roy (2008) demonstrated natural convection in a square enclosure with insulated top wall, hot bottom wall and cold side walls. It was found that heatline concept is very much needed for optimal thermal management and also helps in the understanding of the energy distribution for the food processing application to store food for a long time.

Banerjee et al. (2008) carried out steady state simulation for natural convection with a bi-heater configuration for the analysis of passive electronic cooling. Deng (2008) studied laminar natural convection due to discrete heat source-sink pairs in a two dimensional cavity. They analyzed the influence of arrangement of sources and sinks on fluid flow and heat transport characteristics.

Basak et al. (2009) studied heatline concept for a trapezoidal enclosure by varying Rayleigh number in the range of 10^3 -10^5, Prandtl number ($0.026 \leq Pr \leq 1000$) and at various tilted angles ($\Phi = 45^0, 30^0$ and 0^0). It was observed that the heatlines were perpendicular to the isotherms during conduction dominant region. Basak et al. (2009) performed thermal hydraulic studies for an inverted triangular cavity by considering heatline concept. The study was carried out with wide range of Rayleigh number (10^2 to 10^5) and Prandtl number (0.015, 0.026, 0.7 and 1000). It was found that heatlines are perfectly normal to the isotherm during conduction dominant heat transfer. However, with the increase of Rayleigh number (Ra) to 10^4 due to the initiation of convection, the flow patterns get distorted.

Waheed (2009) made use of heat function formulation to investigate the heat transport in a square porous cavity by employing finite-difference method. It was concluded that, heatlines and heat function enhance the understanding of distribution of heat.

Hooman et al. (2009) numerically investigated the influence of temperature dependent viscosity on natural convection for saturated porous media. Arrhenius model was employed to incorporate the temperature dependent viscosity. It was mention that of heatlines and energy flux vectors can provide a detailed analysis of thermal transport. In line to Bejan's heatlines, Hooman (2010) introduced energy flux vectors for the visualization of convection. It was mention that the technique of energy flux vector does not to solve other equations in additional to momentum and energy. This approach was noted to reduce the computation time and resource for the visualization of energy flow.

Kaluri and Basak (2010) studied distributed thermal management policy for energy-efficient method of materials processing applications by natural convection. Analysis was carried out by visualizing the heat flow by heatlines. It was found that the heatline approach is useful in visualizing the complex heat flow patterns in the cavity with multiple distributed heat sources.

Kaluri et al. (2010) considered a square cavity with distributed heat sources and analyzed the thermal mixing. Based on heatlines it was observed that distributed heating was more efficient when compared to that of a conventional bottom heating.

Mobedi et al. (2010) employed heat function equation for the visualization of convection and diffusion in a square cavity. Basak et al. (2011) studied natural convection in trapezoidal enclosures by varying boundary conditions. Results were presented in terms of isotherms, streamlines, heatlines, local and average Nusselt numbers for enclosures. Basak et al. (2013) considered conjugate natural convection problem to analyze the magnitude and direction of heat flow inside a square cavity using heatline concept. They varied wall thickness from 0.2 to 0.8 and conductivity ratio (k* = 0.1, 1 and 10). It was found that, as k* increases, intensity of fluid circulation increased irrespective of wall thickness.

Singh et al. (2015) estimated the performance of thermal systems using heatline concept. This concept was used to visualize the flow of heat inside inclined two-dimensional cavities filled with porous media. Brinkman– Forchheimer extended Darcy model was used to solve the momentum equations. At Da = 10^{-5} the stream function magnitudes were small; hence heat lines were normal to isotherms. At higher Darcy number (Da=10^{-2}) stream function and heat function magnitudes were stronger which lead to improved mixing.

Biswal and Basak (2015) studied heat line patterns of various shapes with Dirichlet heat function boundary conditions at various Rayleigh numbers (10^3 and 10^5) and Prandtl numbers (Pr = 0.015 and 7.2). It was concluded that the heatline visualization approach with various heat function boundary conditions can be helpful for the better insight of the energy transport in thermal systems.

Triveni et al. (2015) considered a triangular cavity filled with water and the bottom wall was partially heated. They analysed the natural convective flow by varying Rayleigh number ($10^5 \leq Ra \leq 10^7$). Results were presented in terms of streamlines, isotherms and average Nusselt numbers for various positions of the heater within the enclosure. It was observed that the increase of heat transfer rate depended on increment of Rayleigh number.

Das and Basak (2016) investigated discrete solar heating involving natural convection for different types of domains such as square, triangular and inverted triangular geometries. Isotherms, heatlines, streamlines, local and average Nusselt number for different positions of the heater within enclosure were provided. Lima and Ganzarolli (2016) made use of heatlines to analyze the conjugate heat transfer in an enclosure having internal conducting solid body. It was observed that as the ratio of thermal conductivities of fluid and solid(k*) increases from 0.01 to100 the heat transfer at the solid domains was noted to decrease.

Alsabery et al. (2016) documented natural convection phenomenon in a square enclosure which is filled with nanofluid with sinusoidal heating at the horizontal walls. It was found that the enhancement of heat transfer rate depended on the increment of solid wall thickness. Alam et al. (2016) investigated the thermal transport in a prismatic cavity which is filled with air. It was observed that the heatlines are normal to the isotherms in conduction dominant regime. Further it was mentioned that heatlines along with isotherms give better understanding of energy distribution.

Ahmed (2016) investigated energy transport for thermally anisotropic non-Darcy porous media. The bottom and top lids were made to move in the opposite direction. In this study, the thermal transport was visualized by Bejan's heatline. Ajmera and Mathur (2016) performed experimental and numerical investigation of mixed convection in a rectangular enclosure provided with ventilation ports. The parameters considered for the study were $1.25 \leq AR \leq 2.5$, $3224 \leq Re \leq 6579$, $8.5\times10^6 \leq Gr \leq 1.03\times10^8$ and Richardson number in the range of 0.21–9.58. It was observed that there is a rise in Nusselt number with increase in Reynolds number and aspect ratio. It was also noted that enhancement of heat transfer depended on the height of ventilation ports. A thorough knowledge on heat transport phenomenon in complex domain is vital in designing efficient equipment.

Biswal et al. (2016) visualized the heat and fluid flow distribution of natural convection within titled porous square cavities. The governing equations were extracted using Darcy–Brinkman–Forchheimer model and solved by using finite element method. It was observed that, at higher Darcy number isotherms are distorted compared to lower Darcy number irrespective of modified Prandtl number (Pr_m).

Roy et al. (2016) analyzed distribution of heat and fluid flow inside square cavity filled with fluid saturated porous medium using Bejan's heatline concept. Results were presented in terms of streamlines, isotherms and heatlines. They suggested vertically moving wall to achieve higher heat transfer rate. Anandalakshmi et al. (2019) studied buoyancy induced flows for two-dimensional rhombic shape cavities filled with porous media. It was noted that for higher Darcy number ($Da=10^{-3}$), the magnitude of temperature is maximum at the core region due to which maximum thermal mixing was observed. Tao et al. (2019) gave a critical review by comparing heatline and field synergy principle. It was mentioned that both the tools are independent and help for better insight of thermal transport.

Based on the literature review it can be noted that the concept of heatline visualization can help in great detail for the understanding of thermal transport in complex structures. But the studies pertaining to heatlines for natural convection filled with non – Darcy anisotropic porous media is yet to appear in literature. Therefore, the present work is aimed to analyze the thermal hydraulics in a square cavity filled with anisotropic non-Darcy porous medium with the concept of heatline visualization.

2.8. RESEARCH GAPS IDENTIFIED FROM LITERATURE REVIEW

- Analysis of thermal transport using the concept of heatline visualization in complex domains is scarce.

- Soil liquefaction refers to the decrease in the strength of the cohesionless soil when subjected to shear conditions. The studies pertaining to hydrodynamics for loosely packed anisotropic porous media with shear driven conditions is yet to be carried out.

- The understanding of thermal hydraulics with orientation of solid matrix is necessary for the efficient design of thermal equipment. Visualization of thermal transport via heatlines for non-Darcy anisotropic media is yet to appear in literature.

2.9. OBJECTIVES OF THE PRESENT RESEARCH WORK

- To investigate
  - ✓ Heat transport for various solid geometries through heatline visualization.
  - ✓ Hot spots through isotherms and heatline profiles for various solid geometries with discrete heat source(s).
  - ✓ Hydrodynamics for non-Darcy shear driven flows with anisotropic porous media.
  - ✓ Thermal hydraulics using heatline visualization approach for non-Darcy anisotropic porous media.

CHAPTER 3

MATHEMATICAL FORMULATION AND METHOD OF SOLUTION

3.1 INTRODUCTION

In this chapter, a generalized treatment of the governing equations and the solution methodology broadly applicable to all the four problems taken up in the thesis is presented.

3.2 GOVERNING EQUATIONS

In the present study, the governing equations are varied accordingly with respect to pertinent problem. Governing equations and detailed description of pertinent problem are provided in the respective chapters. A generalized form of the governing equations Eqns. (3.1 – 3.5) pertains to fluid flow and heat transfer for non – Darcy anisotropic porous media involve continuity equation, the two momentum equations, the energy equation and heat function equation. In the present study equations are solved using pseudo transient approach. The governing equations in terms of primitive variables for the transient flow can be written as follows.

Continuity equation:

$$\frac{\partial u}{\partial x}+\frac{\partial v}{\partial y}=0 \tag{3.1}$$

x - Momentum equation:

$$\begin{aligned}\frac{1}{\varepsilon}\frac{\partial u}{\partial t}+\frac{u}{\varepsilon^2}\frac{\partial u}{\partial x}+\frac{v}{\varepsilon^2}\frac{\partial u}{\partial y} &= -\frac{1}{\rho_f}\frac{\partial P_f}{\partial x}+\frac{\mu_f}{\rho_f\varepsilon}\left(\frac{\partial^2 u}{\partial x^2}+\frac{\partial^2 u}{\partial y^2}\right)\\ &-\frac{\mu_f}{\rho_f K_1}\left[u\left(\cos^2\theta+K^*\sin^2\theta\right)+v\left(\left(1-K^*\right)\sin\theta\cos\theta\right)\right]\\ &-\frac{F_1}{\sqrt{K_1}}\left[u\left(\cos^2\theta+\frac{\sqrt{K^*}}{F^*}\sin^2\theta\right)+v\left(\left(1-\frac{\sqrt{K^*}}{F^*}\right)\sin\theta\cos\theta\right)\right]\sqrt{u^2+v^2}\end{aligned} \tag{3.2}$$

y - Momentum equation:

$$\frac{1}{\varepsilon}\frac{\partial v}{\partial t}+\frac{u}{\varepsilon^2}\frac{\partial v}{\partial x}+\frac{v}{\varepsilon^2}\frac{\partial v}{\partial y} \tag{3.3}$$

$$= -\frac{1}{\rho_f}\frac{\partial P_f}{\partial y}+\frac{\mu_f}{\rho_f \varepsilon}\left(\frac{\partial^2 v}{\partial x^2}+\frac{\partial^2 v}{\partial y^2}\right)$$

$$-\frac{\mu_f}{\rho_f K_1}\left[u\left((1-K^*)\sin\theta\cos\theta\right)\right.$$

$$\left.+\,v(K^*\cos^2\theta+\sin^2\theta)\right]-\frac{F_1}{\sqrt{K_1}}\left[u\left(\left(1-\frac{\sqrt{K^*}}{F^*}\right)\sin\theta\cos\theta\right)\right.$$

$$\left.+\,v\left(\frac{\sqrt{K^*}}{F^*}\cos^2\theta+\sin^2\theta\right)\right]\sqrt{u^2+v^2}+g\,\beta\,(T-T_{ref})$$

Energy equation:

$$C_{P_f}\left(\frac{\partial(\sigma T)}{\partial t}+U\frac{\partial T}{\partial x}+V\frac{\partial T}{\partial y}\right)=\frac{1}{\rho_f}\left(k_x\frac{\partial^2 T}{\partial x^2}+k_y\frac{\partial^2 T}{\partial y^2}\right) \tag{3.4}$$

Heat function equation:

$$\frac{\partial^2 H}{\partial x^2}+\frac{\partial^2 H}{\partial y^2}=\frac{\partial(uT)}{\partial y}-\frac{\partial(vT)}{\partial x}+k^*\frac{\partial^2 T}{\partial x\,\partial y}-\frac{\partial^2 T}{\partial x\,\partial y} \tag{3.5}$$

Where, $u=\varepsilon u_f$; $v=\varepsilon v_f$

3.3 SOLUTION PROCEDURE

The integral form of the above governing Eqns. (3.6 - 3.10) are discretized using finite-volume method. Collocated grid formulation is used for the discretization of governing equations which denotes the definition of velocity, pressure, temperature and heat function values at the same set of grid points. The collocated grid arrangement is shown in Fig. 3.1.

Continuity equation

$$\iint_{CS}\vec{V}\bullet\overrightarrow{dA}=0 \tag{3.6}$$

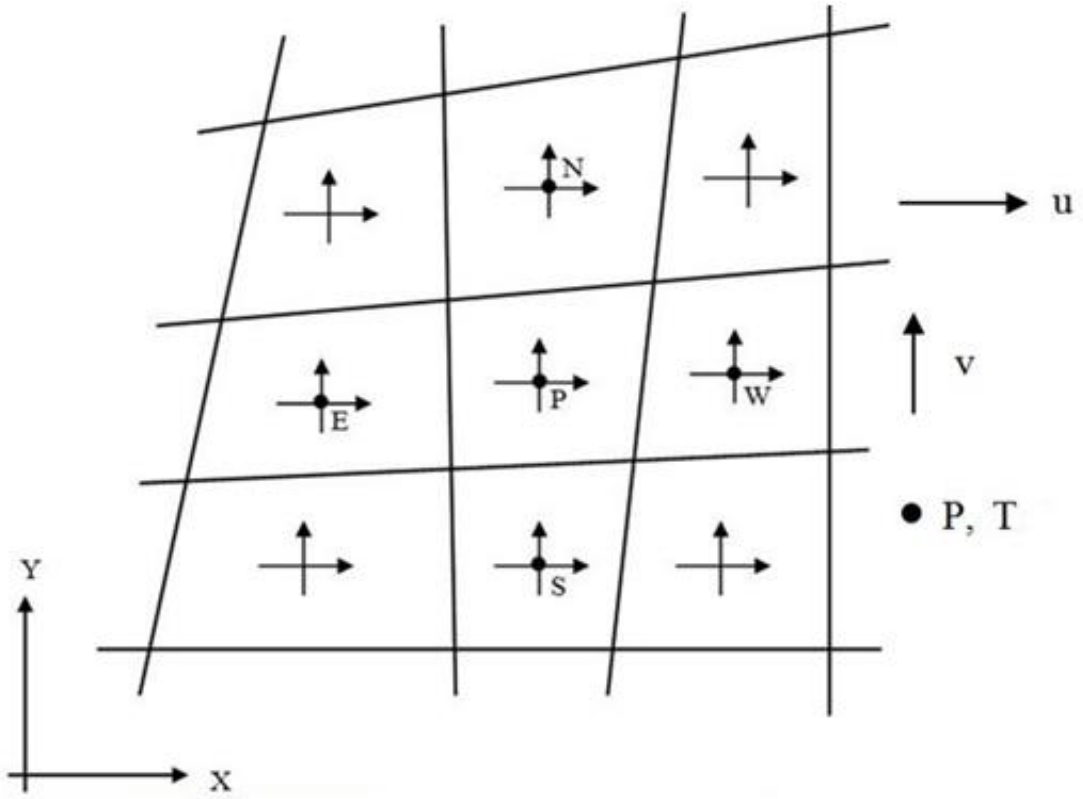

Fig. 3.1. Collocated grid arrangement

x- momentum equation

$$\frac{1}{\varepsilon}\iiint_{\check{C}\forall}\frac{\partial u}{\partial t}d\forall+\frac{1}{\varepsilon^2}\iint_{CS}u\vec{V}\bullet\overrightarrow{dA}=-\frac{1}{\rho_f}\iiint_{\check{C}\forall}\frac{\partial P_f}{\partial x}d\forall+\frac{\mu_f}{\rho_f\varepsilon}\iint_{CS}(\vec{\nabla}u)\bullet\overrightarrow{dA} \tag{3.7}$$

$$-\frac{\mu_f}{\rho_f K_1}\iiint_{\check{C}\forall}A\,d\forall\;-\frac{F_1}{\sqrt{K_1}}\iiint_{\check{C}\forall}B\,d\forall$$

$$A=u\,(\cos^2\theta+K^*\sin^2\theta)+v\big((1-K^*)\,\sin\theta\,\cos\theta\big)$$

$$B=\left[u\left(\cos^2\theta+\frac{\sqrt{K^*}}{F^*}\sin^2\theta\right)+v\left(\left(1-\frac{\sqrt{K^*}}{F^*}\right)\sin\theta\,\cos\theta\right)\right]\sqrt{u^2+v^2}$$

y- momentum equation

$$\frac{1}{\varepsilon}\iiint_{\check{C}\forall}\frac{\partial v}{\partial t}d\forall+\frac{1}{\varepsilon^2}\iint_{CS}v\vec{V}\bullet\overrightarrow{dA}=-\frac{1}{\rho_f}\iiint_{\check{C}\forall}\frac{\partial P_f}{\partial y}d\forall+\frac{\mu_f}{\rho_f\varepsilon}\iint_{CS}(\vec{\nabla}v)\bullet\overrightarrow{dA}$$

$$-\frac{\mu_f}{\rho_f K_1}\iiint_{\check{C}\forall}C\,d\forall-\frac{F_1}{\sqrt{K_1}}\iiint_{\check{C}\forall}D\,d\forall+\iiint_{\check{C}\forall}g\,\beta\,(T-T_{ref})d\forall \tag{3.8}$$

$$C=\left[u\left((1-K^*)\sin\theta\cos\theta\right)+v(K^*\cos^2\theta+\sin^2\theta)\right]$$

$$D=\left[u\left(\left(1-\frac{\sqrt{K^*}}{F^*}\right)\sin\theta\cos\theta\right)+v\left(\frac{\sqrt{K^*}}{F^*}\cos^2\theta+\sin^2\theta\right)\right]\sqrt{u^2+v^2}$$

Energy equation:

$$C_{P_f}\iiint_{\check{C}\forall}\frac{\partial(\sigma T)}{\partial t}d\forall+\iint_{CS}T\vec{V}\bullet\overrightarrow{dA}=\frac{1}{\rho_f}\iint_{CS}(\overrightarrow{\nabla kT})\bullet\overrightarrow{dA} \tag{3.9}$$

Heat function equation:

$$\iint_{CS}(\vec{\nabla}H)\bullet\overrightarrow{dA}=\iint_{CS}H\vec{V}\bullet\overrightarrow{dA} \tag{3.10}$$

Discretization of Eqns. (3.6 – 3.10) proceed as

$$\iint_{CS}\vec{V}\bullet\overrightarrow{dA}=(u_e-u_w)^{n+1}\Delta y+(v_n-v_s)^{n+1}\Delta x \tag{3.11}$$

$$\frac{1}{\varepsilon}\iiint_{\check{C}\forall}\frac{\partial u}{\partial t}d\forall=\frac{1}{\varepsilon}\left(\frac{u_P^{n+1}-u_P^n}{\Delta t}\right)\forall_{cell} \tag{3.12}$$

$$\frac{1}{\varepsilon^2}\iint_{CS}u\vec{V}\bullet\overrightarrow{dA}=\frac{1}{\varepsilon^2}\left[(u_e^a u_e-u_w^a u_w)^n\Delta y+(u_n^a v_n-u_s^a v_s)^n\Delta x\right] \tag{3.13}$$

$$\frac{1}{\rho_f}\iiint_{\check{C}\forall}\frac{\partial P_f}{\partial x}d\forall=\frac{1}{\rho_f}\left(\frac{P_e^{n+1}-P_w^n}{\Delta x}\right)\forall_{cell} \tag{3.14}$$

$$\frac{1}{\rho_f}\iiint_{\check{C}\forall}\frac{\partial P_f}{\partial y}d\forall=\frac{1}{\rho_f}\left(\frac{P_n^{n+1}-P_s^n}{\Delta y}\right)\forall_{cell} \tag{3.15}$$

$$\frac{\mu_f}{\rho_f\varepsilon}\iint_{CS}\left(\vec{\nabla}u\right)\bullet\overrightarrow{dA}=\frac{\mu_f}{\rho_f\varepsilon}\left[\frac{u_E^n-2u_P^n+u_W^n}{\Delta x}\Delta y+\frac{u_N^n-2u_P^n+u_S^n}{\Delta y}\Delta x\right] \tag{3.16}$$

$$\iiint_{\check{C}\forall} g\,\beta\,(T-T_{ref})d\forall=g\,\beta\,(T-T_{ref})\forall_{cell} \tag{3.17}$$

$$\frac{\mu_f}{\rho_f K_1}\iiint_{\check{C}\forall} A\,d\forall=\frac{\mu_f}{\rho_f K_1}(A)\forall_{cell} \tag{3.18}$$

$$\frac{F_1}{\sqrt{K_1}}\iiint_{\check{C}\forall} B\,d\forall=\frac{F_1}{\sqrt{K_1}}(B)\forall_{cell} \tag{3.19}$$

$$C_{P_f}\iiint_{\check{C}\forall}\frac{\partial(\sigma T)}{\partial t}d\forall=C_{P_f}\sigma\left(\frac{T_P^{n+1}-T_P^n}{\Delta t}\right)\forall_{cell} \tag{3.20}$$

$$\iint_{CS}T\vec{V}\bullet\overrightarrow{dA}=(T_e^a u_e-T_w^a u_w)^n\Delta y+(T_n^a v_n-T_s^a v_s)^n\Delta x \tag{3.21}$$

$$\frac{1}{\rho_f}\iint_{CS}\left(\overrightarrow{\nabla k}T\right)\bullet\overrightarrow{dA}=\frac{1}{\rho_f}\left[k_x\frac{T_E^n-2T_P^n+T_W^n}{\Delta x}\Delta y+k_y\frac{T_N^n-2T_P^n+T_S^n}{\Delta y}\Delta x\right] \tag{3.22}$$

$$\iint_{CS}\left(\vec{\nabla}H\right)\bullet\overrightarrow{dA}=\frac{H_E^n-2H_P^n+H_W^n}{\Delta x}\Delta y+\frac{H_N^n-2H_P^n+H_S^n}{\Delta y}\Delta x \tag{3.23}$$

Here, $\forall_{cell}$ represents cell volume dx • dy, (n + 1) and n indicates to the next and current time level of u_e, u_w etc., which indicates the face-centered values of the advecting velocities. u_e^a, u_w^a etc. refers the face-centered values of the advected velocities. This difference comes up due to the fact that momentum components themselves can be transported by the velocity field. The advecting velocity components are determined using a central-difference scheme for a uniform mesh,

$$\mathrm{u_e^n} = \frac{\mathrm{u_E^n} - \mathrm{u_P^n}}{2}$$

Advected momentum velocity terms can be represented by u_e^a, u_w^a etc. and these terms can be solved by using the first order upwind scheme (FOU) or second order upwind scheme (SOU) or QUICK for appropriate upstream biasing.

After discretization, the momentum equations can be written as

$$\mathrm{u_P^{n+1}} = \mathrm{u_P^n} + \mathrm{ADVX^n} + \mathrm{PRX^{n+1}} + \mathrm{DIFFX^n} - \mathrm{STX^n} \tag{3.24}$$

$$\mathrm{v_P^{n+1}} = \mathrm{v_P^n} + \mathrm{ADVY^n} + \mathrm{PRY^{n+1}} + \mathrm{DIFFY^n} - \mathrm{STY^n} + \mathrm{GR^n} \tag{3.25}$$

Here, ADV represents advection term, PR indicates pressure term, DIFF denotes diffusion term, ST refers source term and GR denotes gravity term.

Cell centered velocities can be calculated by dropping pressure terms in Eqns. (3.24-3.25)

$$\widetilde{\mathrm{u_P}} = \mathrm{u_P^n} + \mathrm{ADVX^n} + \mathrm{DIFFX^n} - \mathrm{STX^n} \tag{3.26}$$

$$\widetilde{\mathrm{v_P}} = \mathrm{v_P^n} + \mathrm{ADVY^n} + \mathrm{DIFFY^n} - \mathrm{STY^n} + \mathrm{GR^n} \tag{3.27}$$

Once the velocities are calculated by using Eqns. (3.26 - 3.27), velocities in $(n+1)^t$ level are updated pressure terms at n^t level.

$$u_P^* = \widetilde{u_P} - \frac{\Delta t}{\rho_f}\left(\frac{P_E^n - P_W^n}{\Delta x}\right) \tag{3.28}$$

$$v_P^* = \widetilde{v_P} - \frac{\Delta t}{\rho_f}\left(\frac{P_N^n - P_S^n}{\Delta x}\right) \tag{3.29}$$

3.4. Overall Steps in the Solution Algorithm

1. Assume guess pressure field $\tilde{P}$, at the start of each time step.
2. Solve guess velocities $\tilde{u}$ and $\tilde{v}$, using the guess pressure $\tilde{P}$ in the momentum equations.
3. From guess velocity field $\tilde{v}$, find the continuity residue $\nabla \cdot \tilde{v}$ at every pressure node.
4. Solve the Poisson pressure correction equations $\nabla^2 P' = \frac{\rho_f}{\Delta t}\left(\nabla \cdot \tilde{v}\right)$.
5. Update $P^{n+1} = \tilde{P} + P'$

   $u^{n+1} = \tilde{u} + u'$

   $v^{n+1} = \tilde{v} + v'$

   Where $u' = -\frac{\Delta t}{\rho_f}\frac{\partial P'}{\partial x}$, $v' = -\frac{\Delta t}{\rho_f}\frac{\partial P'}{\partial y}$
6. After updating of u and v the correct pressure P is treated as $\tilde{P}$ and the same steps are continued until a converged solution is obtained.

Gauss-Seidel point by point iteration method is used for the solution of all governing equations. The iteration process is continued till the convergence criterion is satisfied. The convergence is defined by the following equation

$$\frac{\sum_{i,j}\left|\zeta_{i,j}^{\,n} - \zeta_{i,j}^{\,n-1}\right|}{\sum_{i,j}\left|\zeta_{i,j}^{\,n}\right|} < 10^{-8} \tag{3.30}$$

where ζ in Eqn. (3.30) stands for u,v, T and H variables

The validation of present numerical procedure is carried out by comparing extensively with wide range of numerical data. The validation for numerical procedure and formulation may be observed in respective chapters (4-7).

3.5 CLOSURE

The details provided in the present chapter pertaining to governing equations and numerical methodology can be treated as generalized formulation. In the subsequent chapters based on the problem description the governing equations are boiled down into the required form and the parametric investigation has been performed.

CHAPTER 4

VISUALIZATION OF THERMAL TRANSPORT IN 2-D SOLID GEOMETRIES

4.1 INTRODUCTION

Applications such as heat exchangers, nuclear fuel assemblies, electronic components, biomedical engineering, etc. involve intricate geometries for which the thermal transport analysis is very complex. For the efficient design of these equipment a thorough analysis of heat transport characteristics is needed. Compared to the experimental method, numerical simulation can provide an insight of thermal hydraulics in various shapes. Kimura and Bejan (1983) introduced the concept of heat function and heatlines to visualize the thermal transport.

In the earlier chapter (chapter 3) the details pertaining to governing equations in generalized form and numerical formulation for thermal hydraulics in anisotropic porous media is given. In the present chapter the thermal transport for various solid domains is analyzed in terms of isotherms and heatlines. Initially, the numerical formulation pertaining to thermal transport based on diffusion in various shapes is discussed followed by heatline visualization in these domains. Subsequently, the study is extended for various domains with discrete heat sources. Further, hydrodynamics for shear driven flows in anisotropic porous cavity flows is discussed. Additionally, thermal hydraulics for anisotropic porous media is analyzed in terms of stream lines, isotherms and heatlines.

Thompson et al. (1982) made use of non-orthogonal curvilinear grid and developed new computational techniques to analyze fluid flow and heat transfer characteristics. The various domains is mapped to a simple computational domain and the governing equations are written in terms of generalized curvilinear coordinates. Because of its simplicity in programming, the non – staggered (collocated) grid has gained popularity and Perić et al. (1988) reported that the collocated grid gave more accurate results than the staggered arrangement.

It may be noted that, numerical methodologies were developed to analyse the flow and heat transport in various shapes. Generation of grid for various shapes is a tedious task. In order

to overcome the difficulty in grid generation, in the present work a generalized code is developed to read the mesh that is generated using a meshing software GAMBIT. A collocated grid based finite volume solver is developed for the analysis of thermal transport in various domains. It may be noted that based on previous studies visualization of heatlines can play a prominent role for the better insight of thermal transport. Therefore, the present study numerical results are presented in terms of temperature distribution and heatlines in 2D domains with the discretely heated bottom wall.

4.2 THERMAL TRANSPORT IN TWO DIMENSIONAL DOMAINS

4.2.1 Physical Domain and Mathematical Formulation

Two dimensional computational solid domains with boundary conditions are shown in Fig. 4.1. The generalized governing equations Eqns. (3.1 - 3.5) based on the present condition reduce to the diffusion equation.

The governing equation for heat transport in various domains in the integral form can be given as

$$\int_{\Delta V} \frac{\partial}{\partial x}\left(k\frac{\partial T}{\partial x}\right) dxdy + \int_{\Delta V} \frac{\partial}{\partial y}\left(k\frac{\partial T}{\partial y}\right) dxdy = 0 \tag{4.1}$$

Diffusive flux through the east face can be expressed as

$$\begin{aligned} J_{De} &= \sum \left(k\frac{\partial T}{\partial x}\right)_e A_{ex} + \sum \left(k\frac{\partial T}{\partial y}\right)_e A_{ey} \\ J_{De} &= \left(\frac{k_e A_{ex}^1}{V_e}\right)\left[\{A_{ex}^1(T_E - T_P) + A_{ex}^2(T_{ne} - T_{se})\}\right] \\ &\quad + \left(\frac{k_e A_{ey}^1}{V_e}\right)\left[\{A_{ey}^1(T_E - T_P) + A_{ey}^2(T_{ne} - T_{se})\}\right] \end{aligned} \tag{4.2}$$

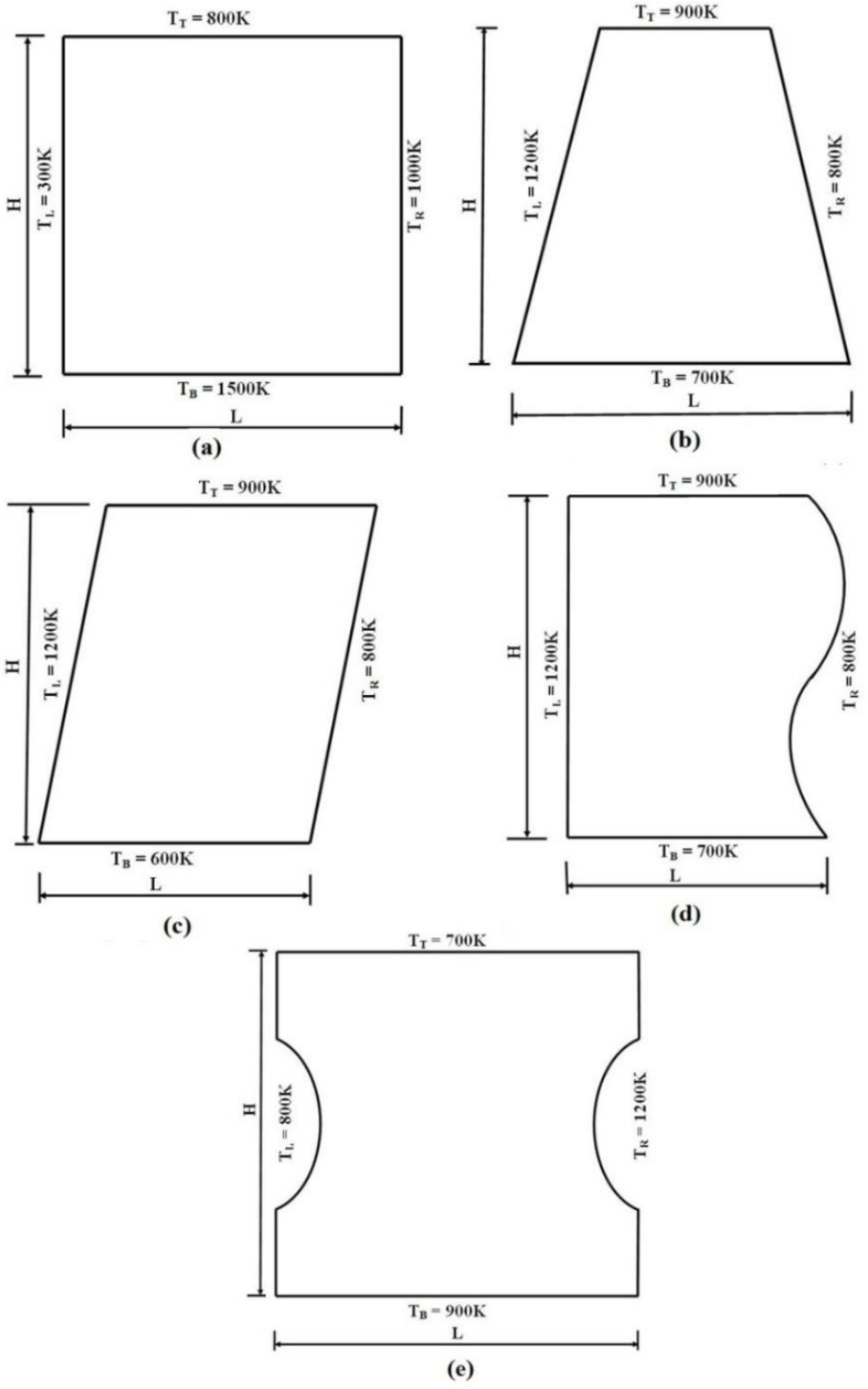

Fig. 4.1. Computational solid domains with the boundary conditions

Diffusive flux through the east face expressed as a function of the projected areas and the values of temperature (T) at neighbouring nodes are shown in Fig 4.2.

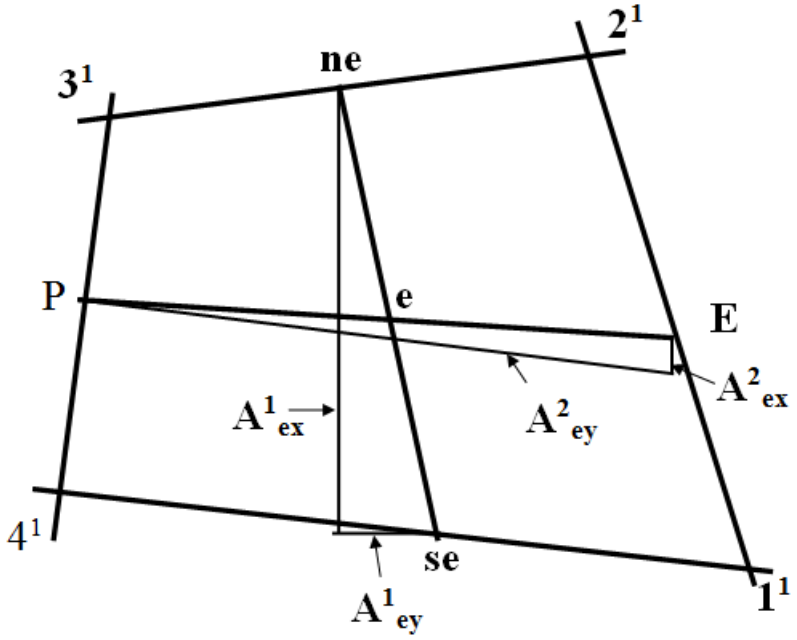

Fig. 4.2. Area Vector for face 'e'

A^1_{ex} and A^2_{ex} represents the orthogonal and non-orthogonal area in x direction for the east face of the control volume.

The areas and volume associated with face 'e' are given by

A^1_{ex} = projection of area A^1_e along X-axis $= (Y_{ne} - Y_{se})$

A^1_{ey} = projection of area A^1_e along Y-axis $= -(X_{ne} - X_{se})$

A^2_{ex} = projection of area A^2_e along X-axis $= -(Y_E - Y_P)$

A^2_{ey} = projection of area A^2_e along Y-axis $= (X_E - X_P)$

V_e = volume of the control volume associated with e

$= (X_E - X_P)(Y_{ne} - Y_{se}) - (X_{ne} - X_{se})(Y_E - Y_P)$

Simplification of above Eqn. (4.2),

$$J_{De} = d_1^e(T_E - T_P) + d_2^e(T_{ne} - T_{se}) \quad (4.3)$$

Where

$$d_e^1 = \frac{k_e}{V_e}\left[(A_{ex}^1 A_{ex}^1) + (A_{ey}^1 A_{ey}^1)\right]; \qquad d_e^2 = \frac{k_e}{V_e}\left[(A_{ex}^1 A_{ex}^2) + (A_{ey}^1 A_{ey}^2)\right]$$

Similarly, J_{Dw}, J_{Dn} and J_{Ds} can be obtained.

The net diffusive flux contribution for all sides of the cell can be brought into the form

$$J_D = -\left[\left\{\left(k\frac{\partial T}{\partial x}\right)_e A_{ex} + \left(k\frac{\partial T}{\partial y}\right)_e A_{ey}\right\} - \left\{\left(k\frac{\partial T}{\partial x}\right)_w A_{wx} + \left(k\frac{\partial T}{\partial y}\right)_w A_{wy}\right\} + \left\{\left(k\frac{\partial T}{\partial x}\right)_n A_{nx} + \left(k\frac{\partial T}{\partial y}\right)_n A_{ny}\right\} - \left\{\left(k\frac{\partial T}{\partial x}\right)_s A_{sx} + \left(k\frac{\partial T}{\partial y}\right)_s A_{sy}\right\}\right] \quad (4.4)$$

$$J_D = -\{d_e^1 T_E + d_w^1 T_W + d_n^1 T_N + d_s^1 T_S - (d_e^1 + d_w^1 + d_n^1 + d_s^1) T_P + [b_{no}]\} \quad (4.5)$$

Where

$$b_{no} = (d_e^2 + d_w^2) T_{ne} - (d_n^2 + d_w^2) T_{nw} - (d_e^2 + d_s^2) T_{se} - (d_w^2 + d_s^2) T_{sw}$$

The term b_{no} arises as a result of non-orthogonality of the mesh which vanishes when the grid becomes orthogonal. The corner values are approximated in terms of four surrounding nodal values as shown in Fig. 4.3.

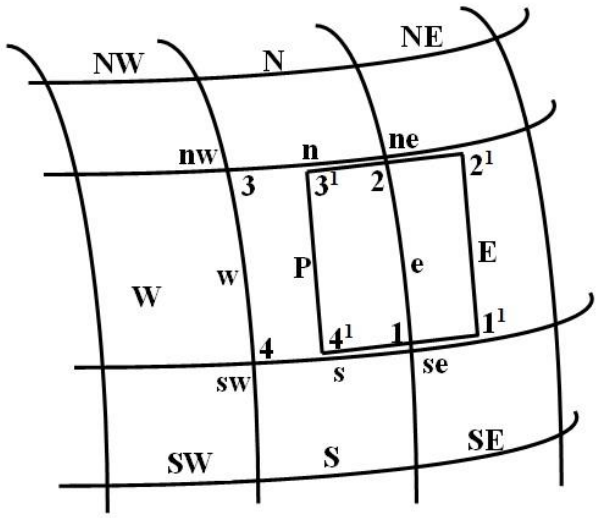

Fig. 4.3. Typical control volume

$$T_{ne} = \frac{1}{4}(T_N + T_E + T_P + T_{NE}) \quad (4.6)$$

Similarly, T_{nw}, T_{se} and T_{sw} can be obtained.

4.2.2. Method of Solution

The grid is generated in GAMBIT and is exported as neutral file. GAMBIT neutral files contain the information of mesh data, boundary conditions or solution data in ASCII file format. To read the mesh data from the GAMBIT neutral file, a code has been developed. This code acts as the bridge between the present in-house finite volume numerical code and meshing software. This reduces the burden of grid generation for various shapes.

The steps followed in the present numerical methodology is given as follows

- Modeling, meshing, selection of boundary conditions and fluid/solid domain using GAMBIT
- Exporting of mesh data in the neutral file format
- Reading of mesh data in ASCII format
- Allocation of suitable boundary conditions for boundary nodes
- Solving the integral form of governing equation (Eqn. (4.1)) using collocated grid based finite volume approach.
- Solving of the algebraic equations using the Gauss-Seidel iterative method
- Check for the convergence criteria
- Plotting of the obtained results using post processing software (TEC PLOT)

4.2.3. Grid Generation and Reading

As the objective of the present study is to check the robustness and validity of the adopted numerical methodology, non-uniform grids with different aspect ratios are taken. Grid independent studies have been performed and made sure the results are independent of computational grid. The grid has been generated for the considered various domains and is shown in Fig. 4.4. Fig. 4.4 (a) provides a non-uniform grid for a square domain whereas Figs. 4.4 (b) – (e) provides the employed grid for non – orthogonal geometries. It may be noted that in this approach instead of writing code for mesh generation, a code has been developed to link the data

from GAMBIT to the developed Finite Volume code. The limitation of the considered approach is that the mesh should be of quadrilateral type only.

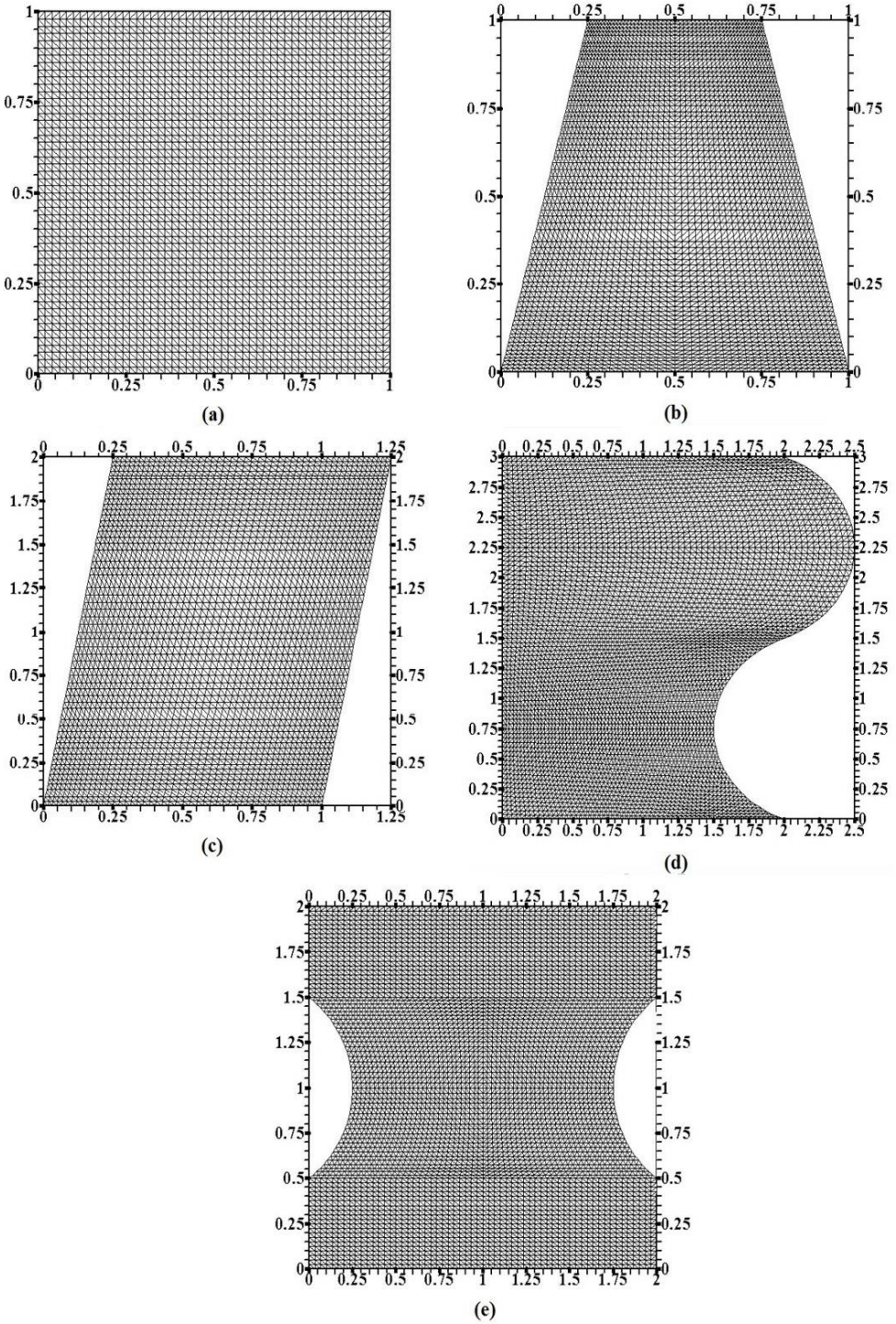

Fig. 4.4. Grid employed for various domains with non uniform grid (a) 60×80, (b) 50×70, (c) 50×60, (d) 60×80 and (e) 60×80.

4.2.4. Results and Discussion

The results thus obtained by solving the heat transport-diffusion equation with Dirichlet condition are shown in Fig. 4.5. To check the validity of the present numerical methodology, the considered various geometries are also solved using commercial CFD code ANSYS Fluent. Fig. 4.5 provides the isotherms which give a qualitative comparison of results. The left side of Fig. 4.5 gives the isotherms obtained from the present study and right side from ANSYS Fluent. In order to further check the validity of the present code(s), the quantitative comparison of the results has been carried out with ANSYS Fluent by plotting mid plane temperature profile and is shown in Fig.4.6. Fig. 4.5 (a) shows the temperature contours for a square domain. Due to the maximum temperature at the bottom wall and minimum temperature at the left wall the temperature gradients are observed to be more near the bottom and left walls when compared to the rest of the domain. Fig. 4.5 (b) shows the temperature contours for a trapezoidal cross section. The thermal transport in the skewed domain is simulated and is provided in Fig. 4.5(c). Further to

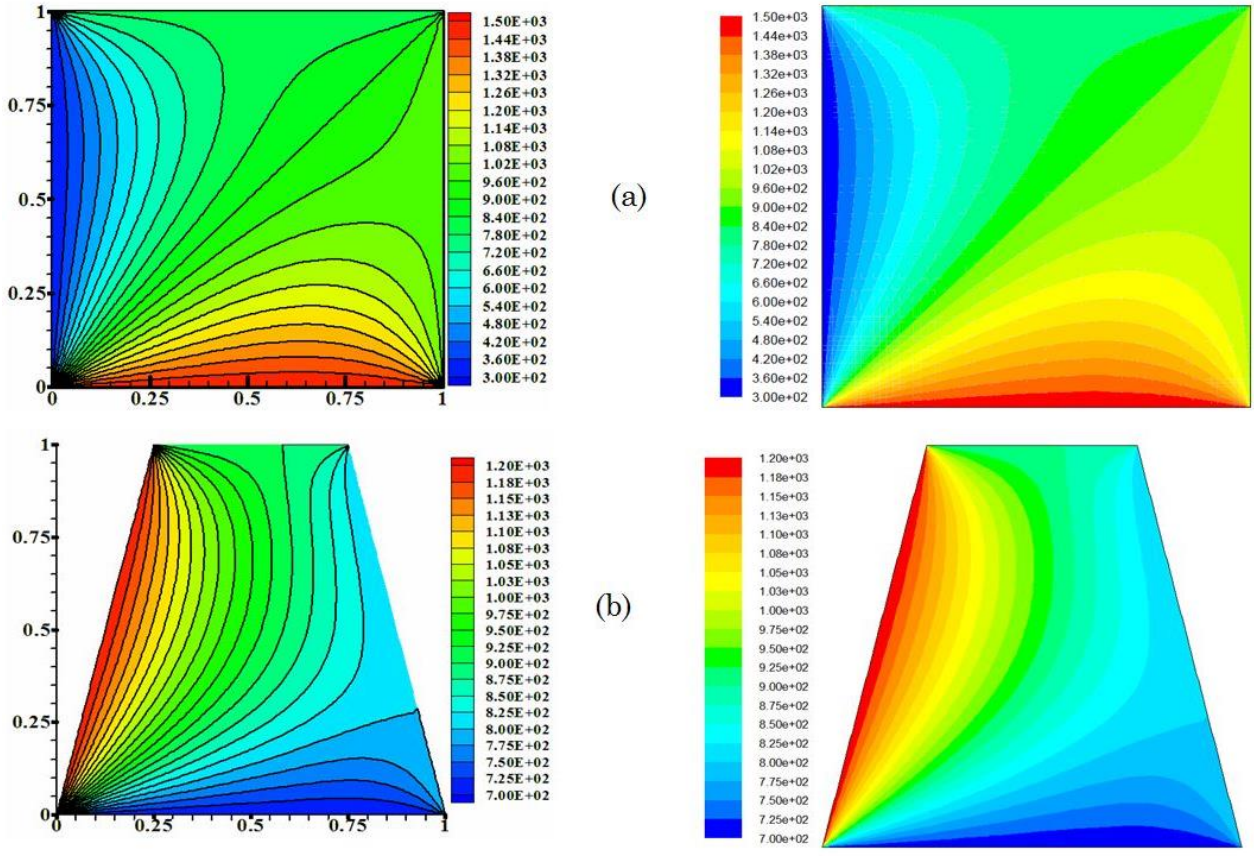

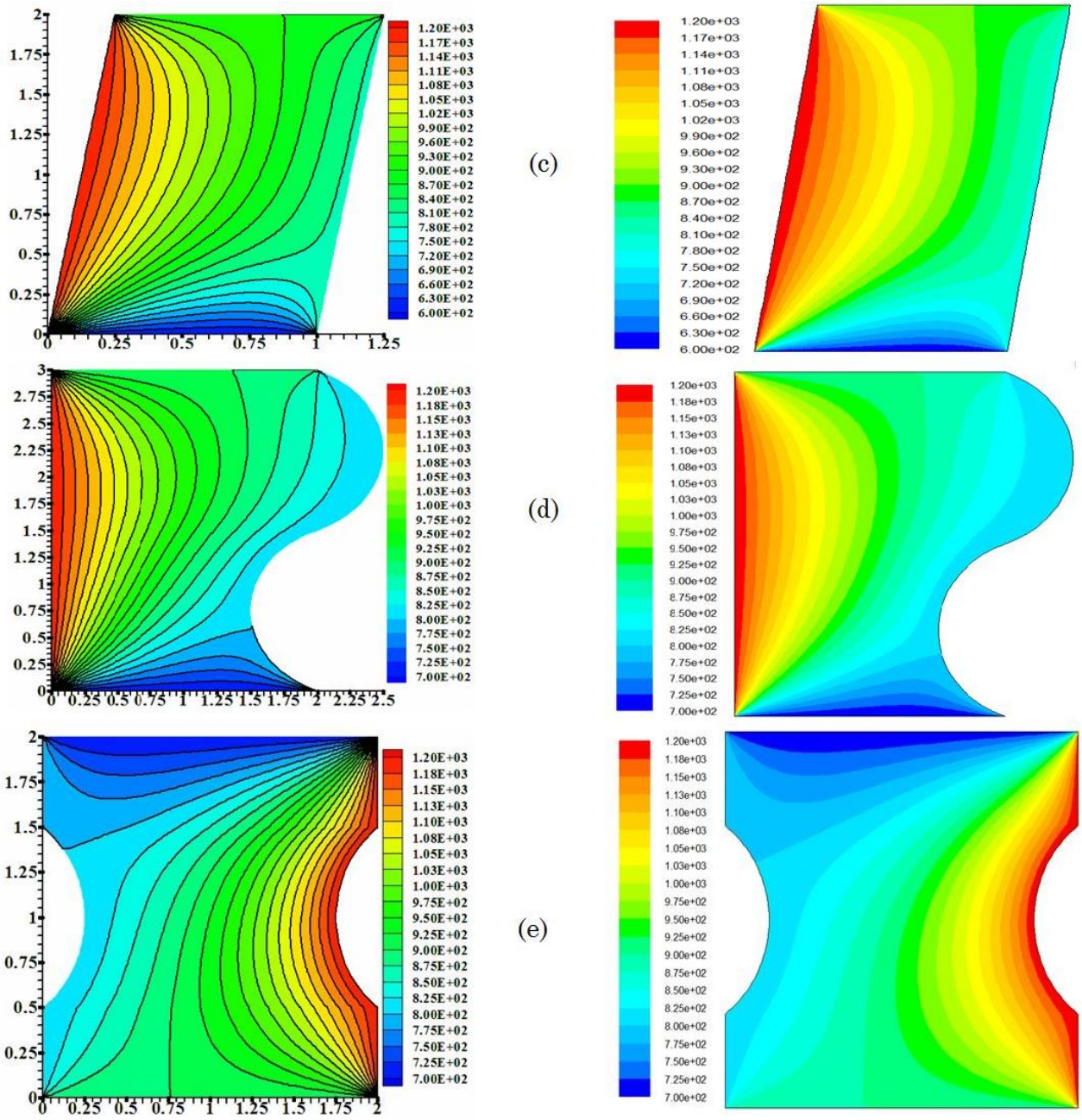

Fig 4.5. Comparison of isotherms with commercial CFD code (ANSYS Fluent)

analyze the thermal transport in domains with curvature, isotherms have been plotted for these geometries and provided in Figs. 4.5 (d) - (e). From Figs. 4.5 and 4.6 it may be noted that the results obtained from the present numerical methodology exactly matched with the results obtained from a commercial CFD package ANSYS Fluent.

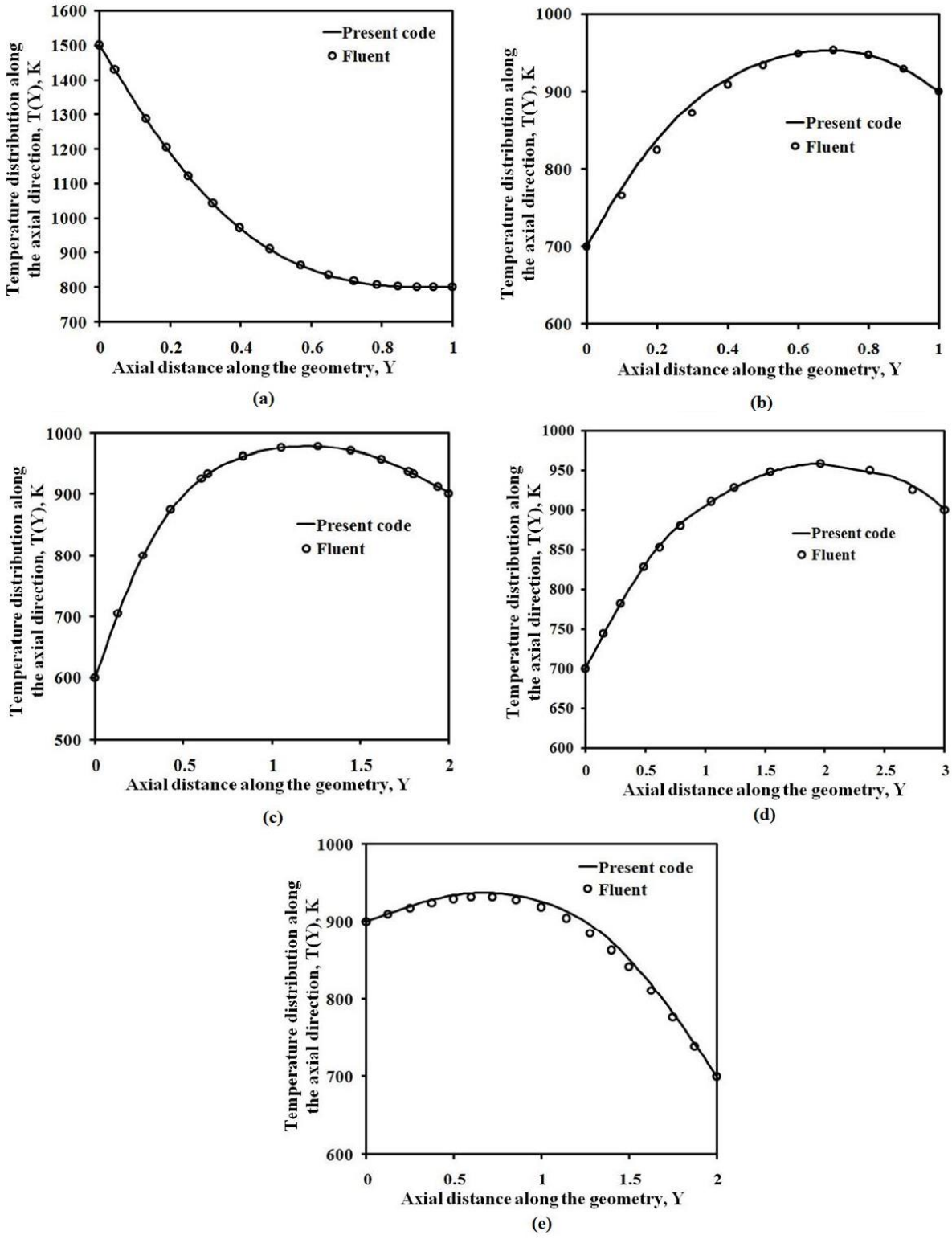

Fig. 4.6. Comparison of mid plane temperature profile with commercial CFD code (ANSYS Fluent)

4.3. VISUALIZATION OF ENERGY TRANSPORT IN 2-D SOLID GEOMETRIES

4.3.1. Physical Domain and Mathematical Formulation

Various computational solid domains with their boundary conditions are shown in Fig. 4.7(a)–(e). The considered computational solid domains are of height H and width L. The side walls are maintained at constant temperature 200K (T_c) and the bottom is maintained at constant temperature 300K (T_h). The top boundary of the geometries is thermally insulated.

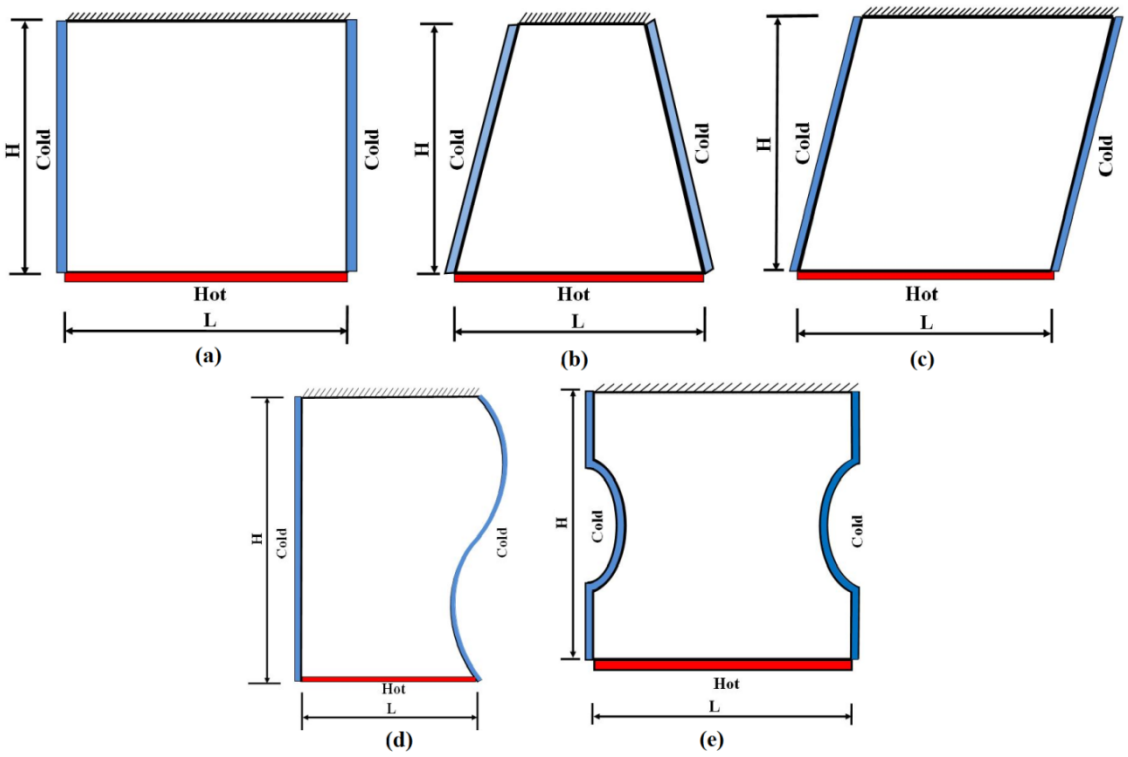

Fig. 4.7. Schematic diagram of the computational solid domains with the boundary condition

The diffusion and heatline equations to analyze the energy transport for the above 2D domains Figs. 4.7 (a)-(e) can be given as follows.

Diffusion equation:

$$\int_{\Delta V} \frac{\partial}{\partial x}\left(k\frac{\partial T}{\partial x}\right) dxdy + \int_{\Delta V} \frac{\partial}{\partial y}\left(k\frac{\partial T}{\partial y}\right) dxdy = 0 \qquad (4.7)$$

Heat function equation:

$$\int_{\Delta V}\frac{\partial}{\partial x}\left(\frac{\partial H}{\partial x}\right)dxdy+\int_{\Delta V}\frac{\partial}{\partial y}\left(\frac{\partial H}{\partial y}\right)dxdy=0 \tag{4.8}$$

The following details given in Eqns. (4.9 – 4.14) can be taken to attain Eqn. (4.8).

The steady energy conservation equation without source term (Costa (2006)) can be given as

$$\frac{\partial}{\partial x}\left[\rho_f u c_p(T-T_0)-\left(k\frac{\partial T}{\partial x}\right)\right]+\frac{\partial}{\partial y}\left[\rho_f v c_p(T-T_0)-\left(k\frac{\partial T}{\partial y}\right)\right]=0 \tag{4.9}$$

The net flow of energy in x-direction:

$$\frac{\partial H}{\partial y}=\rho_f C_P u(T-T_0)-k\frac{\partial T}{\partial x} \tag{4.10}$$

The net flow of energy in y-direction:

$$-\frac{\partial H}{\partial x}=\rho_f C_P v(T-T_0)-k\frac{\partial T}{\partial y} \tag{4.11}$$

As there is no flow (u = v =0) the Eqns. (4.10 and 4.11) reduce to Eqns. (4.12 and 4.13). Therefore, the heat lines become identical to the heat flux lines which is used to visualize the study of heat conduction phenomena.

The net flow of energy in x-direction:

$$\frac{\partial H}{\partial x}=-k\frac{\partial T}{\partial y} \tag{4.12}$$

The net flow of energy in y-direction:

$$-\frac{\partial H}{\partial y}=-k\frac{\partial T}{\partial x} \tag{4.13}$$

Differentiating Eqn. (4.12) with respective to x and Eqn. (4.13) with y and by adding the equations, Eqn. (4.14) can be obtained

$$\frac{\partial^2 H}{\partial x^2}+\frac{\partial^2 H}{\partial y^2}=0 \tag{4.14}$$

The Eqns. (4.7- 4.8) can be converted to non- dimensional form by using the following non-dimensional parameters.

$\theta = \frac{T-T_c}{T_h-T_c}$; $\Pi = \frac{H}{(T_h-T_c)k}$; $x^* = \frac{x}{L}$; $y^* = \frac{y}{H}$;

The non- Dimensional form of governing equations thus obtained for diffusion and heat function can be given as

$$\frac{\partial^2\theta}{\partial x^{*2}} + \frac{\partial^2\theta}{\partial y^{*2}} = 0 \tag{4.15}$$

$$\frac{\partial^2\Pi}{\partial x^{*2}} + \frac{\partial^2\Pi}{\partial y^{*2}} = 0 \tag{4.16}$$

For sake of convenience '*' is not given in the following integral form of equations.

$$\int_{\Delta V}\frac{\partial}{\partial x}\left(\frac{\partial\theta}{\partial x}\right)dxdy + \int_{\Delta V}\frac{\partial}{\partial y}\left(\frac{\partial\theta}{\partial y}\right)dxdy = 0 \tag{4.17}$$

$$\int_{\Delta V}\frac{\partial}{\partial x}\left(\frac{\partial\Pi}{\partial x}\right)dxdy + \int_{\Delta V}\frac{\partial}{\partial y}\left(\frac{\partial\Pi}{\partial y}\right)dxdy = 0 \tag{4.18}$$

The boundary conditions for Eqn. (4.17) can be referred from Fig. 4.7 and for Eqn. (4.18) (i.e. for heat function) can be given as

A reference value of $\Pi(0, H) = 0$ is assumed as the top left corner

Adiabatic top wall: $y = H; 0 < x \leq L;$

$$\Pi(x, H) = \Pi(0, H) - \int_0^L -\frac{\partial\theta}{\partial y}\Big|_{y=H} dx = 0 \tag{4.19}$$

Cold left wall: $x = 0; H > y \geq 0;$

$$\Pi(0, y) = \Pi(x, H) - \int_0^H -\frac{\partial\theta}{\partial x}\Big|_{x=0} dy \tag{4.20}$$

Cold right wall: $x = L; H > y \geq 0;$

$$\Pi(L, y) = \Pi(x, H) - \int_0^H -\frac{\partial\theta}{\partial x}\Big|_{x=L} dy \tag{4.21}$$

Bottom hot wall: $y = 0; 0 < x \leq L$

$$\Pi(x, 0) = \Pi(0, y) + \int_0^L -\frac{\partial\theta}{\partial y}\Big|_{y=0} dx \tag{4.22}$$

Where x and y are the distances measured along with the horizontal and vertical directions, respectively; θ: dimensionless temperature; Π: dimensionless heat function.

4.3.2. Validation of Code and Computation

To check the robustness of the present numerical methodology, the comparison of the results has been carried out with ANSYS Fluent by plotting isotherms and mid plane temperature profile and is shown in Fig.4.8. (a) - (b). Also, the heatline from the present study are compared with the benchmark solution of Basak and Roy (2008) and is shown in Fig. 4.9.

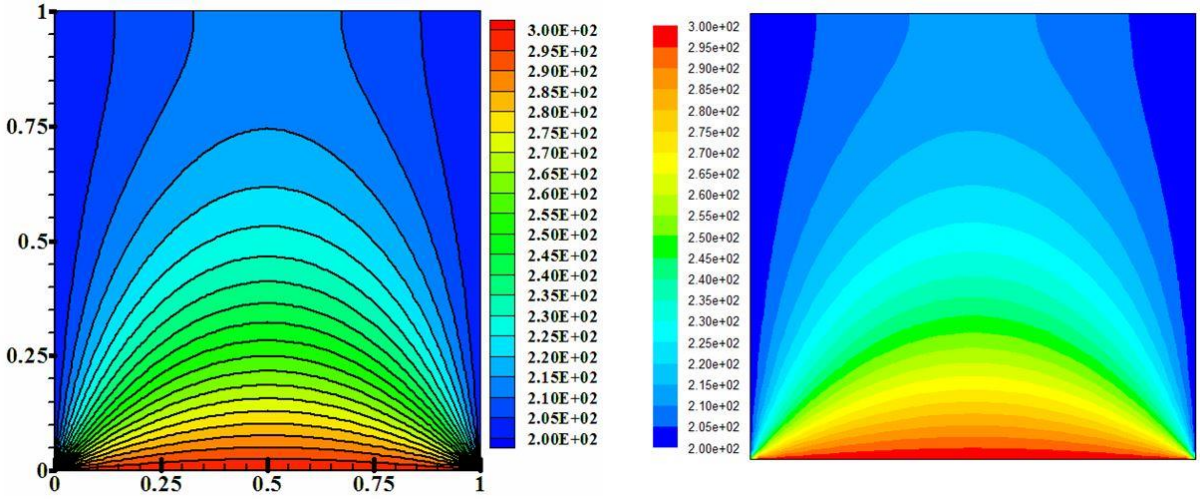

(a)

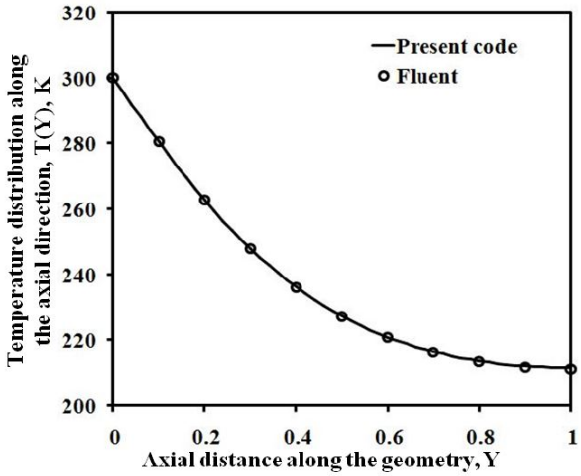

(c)

Fig. 4.8. Comparison of isotherms for (a) present study (left), ANSYS fluent (right) and (b) mid plane temperature profile with commercial CFD code

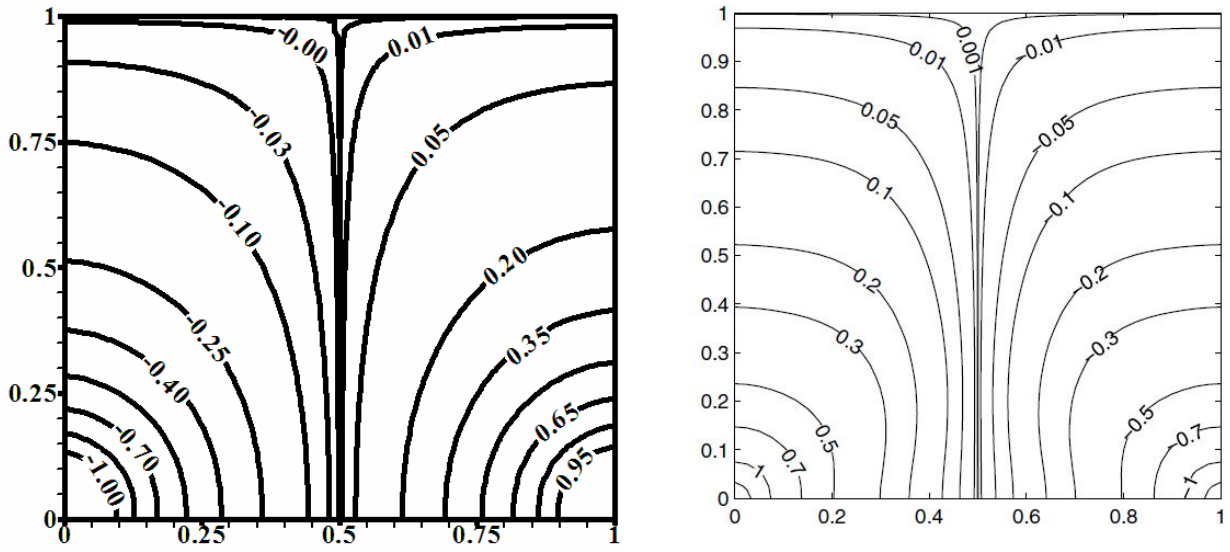

Present Study Basak and Roy (2008)

Fig. 4.9. Comparison of heatlines for the present study and Basak and Roy (2008) in conduction dominant region for Ra=10^3

4.3.3. Results and Discussion

In present work instead of writing code for mesh generation, the grid has been generated by using meshing software GAMBIT. The constraint of the developed code is limited to a quadrilateral grid. Grid independent studies have been performed and made sure the results are independent of computational grid. Grid employed for considered various domains is shown in Fig. 4.4 (a-e). The isotherms and heatlines thus obtained by solving the energy transport equation for the various shapes are shown in Fig. 4.10. The left side of Fig. 4.10 shows the isotherms and the right side shows the heatlines. Based on the isotherm shown in Fig. 4.10 it may be noted that at the bottom surface where hot and cold wall intersect computational singularities are observed. The heatlines showed in Fig. 4.10 (right) clearly indicate the heat flow from the bottom wall to the vertical cold wall. Also, it may be noted that there is no flow of heat from the bottom hot wall to top adiabatic wall. It is to be noted that the dense heatlines indicate higher heat-transfer rates whereas, the courser heatlines indicate lower heat transfer rate.

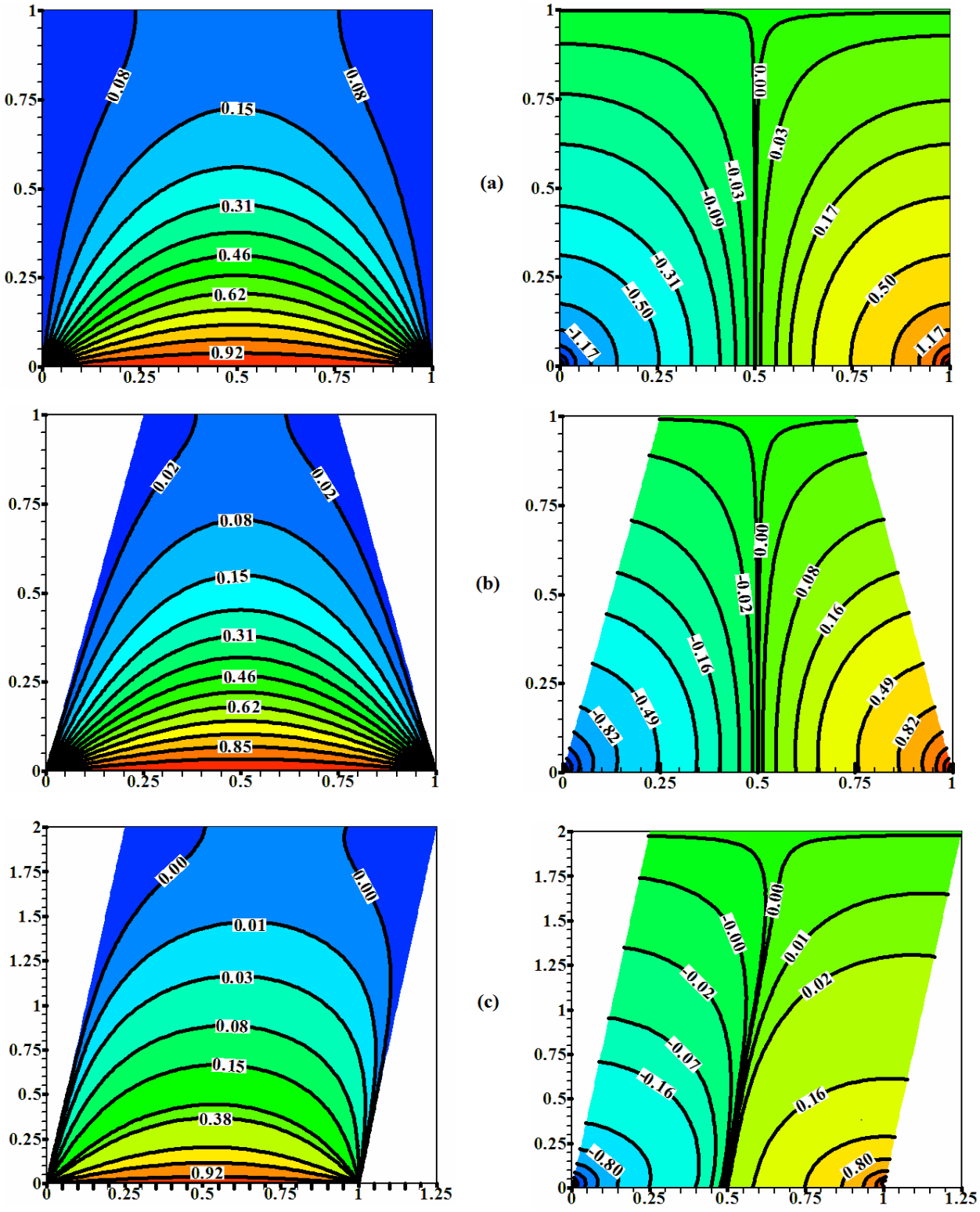
(a)
(b)
(c)

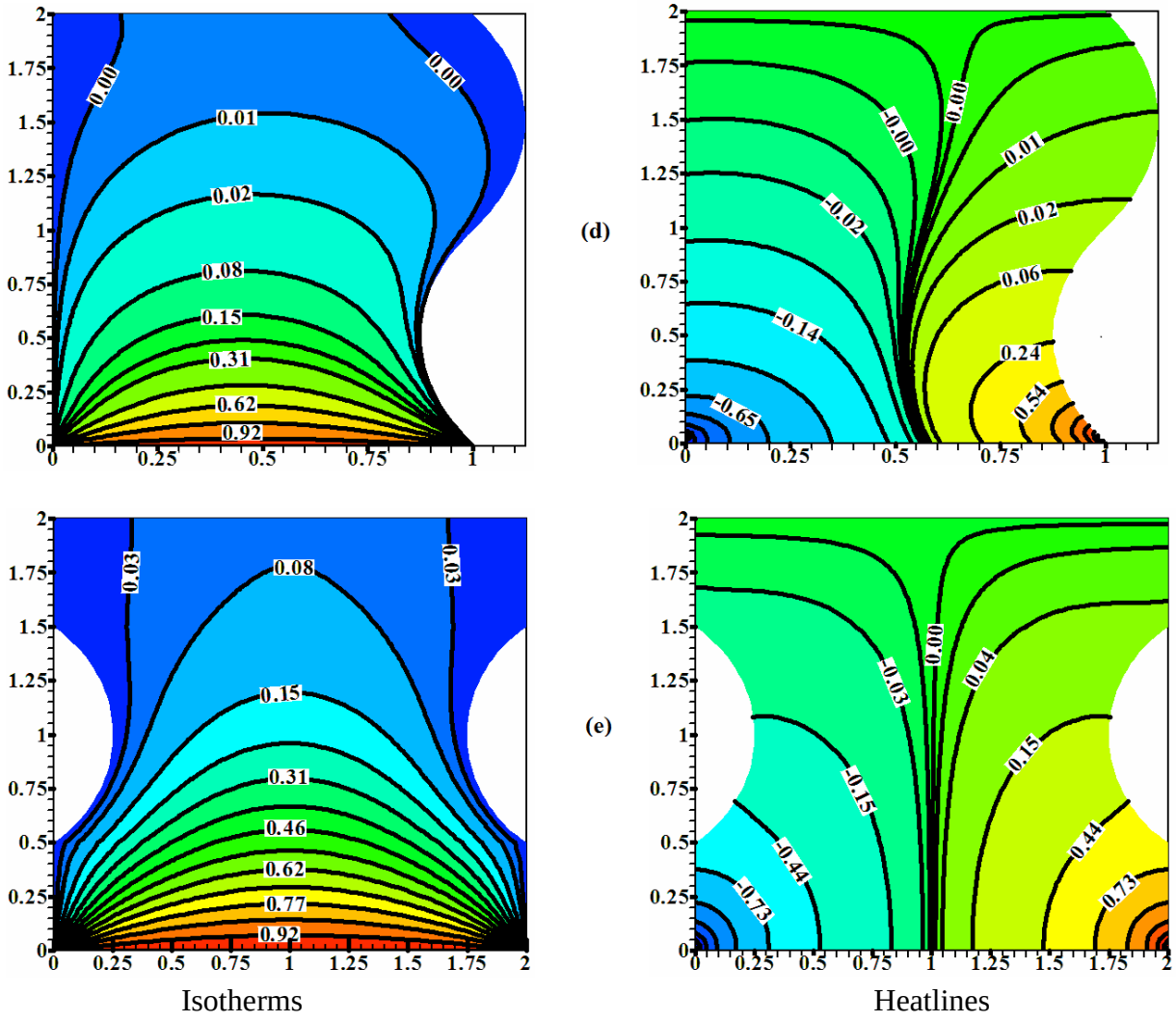

Fig. 4.10. Isotherms (left) and heatlines (right) for different domains

4.4. VISUALIZATION OF ENERGY TRANSPORT IN VARIOUS SHAPES WITH DIFFERENTIALLY HEATED WALLS

4.4.1. Problem Definition and Mathematical Formulation

The computational solid domains with boundary conditions considered in the present study are shown in Fig. 4.11. It consists of two-dimensional computational solid domains of dimensions L×H. The left side wall is maintained at constant temperature 300K (T_c) and serves as a heat sink, and the bottom centre wall (L/2) is maintained at constant temperature 400K (T_h) and serve as a heat source. Other boundaries of the geometries are thermally insulated.

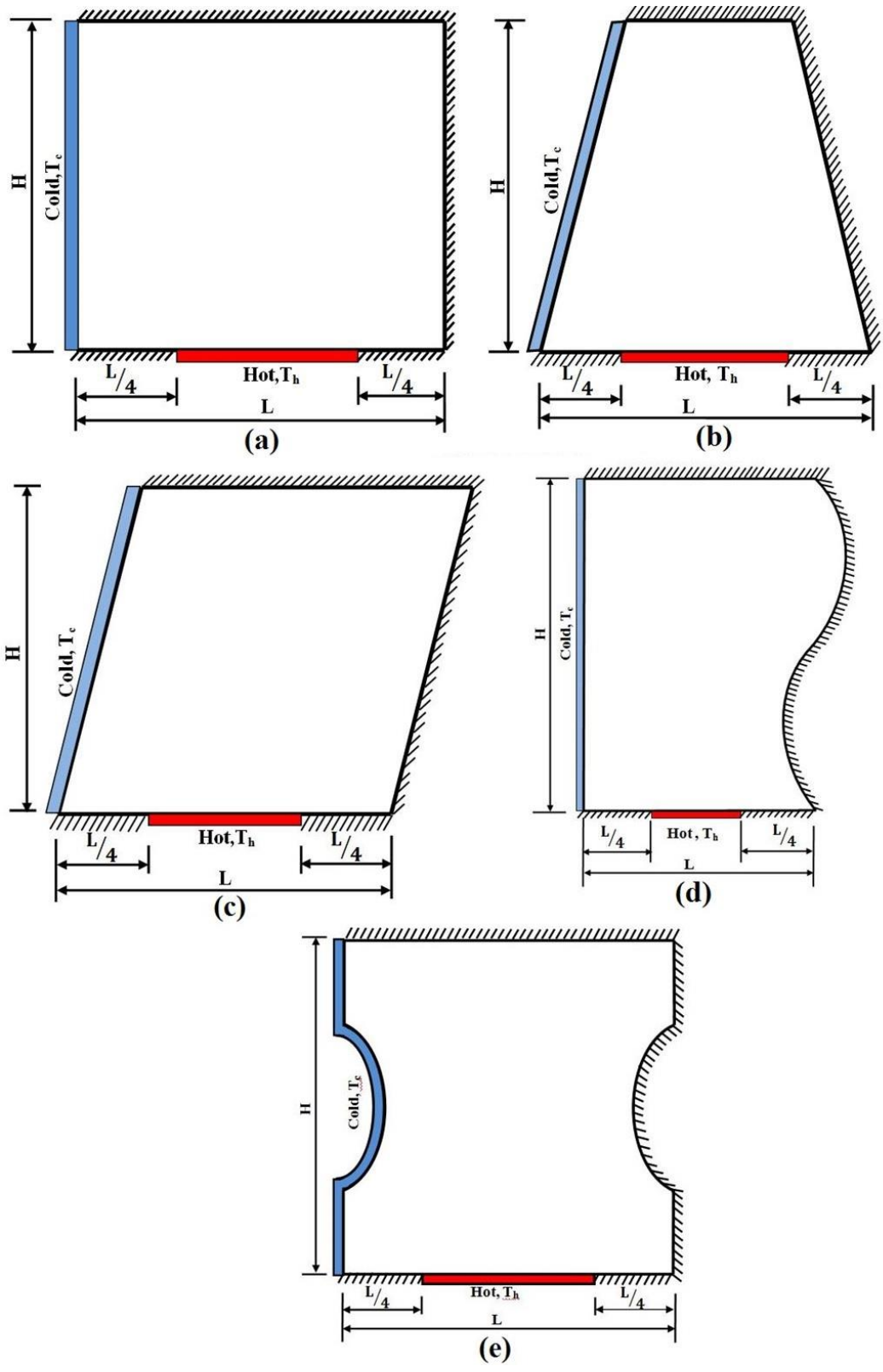

Fig. 4.11. Computational solid domains with the boundary conditions

The non-Dimensional form of governing equations for diffusion and heat function are given in Eqns. (4.17-4.18). The boundary conditions for diffusion equation can be referred from Fig. 4.11.

The boundary conditions for heat function 'Π' at various junction points are as follows.

A reference point, $\Pi(0, H) = 0$ is taken at the top left corner

Adiabatic top wall:$y = H; 0 < x \leq L;$

$$\Pi(\mathrm{x}, \mathrm{H}) = \Pi(0, \mathrm{H}) - \int_0^{\mathrm{L}} -\frac{\partial \theta}{\partial \mathrm{y}}\Big|_{\mathrm{y=H}} \mathrm{dx} = 0 \tag{4.23}$$

Cold left wall:$x = 0; H > y \geq 0;$

$$\Pi(0, \mathrm{y}) = \Pi(\mathrm{x}, \mathrm{H}) - \int_0^{\mathrm{H}} -\frac{\partial \theta}{\partial \mathrm{x}}\Big|_{\mathrm{x=0}} \mathrm{dy} \tag{4.24}$$

Adiabatic right wall: $x = L; H > y \geq 0;$

$$\Pi(L, y) = \Pi(x, H) - \int_0^{H} -\frac{\partial \theta}{\partial x}\Big|_{x=L} dy \tag{4.25}$$

Adiabatic bottom wall: $y = 0; 0 < x_a \leq L/4;$

$$\Pi(x_a, 0) = \Pi(0, y) + \int_0^{L/4} -\frac{\partial \theta}{\partial y}\Big|_{y=0} dx \tag{4.26}$$

Bottom middle portion hot: $y = 0; L/4 < x_b < 3L/4;$

$$\Pi(x_b, 0) = \Pi(x_a, 0) + \int_{L/4}^{3L/4} -\frac{\partial \theta}{\partial y}\Big|_{y=0} dx \tag{4.27}$$

Adiabatic bottom wall: $y = 0; 3L/4 < x_c \leq L$

$$\Pi(x_c, 0) = \Pi(x_b, 0) + \int_{3L/4}^{L} -\frac{\partial \theta}{\partial y}\Big|_{y=0} dx \tag{4.28}$$

4.4.2. Validation

Before performing the validation and parametric investigation grid independent studies have been performed and made sure the results are independent of computational grid. Grid employed for considered various domains in Fig. 4.11 is (a) non-uniform grid (60×80),

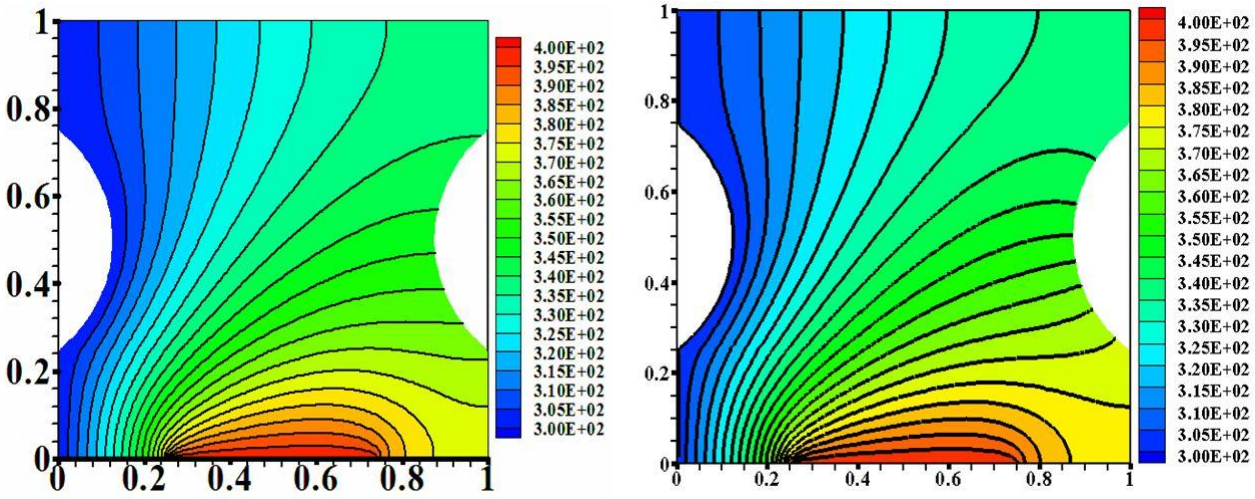

(a)

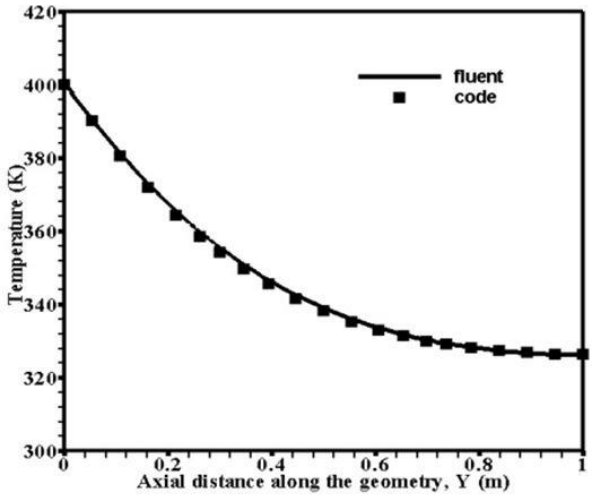

(b)

Fig.4.12. Comparison of isotherms for (a) present study (left), ANSYS fluent (right) and (b) mid plane temperature profile with a commercial CFD code.

(b) non-uniform grid (40×70), (c) non-uniform grid (50×60), (d) uniform grid (80×80) and (e) uniform grid (80×80). To test the validity of the present numerical methodology the results pertaining to temperature distribution with discrete heat source for non-orthogonal geometries has been compared with commercial code ANSYS Fluent and is shown in Fig. 4.12. From Fig. 4.12 (a) gives isotherms from the present study and commercial CFD code ANSYS Fluent and (b) provides a quantitative comparison with ANSYS fluent by plotting mid plane temperature

profile. Based on the above two comparisons it may be noted that the results of present numerical methodology is in good agreement with the results of commercial package ANSYS Fluent. Fig. 4.13 illustrates isotherms and heatlines contours for the computational domain Fig. 4.11(e). Basak and Roy (2008) reported that in conduction dominant regime the isotherms and heatlines are normal to each other. Based on the details provided in Figs. (4.12- 4.13) it is evident that the results obtained from the present numerical methodology agrees with the literature.

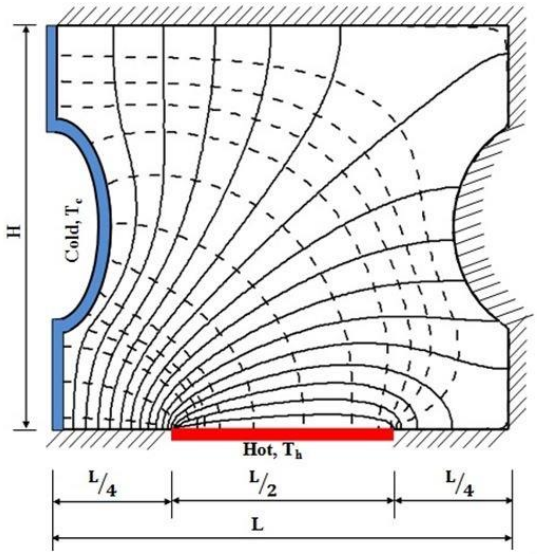

Fig. 4.13. Isotherms (——) and heatlines (- - -) showing normal to each other

4.4.3. Results and Discussion

The left side of Fig. 4.14 shows the isotherms and the right side shows the heatlines for the domains shown in Fig 4.11. Based on the magnitude of isotherms it can be noted that the temperature is maximum at the bottom wall and is distributed towards the left cold wall. Better insight can be noted from the heatlines plotted towards the right side of Fig. 4.14. It may be observed that irrespective of the domain the heatlines are oriented from the bottom hot wall towards the left wall which clearly specifies the direction of heat flow. Based on the magnitude of heatlines it can be noted that the thermal transport is more towards the bottom portion and gradually reduced when moved towards the upper and right portions of the cavity due to its adiabatic nature.

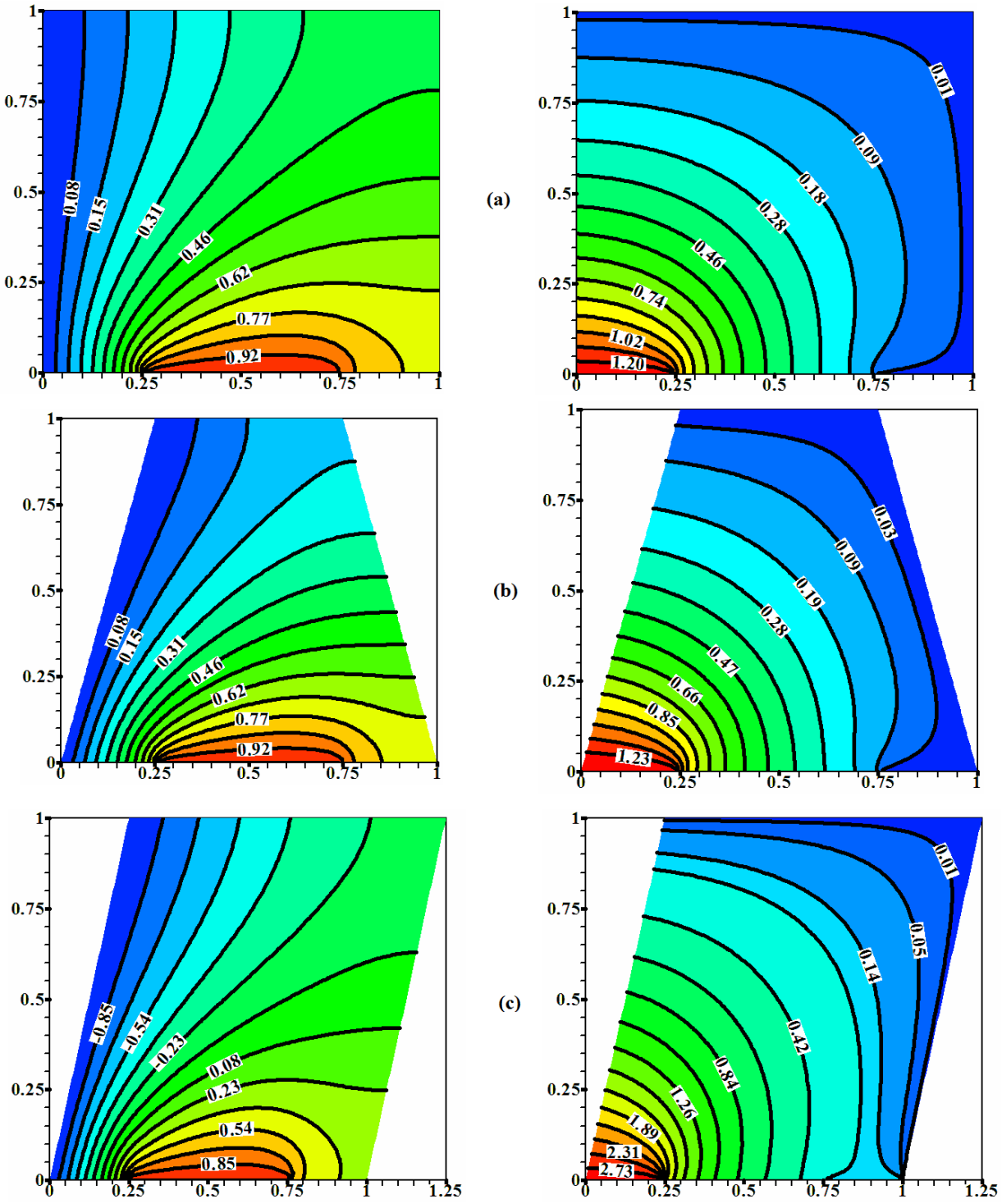
(a)
0.08
0.15
0.31
0.46
0.62
0.77
0.92
0.01
0.09
0.18
0.28
0.46
0.74
1.02
1.20
(b)
0.08
0.15
0.31
0.46
0.62
0.77
0.92
0.03
0.09
0.19
0.28
0.47
0.66
0.85
1.23
(c)
-0.85
-0.54
-0.23
0.08
0.23
0.54
0.85
0.01
0.05
0.14
0.42
0.84
1.26
1.89
2.31
2.73

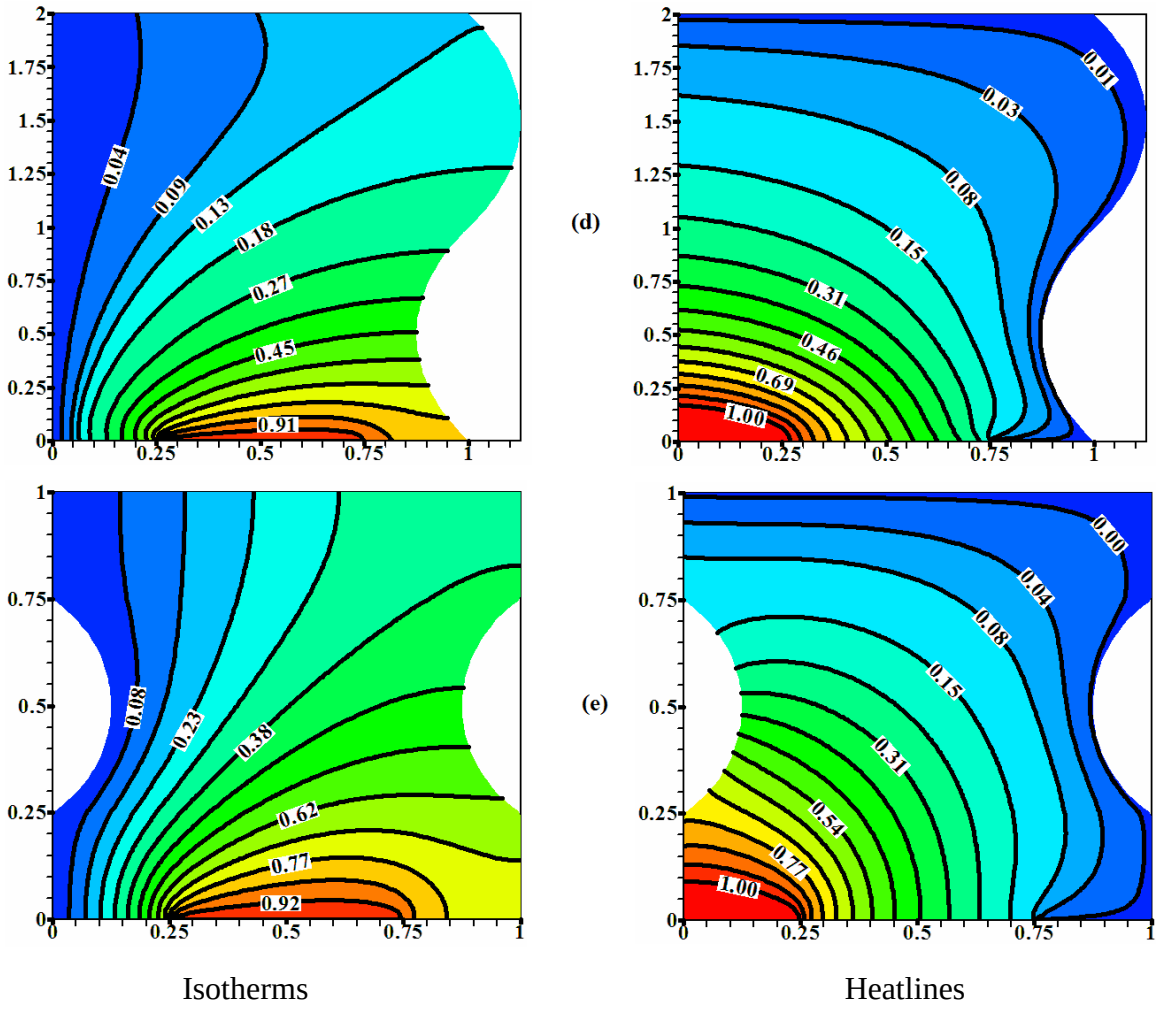

Fig. 4.14 Isotherms (left) and heatlines (right) for different domains

4.5. CONCLUSIONS

The in-house numerical code has been developed to import grid data from the meshing software GAMBIT. A collocated grid based in-house solver is developed for the visualization of thermal transport. The governing equations are discretized using finite volume approach on a Cartesian coordinate system. Results are presented in terms of isotherms, midplane temperature profile and heatlines for the considered geometries. The results thus obtained are rigorously compared with commercial CFD code ANSYS Fluent and heatlines validated with benchmark data. The study deals with diffusion based heat transport where the heatlines are observed to be

normal to the isotherms. Contours for isotherms are plotted to visualize the temperature distribution and heatlines are plotted to assess the energy distribution for the geometries.

Based on the heatlines, it can be concluded that the heatline approach can help for the efficient design of energy systems. The present numerical methodology can be extended for the analysis of thermal hydraulics in various domains.

4.6 CLOSURE

In this chapter, the results are presented in terms of isotherms and heatlines for various shapes to analyze the thermal transport. The present numerical methodology can be extended for the analysis of thermal hydraulics in porous media. The next chapter will deal with the investigation of thermal transport for two-dimensional solid domains with multiple discrete heat sources at the bottom wall.

CHAPTER 5
HEATLINE VISUALIZATION OF THERMAL TRANSPORT IN VARIOUS SOLID DOMAINS WITH DISCRETE HEAT SOURCES AT THE BOTTOM WALL

5.1. INTRODUCTION

In this study five different domains viz. square, trapezoidal, skewed, S-curve and H-curve with discrete heat sources have been considered and the thermal conductivity has been varied from 0.25 to 10 W/mK. The applications include disposal of nuclear wastes, electronic circuits, geothermal areas, food processing industries and cooling of electronic components (Alam et al. (2016); Bondarenko et al. (2019); Krishna et al. (2009); Saravanan et al. (2018); Triveni and Panua (2017)). A thorough understanding of thermal transport in various shapes with a discrete heat source is essential in the design of the above equipment. The concept of Bejan's heatline visualization has been considered for the analysis of thermal transport. The heatlines along with isotherms are expected to provide better insight for the understanding of thermal transport in considered various shapes.

From the earlier works, it can be inferred that several numerical and analytical approaches were adopted for the understanding of heat transport in various shapes. But the analysis of thermal transport with discrete heat sources for various domains in terms of heatlines is scarce. Therefore, the present study aims to analyze in terms of isotherms and heatlines for better insight of thermal transport in these domains.

5.2. PROBLEM DEFINITION AND MATHEMATICAL FORMULATION

The computational domains and boundary conditions considered in the present study are shown in Figs. 5.1. (a)– (e). It consists of two-dimensional geometries of dimensions L×L1. The side walls are maintained at constant temperature 300K (T_c) and serve as a heat sink, two discrete heat sources are located at the bottom wall (L/4) and are maintained at constant heat flux 100

W/m^2(q_1^{II}) and 200 W/m^2 (q_2^{II}) which serve as heat sources (Rout et al. (2012)). Other boundaries of the geometries are thermally insulated.

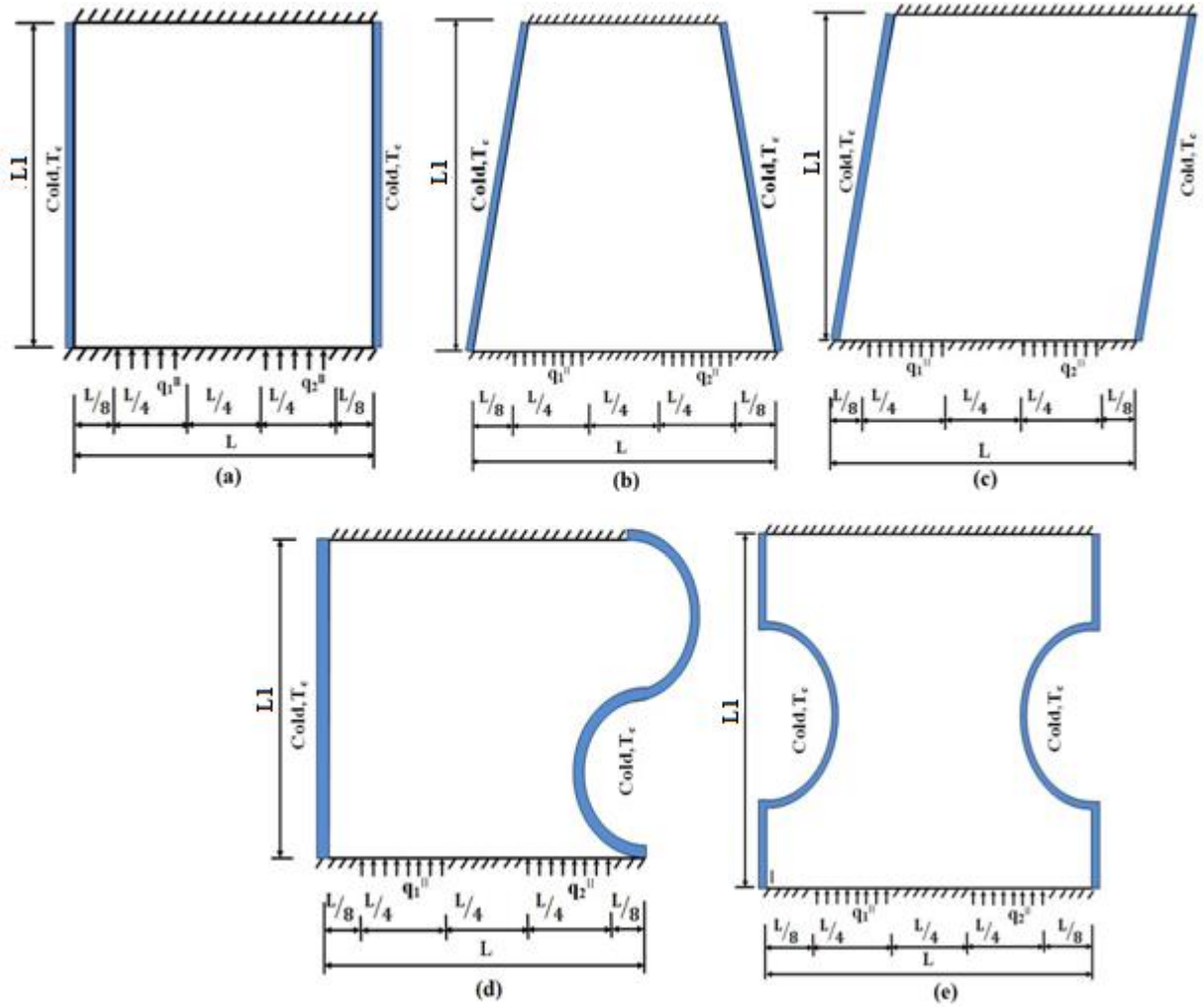

Fig. 5.1. Computational domains and boundary conditions

The governing equations for heat conduction and heat function in the integral form are given in Eqns. (4.7) and (4.8).

The boundary conditions for diffusion equation can be referred to Fig. 5.1 and for heatlines can be given as follows

A reference point, $H(0, L_1) = 0$ is taken at the top left corner

Adiabatic top wall:$y = L_1; 0 < x \leq L;$

$$H(x, L_1) = H(0, L_1) - \int_0^{L_1} -k \frac{\partial T}{\partial y}\Big|_{y=L_1} dx = 0 \quad (5.1)$$

Cold left wall: $x = 0;\ L_1 > y \geq 0;$

$$H(0,y) = H(x,L_1) - \int_0^{L_1} -k\frac{\partial T}{\partial x}\Big|_{x=0} dy \tag{5.2}$$

Cold right wall: $x = L;\ L_1 > y \geq 0;$

$$H(L,y) = H(x,L_1) - \int_0^{L_1} -k\frac{\partial T}{\partial x}\Big|_{x=L} dy \tag{5.3}$$

Adiabatic bottom wall: $y = 0; 0 < x_a \leq L/8;$

$$H(x_a,0) = H(0,y) + \int_0^{L/8} -k\frac{\partial T}{\partial y}\Big|_{y=0} dx \tag{5.4}$$

Bottom wall with heater (q_1"): $y = 0;\ L/8 < x_b < 3L/8;$

$$H(x_b,0) = H(x_a,0) + \int_{L/8}^{3L/8} q_1^{"}\, dx \tag{5.5}$$

Adiabatic bottom wall: $y = 0;\ 3L/8 < x_c \leq 5L/8;$

$$H(x_c,0) = H(x_b,0) + \int_{3L/8}^{5L/8} -k\frac{\partial T}{\partial y}\Big|_{y=0} dx \tag{5.6}$$

Bottom wall with heater (q_2"): $y = 0;\ 5L/8 < x_d \leq 7L/8;$

$$H(x_d,0) = H(x_c,0) + \int_{5L/8}^{7L/8} q_2^{"}\ dx \tag{5.7}$$

Adiabatic bottom wall: $y = 0; 7L/8 < x_e \leq L$

$$H(x_e,0) = H(x_d,0) + \int_{7L/8}^{L} -k\frac{\partial T}{\partial y}\Big|_{y=0} dx \tag{5.8}$$

5.3. SOLUTION METHODOLOGY

The integral form of governing Eqns. (4.7 and 4.8) are discretized for non – orthogonal domains by using the finite volume method. Numerical work has been performed for the various domains using arbitrary quadrilateral mesh. Collocated grid arrangement is chosen which makes the terms in all the governing equations identical leading to simplified programming, minimized program storage and computational time. In this study, the computational domain and its grid are generated in GAMBIT, and the data is exported in neutral file format. The code in C^{++} is implemented to read mesh data from GAMBIT and linked to the in-house finite volume method code for the thermal transport visualization. The set of governing equations Eqns. (4.7 and 4.8) obtained are solved using Gauss-Seidel iterative solver, and a convergence criterion of 10^{-8} is imposed to terminate the iterations.

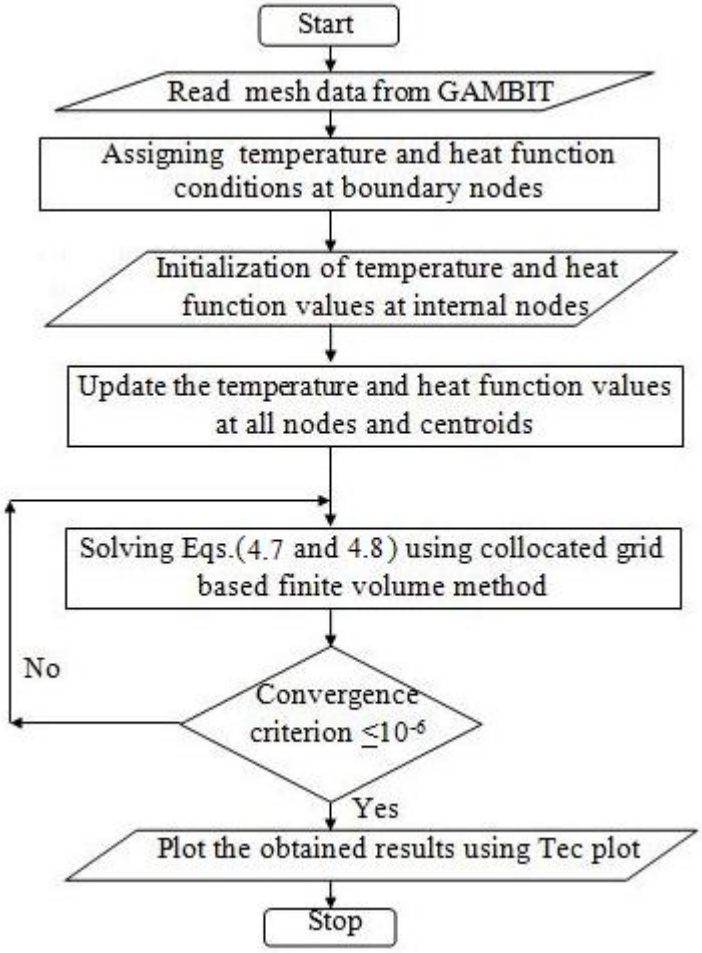

Fig. 5.2. Flow chart for numerical methodology

The steps considered in the present numerical methodology is provided as a flow chart and is shown in Fig. 5.2 and can be summarised as follows:

- Modeling, meshing, selection of boundary conditions and fluid/solid domain using GAMBIT.
- Exporting of mesh data in the neutral file format.
- Reading the mesh data from GAMBIT by in-house developed C^{++} code.
- Assigning temperature and heat function conditions at boundary nodes
- Initialization of temperature and heat function values for internal nodes.
- Solving the integral form of governing equations Eqns. (4.7 and 4.8) based on collocated grid-based finite volume method.
- The solution of algebraic equations is obtained by using the Gauss-Seidel iterative solver.

- Check for the convergence criterion (10^{-8}).
- Obtained results are exported to post-processing software in which contours have been plotted.

5.4. GRID INDEPENDENCE AND VALIDATION

Generation of the grid is an important part of the numerical analysis. A numerical code in C^{++} has been implemented to read a mesh from GAMBIT and linked to the in-house finite

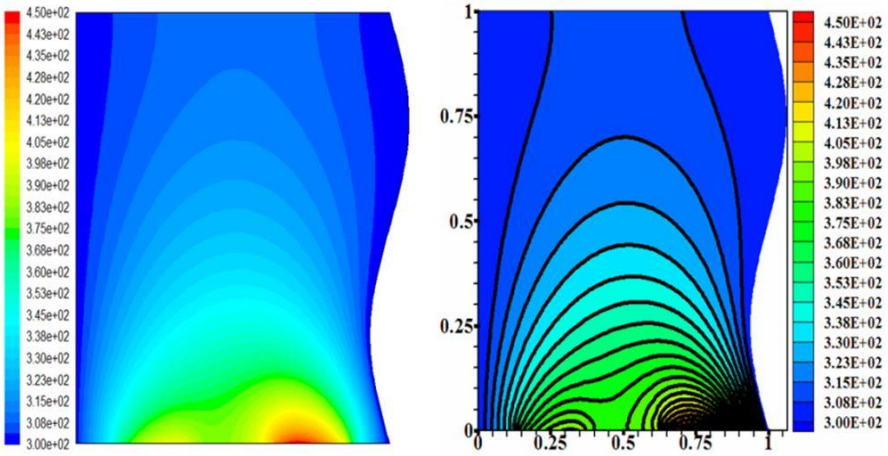

(a)

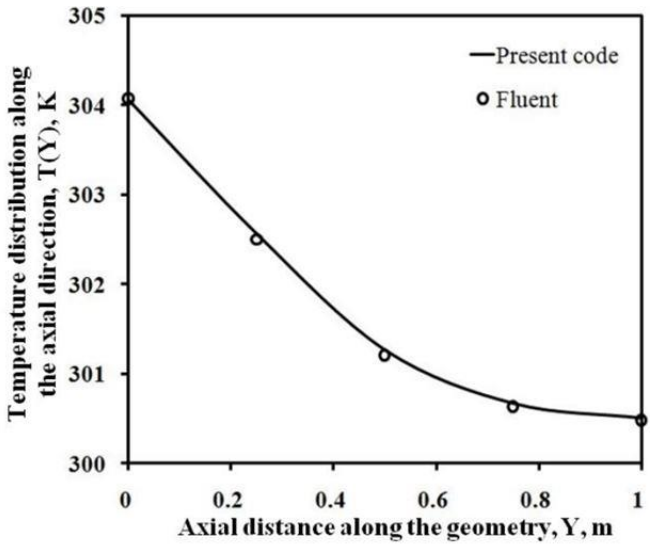

(b)

Fig. 5.3. a) Comparison of isotherms for ANSYS-Fluent (left), present study (right) and b) mid plane temperature profile with commercial CFD code

volume method code for the visualization of thermal transport. Grid independence has been carried out by considering the midplane temperature of the cavity. It is observed that the maximum percentage variation for temperature values between grid sizes 80×80 and 120×120 is less than 1%. Therefore, a grid size of 80 × 80 has been considered for the present study. The computational domain consists of 80 × 80 cells with 20 grid points each, on two discrete heat sources. The thermal conductivity (k) of the computational solid domains is varied between 0.25 W/m K and 10 W/m K. The left-hand side of Fig.5.3(a) gives isotherms from commercial CFD code ANSYS Fluent and the right-hand side gives isotherms from the present study Fig. 5.3(b) provides the quantitative comparison with ANSYS Fluent package by comparing the temperature profile at the midplane.

Based on Fig. 5.3 it can be observed that the present numerical methodology is in good agreement with the commercial code ANSYS Fluent. Fig. 5.4 shows the contours for isotherms and heatlines for the computational domain Fig.5.1 (d). Basak et al. (2008) reported that in conduction dominant regime, the isotherms and heatlines are normal to each other which can be observed from Fig. 5.4. Based on Figs. 5.3 and 5.4 it can be concluded that the present numerical methodology is validated and is in agreement with the literature.

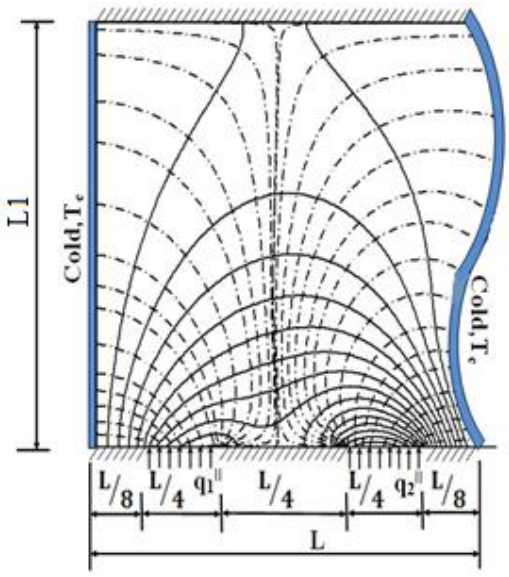

Fig. 5.4. Comparison of isotherms (——) and heatlines (- - -)

5.5. RESULTS AND DISCUSSION

The isotherms (left), and heatlines (right) are presented in Fig. 5.5 (a)–(e) subjected to two distinct heat sources at the bottom wall in the presence of cold side walls and insulated at the remaining boundaries. The thermal conductivity considered for the solid domains shown in Fig. 5.6 is 0.25 W/m K. Based on the isotherms it may be noted that the magnitude of the isotherms is high at the right bottom portion of the geometries due to higher heat flux i.e. 200 W/m^2 (q_2^{II}) and observed to decrease as they move towards the cold side walls i.e 300 K. Also, from the isotherms shown in Fig. 5.5 (left) it may also be observed that they are slightly compressed towards the right bottom corner when compared to the left bottom portion of the cavity. This phenomenon can be explained due to the position of heat flux (200 W/m^2) with a higher magnitude, which is allocated towards the right bottom portion of the cavity. This 200 W/m^2 magnitude heat flux leads to the formation of a hot spot with an isotherm with the highest value when compared to rest of the cavity. The heat from the discrete heat sources has to be dissipated towards the cold walls which are maintained at 300 K. As the temperature gradient

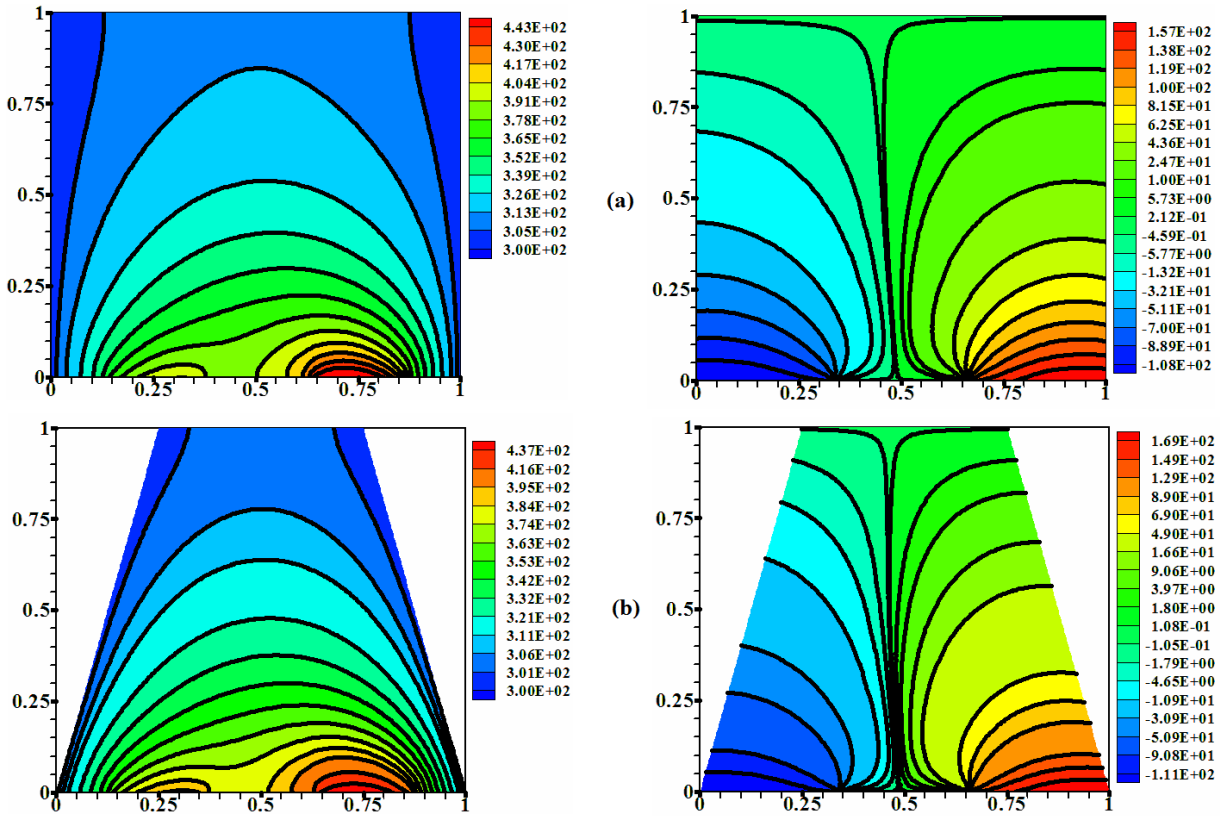

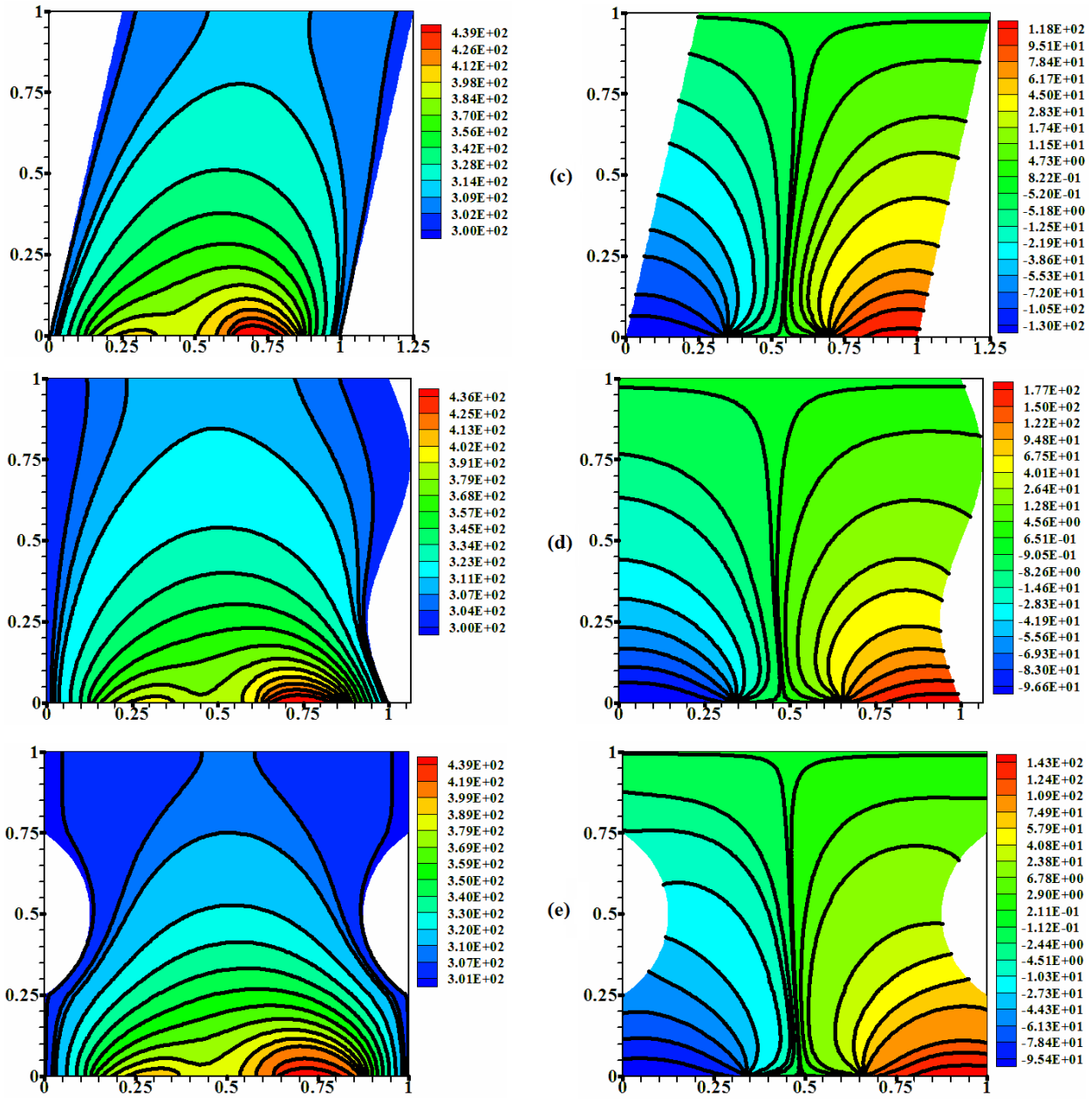

Isotherms Heatlines

Fig. 5.5. Isotherms (left) and heatlines (right) for different various domains (a) Square (b) Trapezoidal (c) Skewed (d) S curve (e) H curve at k= 0.25 W/m K

is more between the right portion of the heat source and cold wall, the isotherms can be observed to be compressed towards the right bottom of the domain. The maximum hot spot temperature for the considered geometries with thermal conductivity 0.25 W/mK is noted at the heat source q_2^{II} (200 W/m^2) placed at the bottom right portion of the cavity. The maximum temperatures

observed are 443 K (square), 437 K (trapezoidal), 439 K (skewed), 436 K (S-curve) and 439 K (H-curve) geometries. This behavior clearly indicates the dependence of geometry configuration on thermal transport.

The heatlines are plotted by assuming the reference point, H=0 at the top left of the adiabatic surface for the geometries shown in Fig. 5.1. Based on the heatlines shown in Fig. 5.5 (right) the heatlines move from discrete heat sources to the cold walls. As the heatlines provide the direction of heat flow, the behavior of heatlines shown in Fig. 5.5. (a-e) indicate the heat transport from discrete heat sources to cold walls. Also, as heat cannot dissipate through the adiabatic walls due to which the heatlines may be noted to be parallel to the adiabatic surfaces. In the present study, the sign convention is based on the direction of heat flow 'H' from the hot to cold walls. The positive sign of 'H' denotes clockwise heat flow and the anti clockwise heat flow is represented by a negative sign of 'H'. It can be noted that the magnitude of heatlines at right wall signifies higher heat transfer rates when compared to rest of the domain. Also, the magnitude of heat function decreases from bottom heat flux portion to the central vertical axis signifying less heat transfer at that zone.

Fig. 5.6 (a-c) illustrates isotherms and heatlines for 'S' curve geometry with the variation of thermal conductivity (k = 0.5, 1 and 10 W/mK) at a constant heat flux condition of 100 W/m^2 (q_1^{II}) and 200 W/m^2 (q_2^{II}). Fig. 5.5 (d) represents 'S' curve geometry with thermal conductivity of 0.25 W/mK. It can be noted that the magnitude of isotherms decreases with the increase in thermal conductivity. This can be inferred due to the increase in heat transfer due to the increase in thermal conductivity. The increase in heat transfer rate tends to decrease in the magnitude of isotherms. Inline to the decrease in the magnitude of temperature, the magnitudes of the heatlines are also observed to decrease due to the decrease in a temperature gradient. Fig. 5.7 (a–e) shows the local temperature distribution along the axial direction at mid-plane drawn with the variation of thermal conductivity (k = 0.25, 0.5, 0.75, 1, 5 and 10 W/m K). Fig.5.7 (a) and (c) shows the magnitude of midplane temperature higher when compared to rest of domain due to variation in size of the cavity at a thermal conductivity of k = 0.25 W/m K. When the size of the domain increases for a material whose thermal conductivity is low the heat can not propagate and leads to higher magnitude for temperature. Also, with the thermal conductivity of k =5 and 10 W/m K,

the magnitude of constant temperature lines are almost the same for the considered geometries. For a thermal conductivity of 0.25 W/mK, the effective heat transport through the domain is less when compared to higher values of thermal conductivity. With the increase in thermal conductivity, the heat transfer rate is observed to increase.

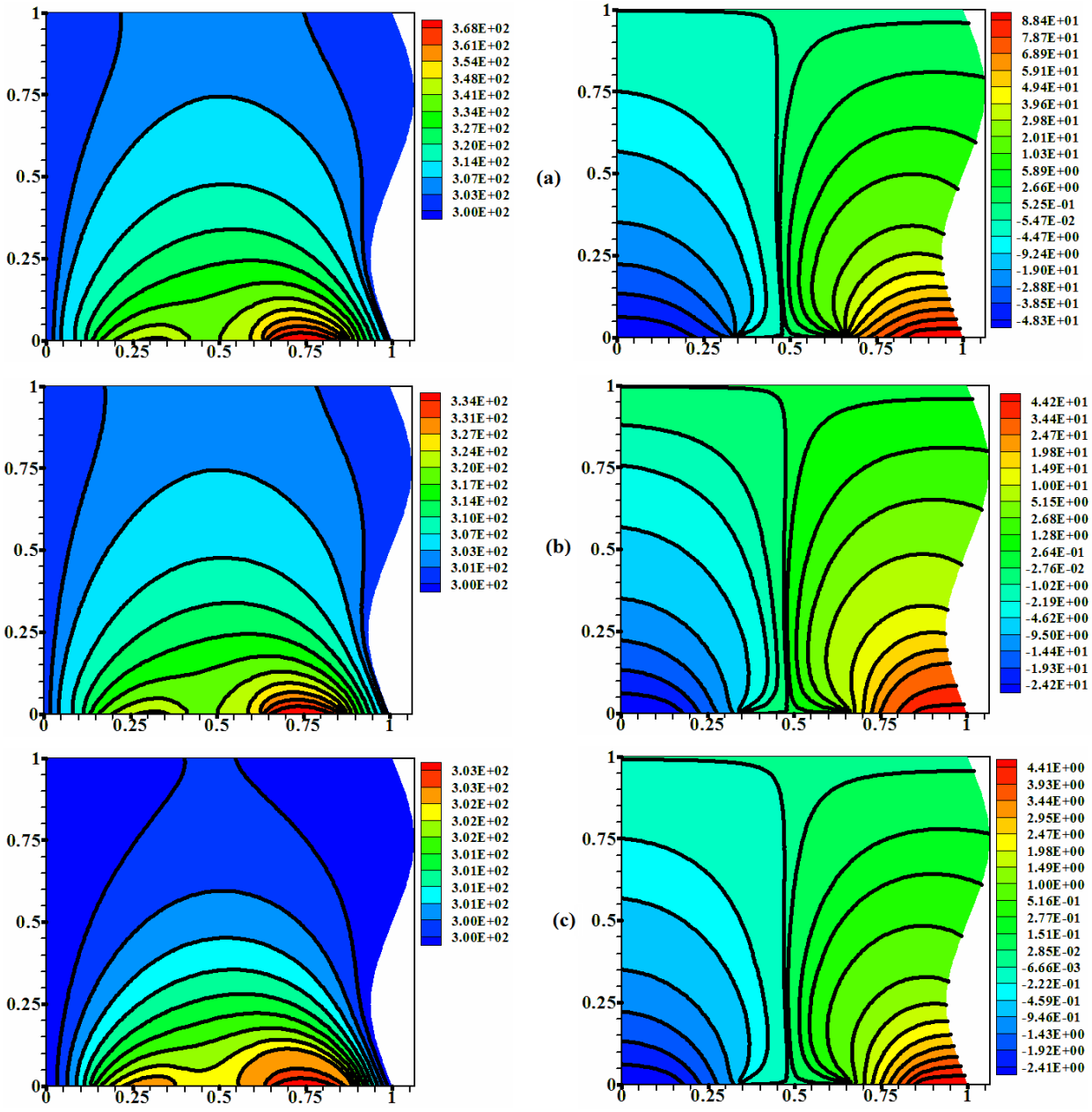

Fig. 5.6. Isotherms (left) and heatlines (right) for S curve geometry with the variation of thermal conductivity (k) (a) 0.5 W/m K (b) 1 W/m K and (c) 10 W/m K

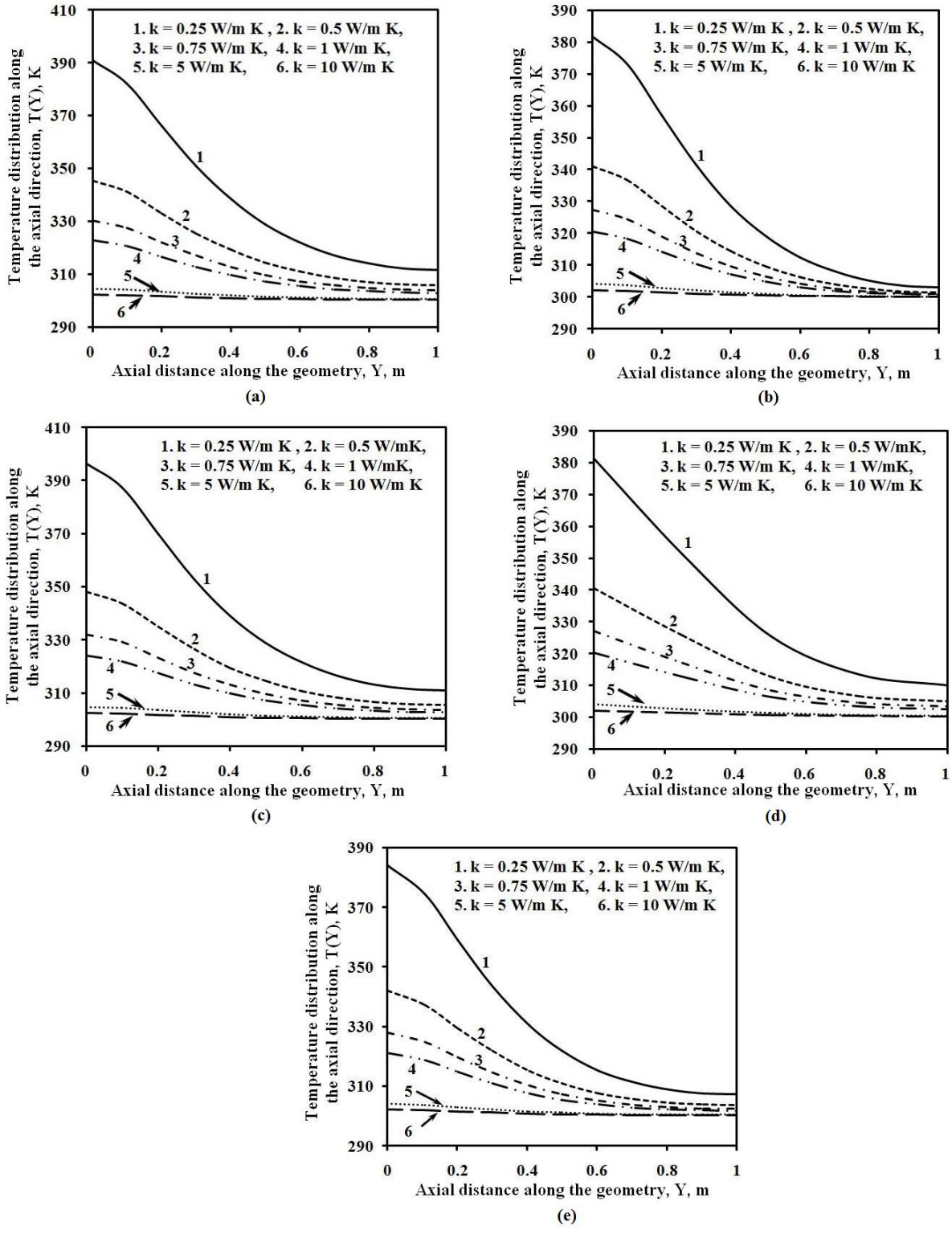

Fig. 5.7. Variation of local temperature distribution vs axial direction along the board with different domains (a) Square, (b) Trapezoidal, (c) Skewed, (d) S curve, (e) H curve

The increase in heat transfer rate leads to a decrease in the magnitude of the midplane temperature. Based on Fig.5.7 it can be noted that with the increase in thermal conductivity from 0.25 to 10 W/m K, the maximum temperature along the vertical midplane for the considered domains decreased by 22.65% (square), 20.90% (trapezoidal), 23.71% (skewed), 20.77% (S-curve) and 21.35% (H-curve) geometries**.**

5.6. CONCLUSIONS

A numerical code in C^{++} has been implemented to read the mesh from GAMBIT and linked to the in-house finite volume method code for the visualization of thermal transport. Results are presented in terms of isotherms and heatlines for the considered geometries. The results thus obtained are compared with ANSYS Fluent. Contours for isotherms are plotted to visualize the temperature distribution and heatlines are plotted to assess the energy transport. The study could reveal that for a domain with lower thermal conductivity the magnitude of temperature increases with the increase in size. The geometry configuration is noted to influence the thermal transport. Based on results it can be observed that the visualization of heatlines provides a better insight of energy transport in domains with discrete heat sources. The study can provide insight for the thermal management of electronic components on various shaped circuit boards.

5.7. CLOSURE

The thermal transport for two-dimensional solid various shapes with two discrete heat sources at the bottom wall is discussed. The study could reveal that for a domain with lower thermal conductivity, the magnitude of temperature increases with the increase in size. The geometry configuration is noted to influence the thermal transport. The next chapter investigates the hydrodynamics for a lid-driven flow saturated with non-Darcy anisotropic porous media.

CHAPTER 6

NUMERICAL INVESTIGATION OF HYDRODYNAMICS FOR A LID DRIVEN NON-DARCY ANISOTROPIC POROUS CAVITY

6.1. INTRODUCTION

The study of lid-driven flow in a porous cavity is not only of academic interest; several other applications include food processing and float glass production (Pilkington (1969)), analysis of ground water flows ((Osinov (2003); Krishna et al. (2008b)), packed-bed catalytic reactors (Oztop (2006)), geophysics, chemical engineering and binary alloy solidification (Haddad (2017); Nield and Bejan (2013)) etc. Generally, earthquakes are associated with soil liquefaction and ground failures. Liquefaction can be referred to the decrease in strength of the saturated cohesion less soil due to the increase in pore water pressure when subjected to shearing stresses. The study pertaining to shear driven flow for porous media can be of great help in the understanding of liquefaction. Vafai and Tien (1981) and Vafai and Kim (1995) employed a local volume averaging technique for porous media and presented a generalized non-Darcy (Brinkman-Forchheimer extended Darcy) formulation. The importance of inertial effects and solid boundary were mentioned to be predominant for highly permeable porous media, high Prandtl number fluids and with large pressure gradients.

Based on the literature review it is observed that the studies pertaining to shear driven porous cavity flows were limited to either isotropic porous media in Darcy/non-Darcy regime or anisotropic porous media in Darcy (tightly packed) regime. Also, the earlier studies could reveal that the anisotropy of the porous matrix could significantly influence transport phenomena (Krishna et al. (2008a); Krishna et al. (2009a); Hu et al. (2017)). To the best of the author's knowledge, the influence of anisotropic parameters of the porous matrix with the variation of lid velocity (Reynolds number), permeability (Darcy number) and porosity on hydrodynamics is yet to be investigated. Therefore, the present study aims to address the above parameters to

understand the flow behaviour for a lid-driven cavity which is impregnated with non-Darcy anisotropic porous media.

6.2. PROBLEM DEFINITION AND MATHEMATICAL FORMULATION

A 2-D orthogonal cavity impregnated with anisotropic porous media with top lid moving at uniform velocity 'U' is considered and is shown in Fig. 6.1. The solid matrix of the porous media is assumed to be homogeneous, saturated with fluid and does not undergo deformation. The effect of anisotropy for the porous media has been considered by varying the principal axes inclination with respect to the gravity vector. The anisotropic properties of the porous medium have been varied in the non-Darcy regime. The influence of pertinent parameters viz. Darcy number ($10^{-5} \leq Da \leq 10^{-2}$), porosity (0.3 and 0.6), permeability ratio (K^*=0.1, 1 and 10), Forchheimer constants ratio (F^*=1, 10 and 100) and principal axes inclination ($\theta=0^o$, 45^o and 90^o) have been considered to understand the hydrodynamics of the porous media. It may be noted that the formulation has been considered based on the pseudo-transient approach and the governing equations (Eqns. 6.1-6.11) pertaining to the present study are given as follows.

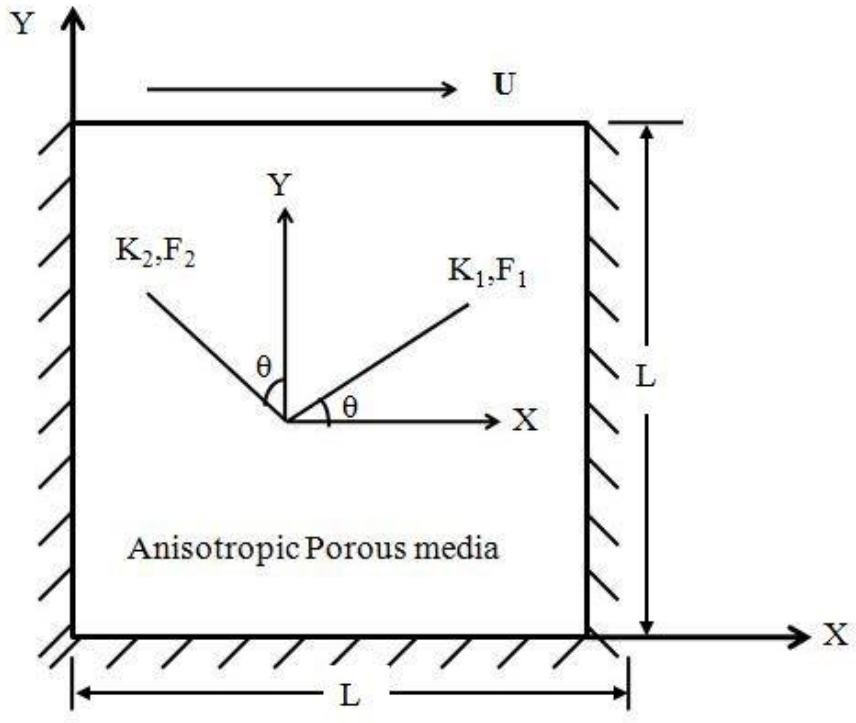

Fig. 6.1. Computational domain

Mass balance:

$$\frac{\partial u}{\partial x}+\frac{\partial v}{\partial y}=0 \tag{6.1}$$

X- Momentum equation:

$$\frac{\rho_f}{\varepsilon}\left[\frac{\partial u}{\partial t}+\frac{u}{\varepsilon}\frac{\partial u}{\partial x}+\frac{v}{\varepsilon}\frac{\partial u}{\partial y}\right]=-\frac{\partial P}{\partial x}+\frac{\mu_f}{\varepsilon}\left(\frac{\partial^2 u}{\partial x^2}+\frac{\partial^2 u}{\partial y^2}\right)-\frac{\mu_f u}{\bar{\bar{K}}}-\bar{\bar{C}}\rho_f u\sqrt{u^2+v^2} \tag{6.2}$$

Y-Momentum equation:

$$\frac{\rho_f}{\varepsilon}\left[\frac{\partial v}{\partial t}+\frac{u}{\varepsilon}\frac{\partial v}{\partial x}+\frac{v}{\varepsilon}\frac{\partial v}{\partial y}\right]=-\frac{\partial P}{\partial y}+\frac{\mu_f}{\varepsilon}\left(\frac{\partial^2 v}{\partial x^2}+\frac{\partial^2 v}{\partial y^2}\right)-\frac{\mu_f v}{\bar{\bar{K}}}-\bar{\bar{C}}\rho_f v\sqrt{u^2+v^2} \tag{6.3}$$

Where

$$\bar{\bar{K}}=\begin{bmatrix}K_1\cos^2\theta+K_2\sin^2\theta & (K_1-K_2)\sin\theta\cos\theta\\ (K_1-K_2)\sin\theta\cos\theta & K_1\sin^2\theta+K_2\cos^2\theta\end{bmatrix} \tag{6.4}$$

$$K^*=\frac{K_1}{K_2} \tag{6.5}$$

$$\bar{\bar{C}}=\begin{bmatrix}C_1\cos^2\theta+C_2\sin^2\theta & (C_1-C_2)\sin\theta\cos\theta\\ (C_1-C_2)\sin\theta\cos\theta & C_1\sin^2\theta+C_2\cos^2\theta\end{bmatrix} \tag{6.6}$$

$$C_1=\frac{F_1}{\sqrt{K_1}}\,C_2=\frac{F_2}{\sqrt{K_2}} \tag{6.7}$$

$$F^*=\frac{F_1}{F_2} \tag{6.8}$$

$$C^*=\frac{C_1}{C_2}=\frac{F^*}{\sqrt{K^*}} \tag{6.9}$$

By applying inverse to permeability tensor and by substituting $K^*=K_1/K_2$, (Eqn. 6.4) can be reduced to

$$\overline{\overline{K^{-1}}}=\frac{1}{K_1}\begin{bmatrix}K^*\sin^2\theta+\cos^2\theta & (1-K^*)\sin\theta\cos\theta\\ (1-K^*)\sin\theta\cos\theta & K^*\cos^2\theta+\sin^2\theta\end{bmatrix} \tag{6.10}$$

Similarly, by substituting (Eqns. 6.7 –6.9) in (Eqn. 6.6), (Eqn. 6.11) can be obtained

$$\bar{\bar{C}}=\frac{F_1}{\sqrt{K_1}}\begin{bmatrix}\cos^2\theta+\frac{\sqrt{K^*}}{F^*}\sin^2\theta & \left(1-\frac{\sqrt{K^*}}{F^*}\right)\sin\theta\cos\theta\\ \left(1-\frac{\sqrt{K^*}}{F^*}\right)\sin\theta\cos\theta & \frac{\sqrt{K^*}}{F^*}\cos^2\theta+\sin^2\theta\end{bmatrix} \tag{6.11}$$

The following non-dimensional parameters can be applied to convert Eqns. (6.1-6.3) to non-dimensional form

$$x^* = \frac{x}{L}; y^* = \frac{y}{L}; u^* = \frac{u}{U}; v^* = \frac{v}{U};\ Da = \frac{K_1}{L^2}; P^* = \frac{P}{\rho_f U^2}; Re = \frac{\rho UL}{\mu_f}; t^* = \frac{tU}{L} \tag{6.12}$$

The non-dimensional form of governing equations thus obtained after substituting (Eqn. 6.12) is as follows. For the sake of convenience, the superscript '*' has been removed

$$\frac{\partial u}{\partial x} + \frac{\partial v}{\partial y} = 0 \tag{6.13}$$

$$\begin{aligned}\left[\frac{1}{\varepsilon}\frac{\partial u}{\partial t} + \frac{u}{\varepsilon^2}\frac{\partial u}{\partial x} + \frac{v}{\varepsilon^2}\frac{\partial u}{\partial y}\right] &= -\frac{\partial P}{\partial x} + \frac{1}{\varepsilon\, Re}\left(\frac{\partial^2 u}{\partial x^2} + \frac{\partial^2 u}{\partial y^2}\right) \\ &- \frac{1}{Re\, Da}\left[u\,(\cos^2\theta + K^* \sin^2\theta)\right. \\ &\left. + v\big((1 - K^*)\sin\theta\cos\theta\big)\right] \\ &- \frac{F_1}{\sqrt{Da}}\left[u\left(\cos^2\theta + \frac{\sqrt{K^*}}{F^*}\sin^2\theta\right)\right. \\ &\left. + v\left(\left(1 - \frac{\sqrt{K^*}}{F^*}\right)\sin\theta\cos\theta\right)\right]\sqrt{u^2 + v^2}\end{aligned} \tag{6.14}$$

$$\left[\frac{1}{\varepsilon}\frac{\partial v}{\partial t}+\frac{u}{\varepsilon^2}\frac{\partial v}{\partial x}+\frac{v}{\varepsilon^2}\frac{\partial v}{\partial y}\right] \tag{6.15}$$

$$= -\frac{\partial P}{\partial y}+\frac{1}{\varepsilon\,Re}\left(\frac{\partial^2 v}{\partial x^2}+\frac{\partial^2 v}{\partial y^2}\right)$$

$$-\frac{1}{Re\,Da}\left[u\left((1-K^*)\sin\theta\cos\theta\right)\right.$$

$$\left.+\,v(K^*\cos^2\theta+\sin^2\theta)\right]-\frac{F_1}{\sqrt{Da}}\left[u\left(\left(1-\frac{\sqrt{K^*}}{F^*}\right)\sin\theta\cos\theta\right)\right.$$

$$\left.+\,v\left(\frac{\sqrt{K^*}}{F^*}\cos^2\theta+\sin^2\theta\right)\right]\sqrt{u^2+v^2}$$

In the above Eqns. (6.14-6.15), $F_1 \approx 0.55$ ((Ward (1964); Krishna et al. (2008b))

Stream function is defined by

$$u=\frac{\partial \psi}{\partial y};\; v=-\frac{\partial \psi}{\partial x} \tag{6.16}$$

6.3. SOLUTION METHODOLOGY

The discretization of the Eqns. (6.13–6.15) has been carried out by the finite volume method. Quadrilateral cells in collocated grid arrangement have been employed. Velocity nodes (for u and v velocity components) and pressure nodes as shown in Fig. 3.1 are placed at the centre of the cells. A non-uniform grid which is based on the cosine function as shown in Fig. 6.2 has been applied. The pressure-velocity coupling has been performed by implementing the SIMPLE algorithm. The convective terms are estimated by the first-order upwind scheme and the diffusive terms by the central difference. The cell face velocities are obtained by linear interpolation. The obtained algebraic system is solved by using the Gauss-Seidel iterative procedure. As given in Eqn. (6.17) once the values for velocities (u and v) attain less than 10^{-8} the iterative process gets terminated.

$$\frac{\sum_{i,j}\left|\Phi_{i,j}^{n}-\Phi_{i,j}^{n-1}\right|}{\sum_{i,j}\left|\Phi_{i,j}^{n}\right|}<10^{-8} \tag{6.17}$$

Where Φ refers to u and v variables

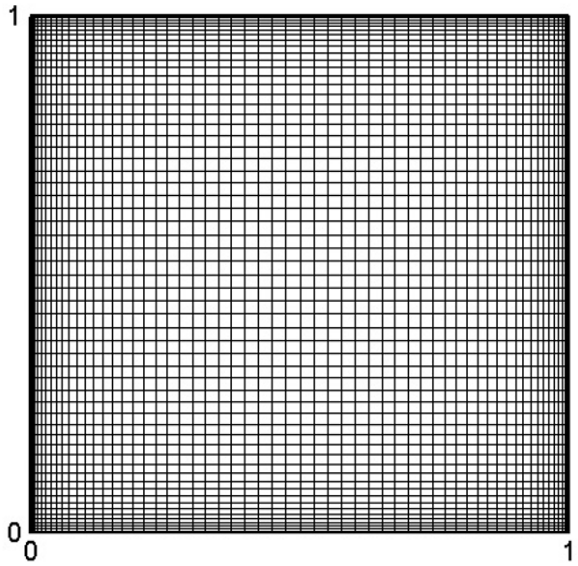

Fig. 6.2. Non-uniform grid (Cosine grid)

6.4. GRID INDEPENDENCE AND VALIDATION

The grid-independent study is very much necessary to ensure the correctness of the employed numerical methodology. Cosine grid as shown in Fig. 6.2 has been employed in the present study. The validation of the present numerical procedure is carried out by comparing with Ghia et al. (1982) , Guo and Zhao (2002) and Krishna et al. (2008b). It is observed that the variation between the grid sizes of 61×61 and 81×81 is observed to be less than 1%. Therefore, a grid size of 61×61 has been employed for further investigation. Porosity can be defined as the ratio of void volume to total volume. If the porosity is tending to one ($\varepsilon \rightarrow 1$), the void volume tends to total volume. Also, permeability can be given as hydraulic conductivity of the porous media i.e. as the magnitude of permeability tends to a very high value the porous medium behaves as a fluid. The non-dimensional form of permeability Eqn. (6.12) can be given as Darcy number. So, the case where the Darcy number tends to a very high value (10^7) and porosity equal to 1, the porous media should behave as a fluid. To check the robustness of the present methodology, the porous media formulation has been tested by initially taking Darcy number as 10^7 and porosity as 0.999. The obtained results are compared with Ghia et al. (1982) and are shown in Fig. 6.3 (a).

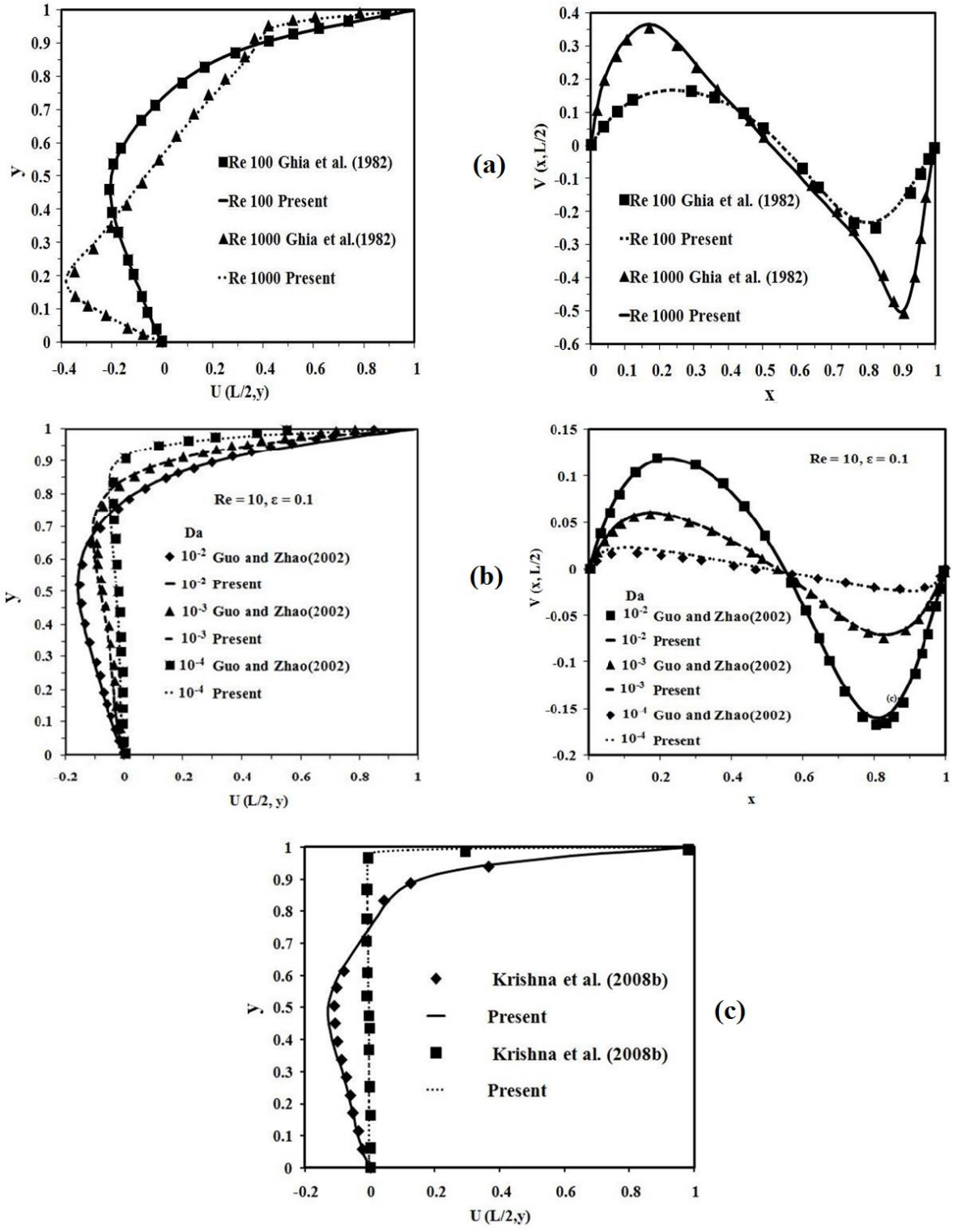

Fig. 6.3. Comparison of the present study (mid plane u and v velocities) with literature (Ghia et al. (1982); Guo and Zhao (2002); Krishna et al. (2008b))

Also, when K*=1, $\theta=0^0$ and F*=1 the porous media should be isotropic in nature. Therefore, the present anisotropic formulation can be boiled down to isotropic porous media by substituting the above parameters. The results thus obtained for isotropic porous media is shown in Fig. 6.3 (b-c). Based on Fig. 6.3 it can be noted that the present numerical formulation is in good agreement with the literature (Ghia et al. (1982); Guo and Zhao (2002); Krishna et al. (2008b)).

6.5. RESULTS AND DISCUSSION

The objective of the present study is to address the effect of anisotropic properties viz. permeability ratio (K*= 0.1, 1 and 10), principal axes inclination ($\theta= 0^o – 90^o$) and Forchheimer constants ratio (F* = 1, 10 and 100) on the hydrodynamics for an anisotropic porous cavity with moving top lid. The Reynolds number considered are 10, 100 and 1000 and the parameters of the porous matrix such as Darcy number ($10^{-5} \leq Da \leq 10^{-2}$) and porosity ($\varepsilon$ = 0.3 and 0.6) have been varied.

The influence of pertinent parameters has been analyzed by studying the behavior of streamlines and maximum stream function value (ψ_{max}). The measurement of the volume flow rate can be given in terms of ψ_{max}. Therefore, the value of ψ_{max} is also considered. In the subsequent sections initially, the effect of Re, Da, and ε are discussed and later the influence of anisotropic properties (K*, F* and θ) on the flow behavior has been addressed.

6.5.1. Effect of Reynolds number (Re):

Fig. 6.4 and Table 6.1 provides the streamlines and ψ_{max} with the variation of Re. Irrespective of Da, ε and K*, the ψ_{max} can be noted to decrease with the increase in Reynolds number. With the Darcy numbers (Da) 10^{-2} and 10^{-3} the porous media can be classified under a non-Darcy regime where the influence of non-linear drag is significant (Krishna et al. (2008b)). Therefore, the behavior of the decrease in ψ_{max} with the increase in Reynolds number can be inferred due to the influence of non-linear drag forces. Also, as the Reynolds number increases due to the increase in inertia for the fluid the vortex can be noted to move from top lid towards the downward portion of the cavity.

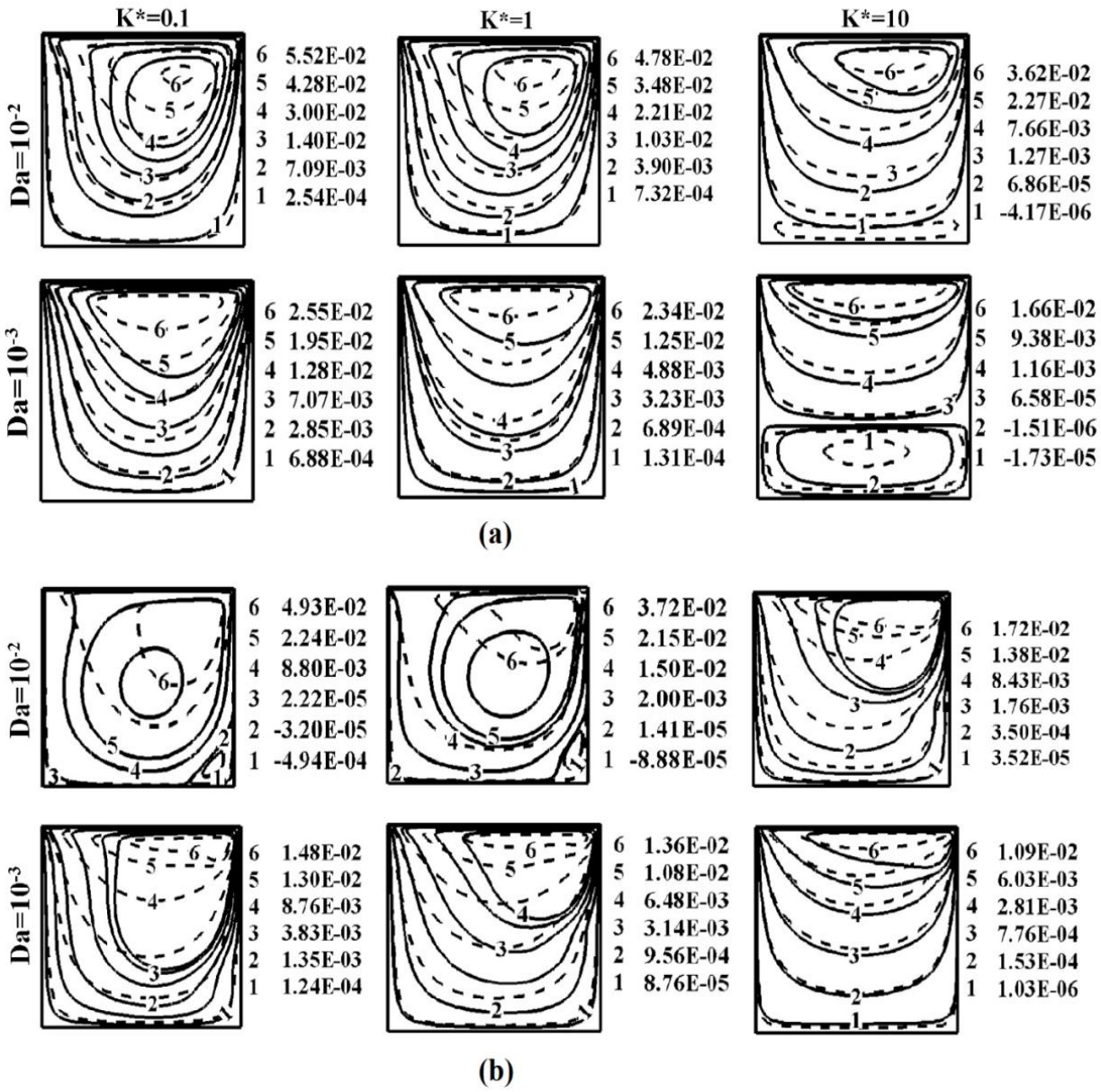

Fig. 6.4. Streamlines for θ=0^0, F*=1 (a) Re =100 (b) Re =1000 with Darcy number (solid line ε=0.3, dotted line ε=0.6)

Table 6.1. Variation of maximum stream function value with Re, Da, ε and K* for F* =1, θ = 0º

Darcy Number (Da)	K*	The maximum Stream function value (ψ_{max})			
		Re =100		Re =1000	
		ε = 0.3	ε = 0.6	ε = 0.3	ε = 0.6
10^{-2}	0.1	0.0755	0.0566	0.0578	0.0367
	1	0.0679	0.0514	0.0486	0.0302
	10	0.0514	0.0407	0.0343	0.0234
10^{-3}	0.1	0.0403	0.0284	0.0326	0.0167
	1	0.0351	0.0263	0.0257	0.0145
	10	0.0275	0.0216	0.0184	0.0126

6.5.2. Effect of Darcy number (Da)

As provided in Eqn. (6.12), Darcy number (Da) can be defined as K_1/L^2 (permeability to reference length square) and is the non-dimensional form of permeability. From Fig. 6.4 and Table 6.1, the ψ_{max} can be observed to increase with the increase of Darcy number. It may be

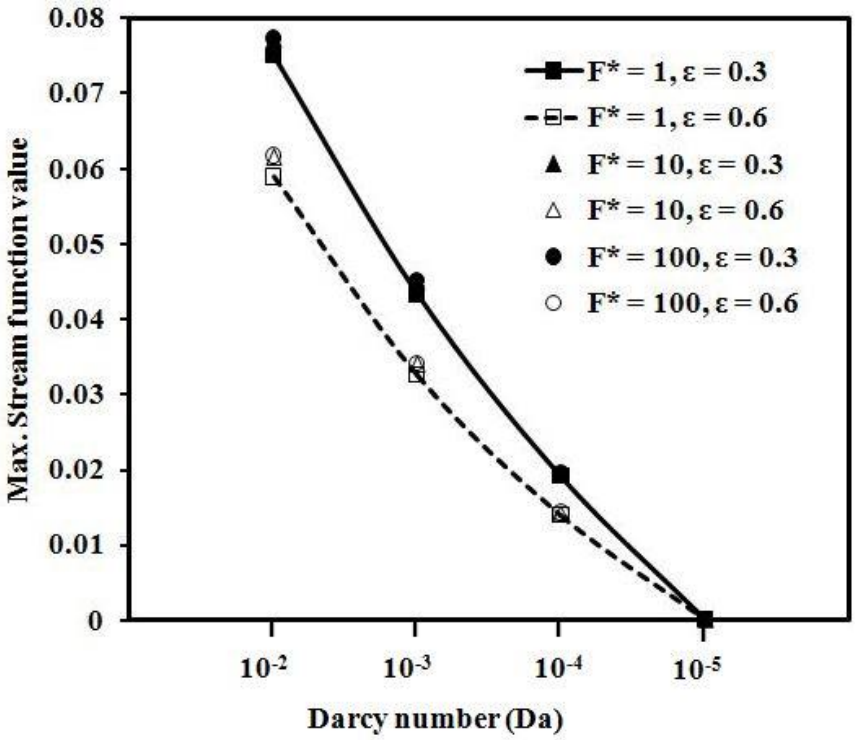

Fig. 6.5. Variation of ψ_{max} with Da and F* for Re = 100, K* = 0.1 and θ = 45°

noted that higher Darcy number represents higher hydraulic conductivity. At higher Darcy number (Da = 10^{-2}) vortex strength is higher when compared to that of 10^{-3}. A decreased trend for the ψ_{max} with the decrease in Darcy number can be noted and can be seen in Fig. 6.5. This decreased trend is due to the decrease in hydraulic conductivity of the porous matrix. Hence, the vortex strength becomes weaker and flow velocity becomes less.

6.5.3. Effect of Porosity (ε):

The solid lines shown in Fig. 6.4 for streamlines represents ε=0.3 and dotted lines for ε=0.6. Variation can be observed between these two porosities for Da = 10^{-2} and 10^{-3}. Also, from Table 6.1, a decrease in ψ_{max} can be noted with the increase in porosity from 0.3 to 0.6. For a given Darcy number (permeability) the hydraulic conductivity remains fixed even with the variation of porosity. An increase in pore size with the increase in porosity leads to the decrease in pore velocity due to which the stream function value can be observed to decrease. The influence of porosity on Darcy number is shown in Fig. 6.5. It may be noted that with the decrease in Darcy number the effect of porosity decreases and nullifies at Da=10^{-5}.

6.5.4. Effect of Permeability Ratio (K*):

The influence of permeability ratio (K*) with the variation of Reynolds number (Re=100 and 1000), Darcy number (Da = 10^{-2} and 10^{-3}) and porosity (ε = 0.3 and 0.6) on the flow behavior is shown in Fig. 6.4. Fig 6.4 (a) shows the streamlines for Re = 100 and Fig. 6.4 (b) for Re=1000. Also, the variation of the ψ_{max} with K* for the above parameters are given in Table 6.1. Based on Eqns. (6.5 and 6.12) it can be noticed that the permeability ratio (K*) is defined as K_1/K_2 and Darcy number (Da) is given as K_1/L^2. As Darcy number is given with regard to K_1 which is assumed to be constant and the permeability K_2 is varied in terms of K*. With $\theta = 0^o$ the porous matrix becomes orthotropic in nature. When K* increases the permeability in the vertical direction (K_2) can be observed to decrease. Hence, the increase in permeability ratio causes vortex strength to become weaker and causes the vortex to move towards the upper portion of the cavity.

Table 6.2. Variation of ψ_{max} with Re, F*, ε, θ and K* for Da = 10^{-2}

K*	Forchheimer ratio (F*)	Angle of inclination (θ)	The maximum Stream function value			
			Re =10		Re =1000	
			ε = 0.3	ε = 0.6	ε = 0.3	ε = 0.6
0.1	1	0	0.0833	0.0731	0.0578	0.0367
		45	0.0838	0.0747	0.0555	0.0357
		90	0.0856	0.0776	0.0572	0.0398
	10	0	0.0836	0.0734	0.0631	0.0418
		45	0.0842	0.0753	0.0587	0.0387
		90	0.0862	0.0785	0.0624	0.0461
	100	0	0.0836	0.0734	0.0635	0.0424
		45	0.0842	0.0753	0.0592	0.0389
		90	0.0863	0.0786	0.0630	0.0469
1	1	0	0.0772	0.0650	0.0486	0.0302
		45	0.0772	0.0650	0.0486	0.0302
		90	0.0772	0.0650	0.0486	0.0302
	10	0	0.0776	0.0664	0.0598	0.0387
		45	0.0781	0.0671	0.0568	0.0371
		90	0.0786	0.0678	0.0593	0.0430
	100	0	0.0777	0.0665	0.0614	0.0405
		45	0.0782	0.0672	0.0579	0.0381
		90	0.0787	0.0679	0.0611	0.0451
10	1	0	0.0579	0.0480	0.0343	0.0234
		45	0.0511	0.0397	0.0352	0.0201
		90	0.0447	0.0340	0.0326	0.0167
	10	0	0.0582	0.0482	0.0455	0.0295
		45	0.0518	0.0403	0.0463	0.0300
		90	0.0455	0.0347	0.0461	0.0307
	100	0	0.0582	0.0483	0.0478	0.0311
		45	0.0518	0.0404	0.0479	0.0319
		90	0.0455	0.0348	0.0485	0.0341

At K* = 10, a secondary vortex can be noted at the bottom of the cavity for Re=100 with the decrease of Darcy number (i.e. from 10^{-2} to 10^{-3}) which is not so for Re=1000. At Re=100 the inertia of the fluid could not overcome the resistance offered by the porous matrix. But with the increase of Reynolds number the fluid could overcome the resistance and move towards the bottom portions of the cavity. The combination of lower Darcy number and higher permeability ratio (Da = 10^{-3}, K* = 10) make the vortex strength poor and lead to the formation of a secondary vortex. From Fig 6.4 (b) it can be noticed that for Re = 1000 and Da = 10^{-2} with the increase in K* the primary vortex from the centre of the cavity moves towards the upper right corner. As the vortex starts moving towards the right, the secondary vortex which is found at the bottom right corner for K*=0.1 starts diminishing with the increase in K* and disappears at K* = 10. With the increase in K* the influence of porosity can be noticed to reduce which can be empathized due to the decline in the magnitude of permeability in the vertical direction.

Fig. 6.6 shows the variation of ψ_{max} with K* and Da for Re = 100, $\theta = 45^0$ and F* = 1. It may be noted that with the decrease in Da and with the increase in K*, the permeability decreases in the direction of K_2 i.e. resistance offered by the porous matrix increases. Due to the decrease of permeability, the influence of porosity and the value of maximum stream function can be noticed to decrease.

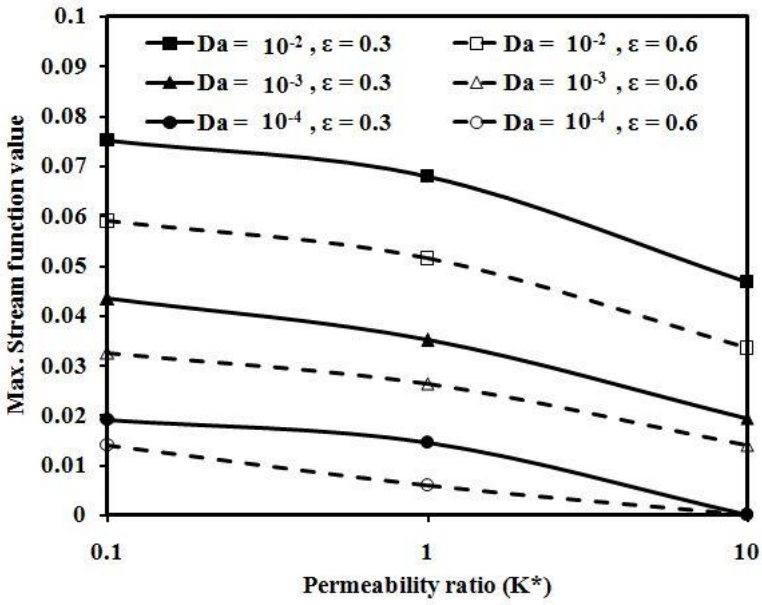

Fig. 6.6. Influence of permeability ratio (K*) on the ψ_{max} with Da for Re = 100, $\theta = 45^0$ and F*=1

6.5.5. Effect of Forchheimer constants ratio (F^*)

Fig. 6.7 shows the streamlines for Re=1000, Da= 10^{-2} and K*=0.1 with the variation of F* (1, 10, 100), θ (0^o, 45^o, 90^o) and ε (0.3, 0.6). Also, Table 6.2 provides the variation of ψ_{max} with Re, F*, ε, θ and K* for Da=10^{-2}. Based on Eqn. (6.8), $F^*=F_1/F_2$ and $F_1 \approx 0.55$ ((Ward (1964); Krishna et al. (2008b)) i.e. the value for F_1 is fixed and with an increase in F* the non-linear drag in F_2 direction decreases. As can be seen from Fig. 6.7, no significant variation in the trend for streamlines is observed with the variation of Forchheimer constants ratio (F^*). Based on the maximum stream function values provided in Table 6.2, the effect of F* is more pronounced at Re=1000 when compared to that of Re=10. Also, for a given value of K*, the influence of F* can be noted to be more for ε = 0.3 when compared to that of 0.6. As F* represents the ratio of Forchheimer constants and its significance comes into picture when inertial forces are dominant. The increase in Reynolds number and a decrease in porosity for a Darcy number leads to an increase in velocity due to which non-linear drag forces become predominant in the non-Darcy regime.

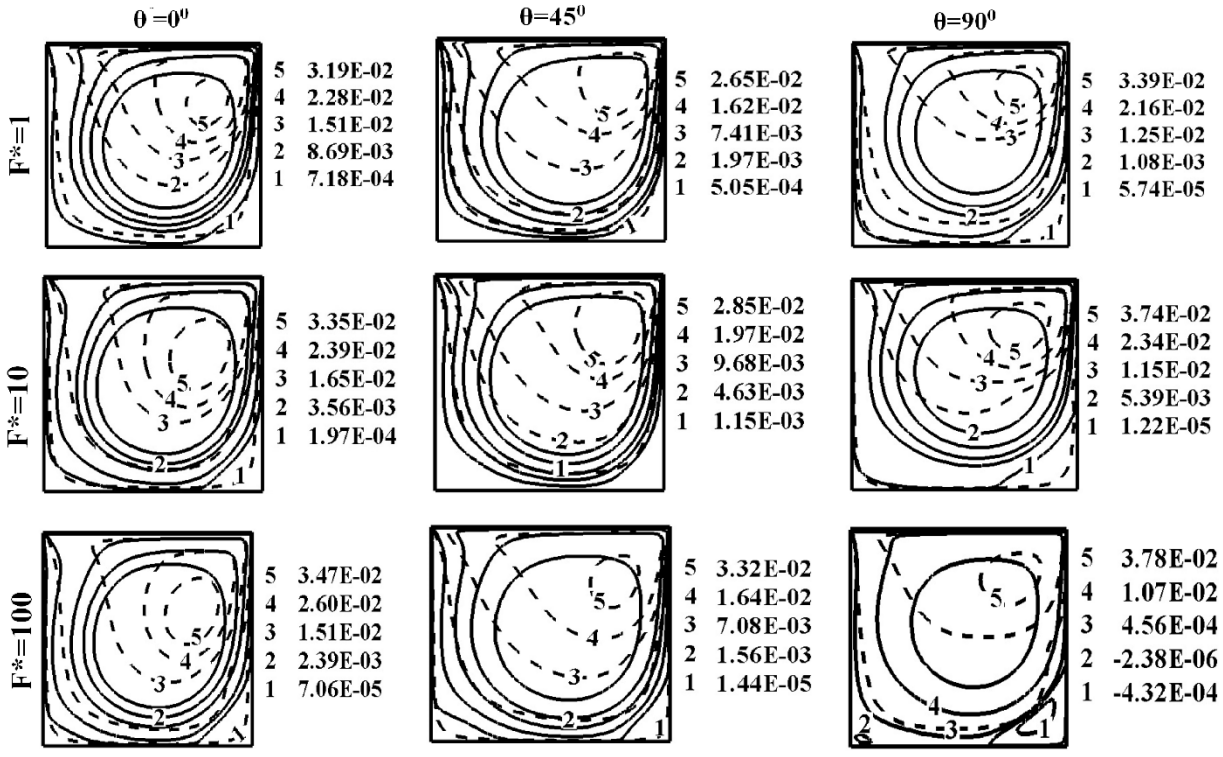

Fig. 6.7. Streamlines for Re=1000, Da=10^{-2} and K*=0.1(solid line ε=0.3, dotted line ε=0.6)

6.5.6. Effect of Principal Axes Inclination (θ)

The streamlines with the variation of θ(0^o, 45^o, 90^o), ε(0.3, 0.6), F*(1, 10, 100) for K*=0.1, Da=10^{-2} and Re=1000 is shown in Fig. 6.7. Also, Table 6.2 provides the maximum stream function values with the variation of K*(0.1, 1, 10), θ (0^o, 45^o, 90^o), ε (0.3, 0.6), F*(1, 10, 100) and Re (10, 1000) for Da=10^{-2}. Based on Eqns. (6.5 and 6.12), for K*<1 the permeability in the direction of K_2 will be greater than K_1 and reverse when K*>1. It can be noticed that as 'θ' increases, the K_1 moves towards the direction of K_2 (Fig. 6.1). For K*= 0.1 as K_2>K_1 the permeability starts decreasing with the increase of 'θ' in the vertical direction and simultaneously increase in the horizontal direction. From the streamlines shown in Fig. 6.7, the vortex can be noted to move towards the right portion of the lid. The reason for this behavior can be inferred to the above explanation of permeability variation in horizontal and vertical directions. In the subsequent sections, the effect of 'θ' on the hydrodynamics with the change of Reynolds number is given.

Re=10

Based on Table 6.2 it is interesting to note that with the variation of 'θ' for Re=10 when K*=0.1 an increasing, and with K*=10 decreasing trends are followed for ψ_{max}. The reason for this behavior can be given due to the variation of permeability in horizontal and vertical directions with 'θ'. For K*=0.1 as $K_2=K_1/K^*$ the magnitude of permeability in K_2 direction is 10 times more to that of K_1. When $\theta=0^o$ the permeability in the vertical direction will be more to that of horizontal. But with the increase of 'θ', the permeability in the horizontal direction starts to increase. This increase in permeability leads to the decrease in obstruction for the circulation of the fluid which results in an increase of ψ_{max}. When K*= 10, the magnitude of K_2 is 10 times less to that of K_1. With the increase of 'θ' as the permeability decreases in the direction of K_2 the maximum stream function value can be noted to decrease.

Re=100

Fig. 6.8 provides the effect of principal axes inclination (θ) on ψ_{max} with the variation of K* and ε for Re=100, Da=10^{-3}, and F*=1. The maximum stream function value for different values of K* (0.1, 1, 10) with the increase of 'θ' follow a similar trend as observed for Re=10. The increase of permeability for K*=0.1 and decrease of permeability for K*=10 in K_2 direction as discussed for Re=10 can be referred to this behavior. As K*=1 refers to the isotropic porous

media, no variation in ψ_{max} is observed. Considerable variation with a similar trend can be noted in ψ_{max} with porosity. The decrease in ψ_{max} with the increase in porosity can be inferred to the decrease in pore velocity.

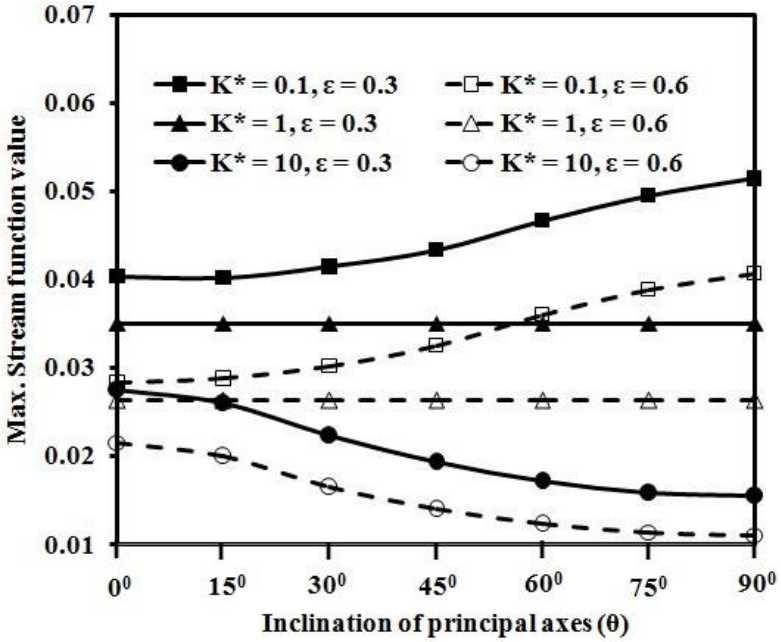

Fig. 6.8. Effect of principal axes inclination (θ) on ψ_{max} with K* for Re =100, Da=10^{-3} and F*= 1

Re=1000

As can be noticed from Table 6.2, the behavior of the maximum stream function value for Re=1000 is not in-line with Re=10 and 100. For K*=0.1, as 'θ' is increased from 0^o – 90^o at first a decreasing and then increasing trend can be noted, whereas for K*=10 an increasing and the decreasing trend is followed. It can be noted that Da=10^{-2} comes under a non-Darcy regime where the influence of non-linear drag forces are significant. This reason can be given for the decrease in the ψ_{max} from Re=10 to 1000. From Fig. 6.1, it can be seen that for K*=0.1 with $\theta=0^o$ the magnitude of permeability is high in the vertical direction, and in the horizontal direction when $\theta=90^o$. At $\theta=45^o$ the porous matrix attains a higher magnitude for permeability inclined at an angle of 45^o to that of vertical and horizontal directions. Due to this behavior of the matrix structure, the fluid will be constrained to move at an angle which results in the reduction of vortex strength by which ψ_{max} reduces. At K*=10, a decrease in permeability (K_2) can be noted. When $\theta=0^o$ the obstruction for flow can be noticed to be more in the vertical direction, and in the

horizontal direction with $\theta=90^o$. But for $\theta=45^o$ as this restriction gets reduced in horizontal and vertical directions the ψ_{max} can be observed to be high.

6.6. CONCLUSIONS

In the present study, lid-driven flow in orthogonal cavity impregnated with anisotropic porous media is investigated numerically by using generalized non-Darcy formulation. The collocated grid based finite volume approach has been adopted to solve the governing equations. The parameters such as Reynolds number (10, 100, 1000), Darcy number ($10^{-5} \leq Da \leq 10^{-2}$), porosity ($\varepsilon$ = 0.3 and 0.6), permeability ratio (K^*=0.1, 1 and 10), Forchheimer constants ratio (F^*=1, 10 and 100) and principal axes inclination ($\theta=0^o$, 45^o and 90^o) have been addressed and the following conclusions can be given.

- At higher Darcy numbers a decrease of maximum stream function value is noticed with the increase of Reynolds number due to the influence of non-linear drag forces.
- For a given Darcy number (permeability) the decrease in porosity leads to an increase in maximum stream function value due to the increase in pore velocity.
- The effect of porosity and Forchheimer constants ratio is observed to be insignificant at a Darcy number of 10^{-5}.
- The vortex is observed to move towards the upper portion (i.e. towards the lid) as the permeability decreases in the vertical direction.
- The influence of the permeability ratio (K*) and principal axes inclination (θ) are observed to play a significant role on hydrodynamics at higher Darcy number (loosely packed porous media). But observed to decrease with the reduction of Darcy number.

6.7. CLOSURE

In this study, lid-driven flow in orthogonal cavity impregnated with anisotropic porous media is investigated by using generalized non-Darcy formulation. The influence of the permeability ratio (K*) and principal axes inclination (θ) are observed to play a significant role on hydrodynamics at higher Darcy number (loosely packed porous media). But observed to decrease with the reduction of Darcy number. The next chapter deals with the numerical analysis of steady-state natural convection inside a square cavity filled with anisotropic porous media.

CHAPTER 7
HEATLINE VISUALIZATION OF BUOYANCY INDUCED FLOWS FOR NON-DARCY ANISOTROPIC POROUS MEDIA

7.1. INTRODUCTION

Fluid flow and heat transfer studies related to free convection in a saturated porous media are being carried out due to its important applications which include geothermal systems (Vafai and Tien (1981)), nuclear reactor safety (Ettefagh et al. (1991)), ground water flow modeling (Lage (1993)), solar power collectors (Saeid and Pop (2005)), food processing (Krishna et al. (2008b)), compact heat exchangers (Swamy et al. (2013) and Sheremet et al. (2015)). It can be noted that most of the real life problems such as extraction of metal alloys from ores, nuclear fuel rod bundle, heat exchanger tubes, geothermal processes etc. are anisotropic in nature. Hence, it is necessary to study the effect of anisotropic properties of the porous medium on the fluid flow and heat transport behavior. Mamou et al. (1998) investigated the problem of natural convection in a cavity filled with anisotropic porous medium. It was reported that permeability ratio and principal axes orientation have more influence on the system stability.

The heatline approach can be used to analyze the performance of thermal systems by visualizing the direction and intensity of heat flow. Visualization of heat flow using heat lines was introduced by Kimura and Bejan (1983). Waheed (2009) numerically studied the natural convection in a square cavity filled with saturated porous medium using heat function formulation solved by finite-difference method. It was concluded that, heatlines and heat function enhance the understanding of distribution of heat in the design of equipment.

Based on the literature review it can be noted that the concept of heatline visualization can help in great detail for the understanding of thermal transport in various structures. But the studies pertaining to heatlines for natural convection filled with non – Darcy anisotropic porous media is yet to appear in literature. Therefore, the present work is aimed to analyze the thermal

hydraulics in a square cavity filled with anisotropic non-Darcy porous medium with the concept of heatline visualization.

7.2. MODEL DESCRIPTION

Fig. 7.1 shows the schematic diagram of a two-dimensional square enclosure filled with anisotropic fluid-saturated porous medium. It is assumed that the solid matrix is homogeneous. No slip condition is applied at the walls. The fluid confined within the porous medium is treated as Newtonian and incompressible. Boussinesq approximation is employed to account for the density variation with respect to temperature. The flow is considered as laminar. Also, a second order velocity term is incorporated in the momentum equations to model the inertia effect. This is more important to analyze convective boundary layer flow over the surface of a body embedded in a high porosity media in non-Darcy regime. The influence of anisotropic parameters (K*, θ, F*, k*) are studied by varying Ra, Da, ε and Pr.

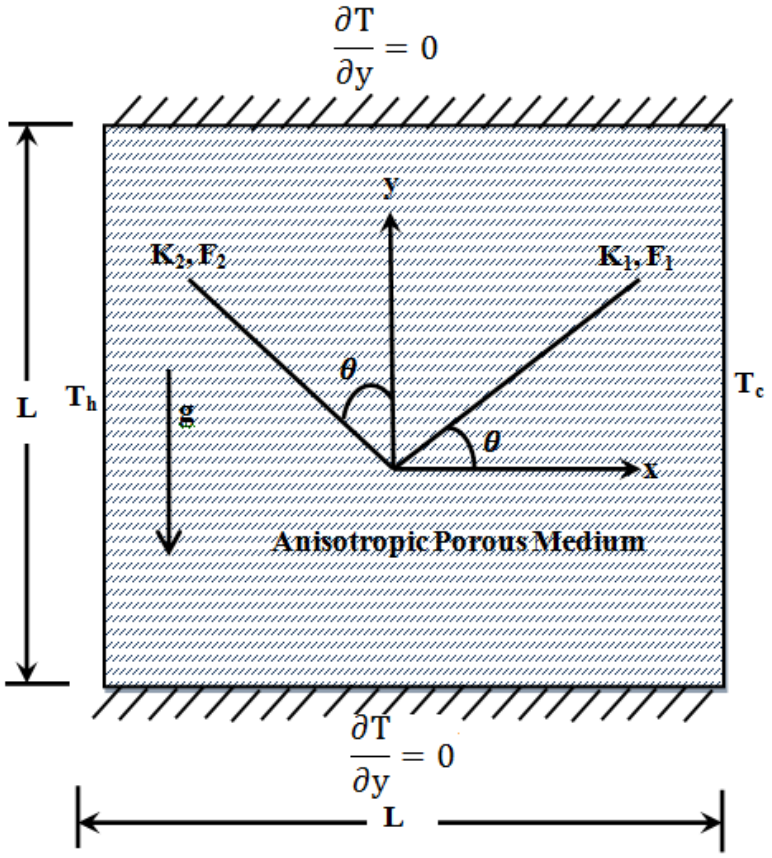

Fig. 7.1. Problem geometry with the boundary condition

7.3. GOVERNING EQUATIONS

The governing equations for buoyancy induced flows for non-Darcy anisotropic porous media are given in Eqns. (7.1 – 7.4) and for heat function are given in Eqns. (7.11 – 7.12). To simplify the analysis, the following assumptions are made

- Properties of the fluid and the porous medium are assumed to be constant
- The cavity walls are impermeable
- Boussinesq approximation is considered to be valid

$$\frac{\partial u}{\partial x}+\frac{\partial v}{\partial y}=0 \tag{7.1}$$

$$\frac{\rho_f}{\varepsilon}\left[\frac{\partial u}{\partial t}+\frac{u}{\varepsilon}\frac{\partial u}{\partial x}+\frac{v}{\varepsilon}\frac{\partial u}{\partial y}\right]=-\frac{\partial P_f}{\partial x}+\frac{\mu_f}{\varepsilon}\left(\frac{\partial^2 u}{\partial x^2}+\frac{\partial^2 u}{\partial y^2}\right)-\frac{\mu_f u}{\bar{\bar{K}}}-\bar{\bar{C}}\rho_f u\sqrt{u^2+v^2} \tag{7.2}$$

$$\frac{\rho_f}{\varepsilon}\left[\frac{\partial v}{\partial t}+\frac{u}{\varepsilon}\frac{\partial v}{\partial x}+\frac{v}{\varepsilon}\frac{\partial v}{\partial y}\right]=-\frac{\partial P_f}{\partial y}+\frac{\mu_f}{\varepsilon}\left(\frac{\partial^2 v}{\partial x^2}+\frac{\partial^2 v}{\partial y^2}\right)-\frac{\mu_f v}{\bar{\bar{K}}}-\bar{\bar{C}}\rho_f v\sqrt{u^2+v^2}+\rho_f\beta g(T-T_c) \tag{7.3}$$

$$\rho_f C_{pf}\left[\frac{\partial(\sigma T)}{\partial t}+u\frac{\partial T}{\partial x}+v\frac{\partial T}{\partial y}\right]=\left[k_x\frac{\partial^2 T}{\partial x^2}+k_y\frac{\partial^2 T}{\partial y^2}\right] \tag{7.4}$$

Where

$$\bar{\bar{K}}=\begin{bmatrix}K_1\cos^2\theta+K_2\sin^2\theta & (K_1-K_2)\sin\theta\cos\theta\\ (K_1-K_2)\sin\theta\cos\theta & K_1\sin^2\theta+K_2\cos^2\theta\end{bmatrix} \tag{7.5}$$

$$\bar{\bar{C}}=\begin{bmatrix}C_1\cos^2\theta+C_2\sin^2\theta & (C_1-C_2)\sin\theta\cos\theta\\ (C_1-C_2)\sin\theta\cos\theta & C_1\sin^2\theta+C_2\cos^2\theta\end{bmatrix} \tag{7.6}$$

$$C_1=\frac{F_1}{\sqrt{K_1}};C_2=\frac{F_2}{\sqrt{K_2}} \tag{7.7}$$

$$F^*=\frac{F_1}{F_2};\ K^*=\frac{K_1}{K_2};C^*=\frac{C_1}{C_2}=\frac{F^*}{\sqrt{K^*}};k^*=\frac{k_y}{k_x} \tag{7.8}$$

By applying inverse to permeability tensor and by substituting $K^*=K_1/K_2$, Eqn. 5 can be reduced to

$$\overline{\overline{K^{-1}}}=\frac{1}{K_1}\begin{bmatrix}K^*\sin^2\theta+\cos^2\theta & (1-K^*)\sin\theta\cos\theta\\ (1-K^*)\sin\theta\cos\theta & K^*\cos^2\theta+\sin^2\theta\end{bmatrix} \tag{7.9}$$

$$\bar{\bar{C}} = \frac{F_1}{\sqrt{K_1}}\begin{bmatrix} \cos^2\theta + \frac{\sqrt{K^*}}{F^*}\sin^2\theta & \left(1 - \frac{\sqrt{K^*}}{F^*}\right)\sin\theta\cos\theta \\ \left(1 - \frac{\sqrt{K^*}}{F^*}\right)\sin\theta\cos\theta & \frac{\sqrt{K^*}}{F^*}\cos^2\theta + \sin^2\theta \end{bmatrix} \tag{7.10}$$

Heat function equation in x and y directions are given by

$$-\frac{\partial H}{\partial x} = \rho C_{Pf} v(T - T_C) - k_y \frac{\partial T}{\partial y} \tag{7.11}$$

$$\frac{\partial H}{\partial y} = \rho C_{Pf} u(T - T_C) - k_x \frac{\partial T}{\partial x} \tag{7.12}$$

Where 'H' is the dimensional heat function.

The following non-dimensional variables are used to non-dimensionalize the governing equations

$$x^* = \frac{x}{L}; y^* = \frac{y}{L}; u^* = \frac{u}{\left(\alpha_x/L\right)}; v^* = \frac{v}{\left(\alpha_x/L\right)};\ Da = \frac{K_1}{L^2}; P^* = \frac{P}{\rho_f U^2}; \alpha_x = \frac{k_x}{\rho_f C_p};\ \tag{7.13}$$

$$t^* = \frac{t}{\left(L^2/\alpha_x\right)}; Pr = \frac{\nu_f}{\alpha_x};\ Ra = \frac{g\beta\Delta T L^3}{\alpha_x \nu_f};\ P^* = \frac{P_f}{\left(\frac{\rho_f \alpha_x^2}{L^2}\right)}; \theta = \frac{T - T_c}{T_h - T_c};\ \Pi = \frac{H}{(T_h - T_c)k_x}$$

Thus, Eqns. (7.1) – (7.4) can be written in non-dimensional form as below. For the sake of convenience '*' is not provided.

$$\frac{\partial u}{\partial x} + \frac{\partial v}{\partial y} = 0 \tag{7.14}$$

$$\left[\frac{1}{\varepsilon}\frac{\partial u}{\partial t} + \frac{u}{\varepsilon^2}\frac{\partial u}{\partial x} + \frac{v}{\varepsilon^2}\frac{\partial u}{\partial y}\right] \tag{7.15}$$

$$= -\frac{\partial P}{\partial x} + \frac{Pr}{\varepsilon}\left(\frac{\partial^2 u}{\partial x^2} + \frac{\partial^2 u}{\partial y^2}\right)$$

$$-\frac{Pr}{Da}\left[u\left(\cos^2\theta + K^*\sin^2\theta\right) + v\left((1 - K^*)\sin\theta\cos\theta\right)\right]$$

$$-\frac{F_1}{\sqrt{Da}}\left[u\left(\cos^2\theta + \frac{\sqrt{K^*}}{F^*}\sin^2\theta\right)\right.$$

$$\left. + v\left(\left(1 - \frac{\sqrt{K^*}}{F^*}\right)\sin\theta\cos\theta\right)\right]\sqrt{u^2 + v^2}$$

$$\left[\frac{1}{\varepsilon}\frac{\partial v}{\partial t}+\frac{u}{\varepsilon^2}\frac{\partial v}{\partial x}+\frac{v}{\varepsilon^2}\frac{\partial v}{\partial y}\right] \tag{7.16}$$

$$= -\frac{\partial P}{\partial y}+\frac{Pr}{\varepsilon}\left(\frac{\partial^2 v}{\partial x^2}+\frac{\partial^2 v}{\partial y^2}\right)$$

$$-\frac{Pr}{Da}\left[u\left((1-K^*)\sin\theta\cos\theta\right)\right.$$

$$\left.+\,v(K^*\cos^2\theta+\sin^2\theta)\right]-\frac{F_1}{\sqrt{Da}}\left[u\left(\left(1-\frac{\sqrt{K^*}}{F^*}\right)\sin\theta\cos\theta\right)\right.$$

$$\left.+\,v\left(\frac{\sqrt{K^*}}{F^*}\cos^2\theta+\sin^2\theta\right)\right]\sqrt{u^2+v^2}+Ra.Pr.\theta$$

$$\frac{\partial(\sigma\theta)}{\partial t}+u\frac{\partial\theta}{\partial x}+v\frac{\partial\theta}{\partial y}=\frac{\partial^2\theta}{\partial x^2}+k^*\frac{\partial^2\theta}{\partial y^2} \tag{7.17}$$

$F_1\approx0.55$ ((Ward (1964); Krishna et al. (2008b)) is considered in Eqns. (7.15) - (7.16).

Boundary conditions with respect to the geometry shown in Fig. 7.1 are as follows

At the left (hot) wall

$$u=0, v=0, \theta=1, x=0,\ \ 0\leq y\leq 1 \tag{7.18}$$

At the right (cold) wall

$$u=0, v=0, \theta=0, x=1,\ \ 0\leq y\leq 1 \tag{7.19}$$

At the bottom and top walls

$$u=0;\ v=0;\ \frac{\partial\theta}{\partial y}=0;\ y=0;\ y=1;\ \ 0\leq x\leq 1 \tag{7.20}$$

The flow behavior is analyzed by using the stream function (ψ), the definition of which is given such that

$$u=\frac{\partial\psi}{\partial y};\ v=-\frac{\partial\psi}{\partial x} \tag{7.21}$$

The heat transfer coefficient in terms of the local Nusselt number at left wall (Nu_l) is defined by

$$Nu_l=\left(\frac{\partial\theta}{\partial x}\right)_{x=0} \tag{7.22}$$

The average Nusselt numbers at the left wall is given by

$$\overline{Nu_l} = -\int_0^1 \frac{\partial\theta}{\partial x}\Big|_{x=0} dy \tag{7.23}$$

The dimension less heat function (Π) value is obtained from conductive heat fluxes $(-\frac{\partial\theta}{\partial y}, -\frac{\partial\theta}{\partial x})$ as well as convective heat fluxes (uθ, vθ).

$$-\frac{\partial\Pi}{\partial x} = v\theta - k^*\frac{\partial\theta}{\partial y} \tag{7.24}$$

$$\frac{\partial\Pi}{\partial y} = u\theta - \frac{\partial\theta}{\partial x} \tag{7.25}$$

Where 'Π' is the non-dimensional heat function for the fluid

Assuming that 'Π' is a continuous function to its second order derivatives yield a single equation for heat function

$$\frac{\partial^2\Pi}{\partial x^2} + \frac{\partial^2\Pi}{\partial y^2} = \frac{\partial(u\theta)}{\partial y} - \frac{\partial(v\theta)}{\partial x} + k^*\frac{\partial^2\theta}{\partial x\,\partial y} - \frac{\partial^2\theta}{\partial x\,\partial y} \tag{7.26}$$

The boundary conditions of non-dimensional heat function are as follows.

A reference value of heat function (Π) is assumed as 0 at x=0, y= 0, hence Π (0,0) = 0.

Bottom wall $(0 < x \leq 1)$

$$\text{At } y = 0: \Pi(x,0) = \Pi(0,0) - \int_0^x \left(v\theta - k^*\frac{\partial\theta}{\partial y}\right) dx = \int_0^x k^*\frac{\partial\theta}{\partial y} dx = 0 \tag{7.27}$$

Left wall $(0 < y \leq 1)$

$$\text{At } x = 0: \ \Pi(0,y) = \Pi(0,0) + \int_0^y \left(u\theta - \frac{\partial\theta}{\partial x}\right) dy = -\int_0^y \frac{\partial\theta}{\partial x}\Big|_{x=0} dy \tag{7.28}$$

Right wall $(0 < y \leq 1)$

$$\text{At } x = 1: \ \Pi(1,y) = \Pi(x,0) + \int_0^y \left(u\theta - \frac{\partial\theta}{\partial x}\right) dy = -\int_0^y \frac{\partial\theta}{\partial x}\Big|_{x=1} dy \tag{7.29}$$

Top wall $(0 < x \leq 1)$

$$\text{At } y = 1: \ \Pi(x,1) = \Pi(0,y) - \int_0^x \left(v\theta - k^*\frac{\partial\theta}{\partial y}\right) dx = -\int_0^y \frac{\partial\theta}{\partial x}\Big|_{x=0} dy = \overline{Nu_l} \tag{7.30}$$

7.4. SOLUTION METHODOLOGY

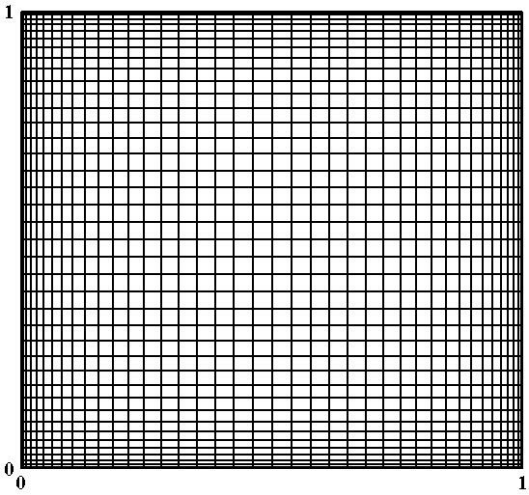

Fig. 7.2. Non-uniform grid (Cosine grid).

The numerical simulations are performed using the finite volume formulation of Eqns. (7.14 - 7.17 and 7.26) with the boundary conditions as given in Eqns. (7.18 - 7.20 and 7.27-7.30). In the present study, the grid is generated by dividing the computational domain into quadrilateral cells. Collocated grid arrangement has been employed where the velocities, pressure, temperature and heat function (u, v, p, T and H) are located at the cell centers as shown in Fig. 3.1. To obtain the values of primitive variables at cell faces, linear interpolation using the values at cell centers is applied which gives second order accuracy. Cosine grid has been considered as shown in Fig. 7.2. The convective terms of Eqns. (7.15–7.17) are discretized using a first order upwind scheme and the diffusion terms with the central difference scheme. The pressure and velocity terms of Eqns. (7.15 – 7.16) are coupled using the SIMPLE algorithm. In order to attain accurate solution, the mass conservation needs to be assured for which convergence criteria need to be given. Based on this criteria the iterative process gets terminated. In the present numerical methodology convergence criterion is given by Eqn. (7.31) and is set to 10^{-8}.

$$\frac{\sum_{i,j}\left|\Phi_{i,j}^{n}-\Phi_{i,j}^{n-1}\right|}{\sum_{i,j}\left|\Phi_{i,j}^{n}\right|}<10^{-8} \tag{7.31}$$

Where Φ refers to u, v, θ and Π variables

It may be noted that for the employed porous media formulation a convergence criterion of 10^{-8} is observed to satisfy the mass conservation. With a further decrease in convergence criteria, no difference in end solution is noted but significantly increased the computational time. To attain solution for all depended variables in Eqns. ((7.15-7.17) and (7.26)) an under relaxation factor is taken as 0.4.

7.5. GRID INDEPENDENCE STUDY AND VALIDATION

Grid independence study is important to determine the grid size that should be used. In the present study non-uniform (cosine) grid has been considered as shown in Fig. 7.2. The grid independence study is carried out for the case: Ra = 10^7, Da = 10^{-6}, ε = 0.4, θ = 0°, K* = 1, k* = 1, F*=1 and Pr = 1. It is observed that the percentage deviation between 41 × 41 and 61 × 61 is less than 1%. Therefore, a grid size of 41× 41 is considered for the simulations.

7.5.1. Validation

The correctness of the developed numerical algorithm is tested with the classical problem of differentially heated porous cavity. For the code validation, a square porous cavity with differential isothermal vertical walls and adiabatic horizontal walls is considered. Based on Eqn. (7.13) it can be noted that Darcy number is given by permeability to reference length square. As permeability refers to hydraulic conductivity, with the increase of permeability (Darcy number) to very large value the restriction of the solid matrix should be reduced to zero. Also, as the porosity is defined as the ratio of void volume to the total volume and with $\varepsilon \rightarrow 1$, the void volume should tend to total volume. By referring to the details of Darcy number tending to a very large value and porosity tending to one, the porous media should behave as a fluid. To check the validity of present formulation the average Nusselt number is calculated for different Rayleigh numbers (Ra = 10^3, 10^4,10^5 and 10^6) and by taking remaining parameters as K* = 1, k* =1, F* =1, θ = 0^o, Pr = 0.71, Da =10^6, ε =0.9999. The numerical results are compared with the available published works of Davis and Jones (1983) and Krishna et al. (2008) and is shown in Table 7.1. To check the robustness for a wide range of isotropic and anisotropic parameters the obtained results are compared with (Nithiarasu et al. (1997), Ni and Beckermann (1991), and Krishna et al. (2008b)) and are given in Table 7.2. Further to check the robustness and validity of the present numerical methodology and code for anisotropic porous media the comparison is

Table 7.1: Comparison of present work with literature for fluid (K* = 1, k* =1, F* =1, θ = 0º, Pr = 0.71, Da =10^6, ε =0.999)

S.No	Ra	Average Nusselt number		
		Davis and Jones (1983)	Krishna et al. (2008b)	Present
1	10^3	1.116	1.128	1.143
2	10^4	2.234	2.244	2.252
3	10^5	4.51	4.526	4.515
4	10^6	8.798	8.846	8.779

Table 7.2: Comparison of present work with literature for porous media with F* =1 and Pr = 1

S.No	Ra	Da	ε	K^*	k*	θ°	Average Nusselt number		
							Nithiarasu et al. (1997)	Krishna et al. (2008b)	Present
1	10^8	10^{-6}	0.9	1	1	0	3.00	3.07	3.129
2	10^7	10^{-6}	0.4	1	1	0	1.079	1.086	1.077
3	10^6	10^{-4}	0.6	1	1	0	2.725	2.706	2.646
4	10^5	10^{-4}	0.4	1	1	0	1.067	1.072	1.064
5	$5x10^5$	10^{-2}	0.9	1	1	0	6.70	6.61	6.109
6	10^4	10^{-2}	0.6	1	1	0	1.53	1.498	1.460
7	10^3	10^{-2}	0.4	1	1	0	1.01	1.01	1.008
8	$5 x10^5$	10^{-3}	0.6	10^{-3}	1	90	4.560	4.489	4.688
9	$5 x10^7$	10^{-5}	0.6	10^2	1	45	1.174	1.122	1.149
10	$5 x10^5$	10^{-3}	0.6	10^2	1	45	1.170	1.121	1.126
11	$5 x10^5$	10^{-3}	0.6	10^{-2}	1	0	4.729	5.064	5.364
							Ni and Beckermann (1991)	Krishna et al. (2008b)	Present
12	10^8	10^{-6}	0.9	1	0.1	0	3.721	3.645	3.715
13	10^8	10^{-6}	0.9	1	1	0	3.102	3.070	3.139
14	10^8	10^{-6}	0.9	1	10	0	1.842	1.871	1.918
15	10^9	10^{-6}	0.9	1	0.1	0	14.297	13.849	14.210

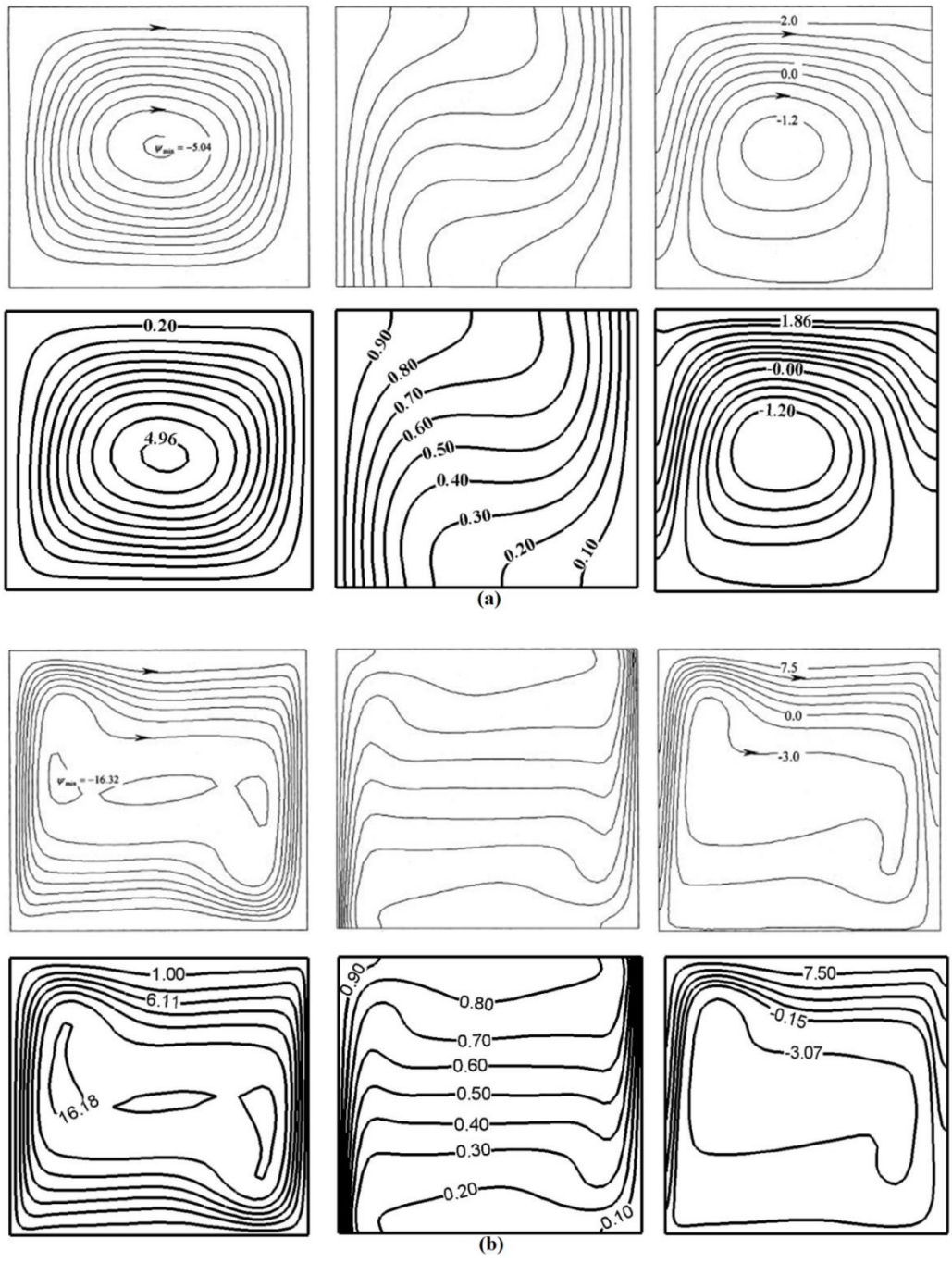

Fig. 7.3. Comparison of the Streamline (left), isotherm (center), heatline (right) of the present work (bottom row) by taking Da =10^6, ε =0.999, K* = 1, k* =1, F* =1, θ = 0^o and Pr = 0.71 with Biswal and Basak (2015) (top row) at (a) Ra = 10^4 and (b) Ra = 10^6 for fluid.

made with Biswal and Basak (2015). Fig. 7.3 shows the comparison in terms for streamlines, isotherms and heatlines with the classical problem of differentially heated cavity with fluid for Ra = 10^4 and Ra =10^6. Based on the results shown in Tables (7.1 and 7.2) and Fig. 7.3 it can be noted that the present methodology is good agreement with the literature and can be extended further for parameters investigation.

7.6. RESULTS AND DISCUSSION

This section illustrates the influence of various non-dimensional parameters such as permeability ratio (K*= 0.1, 1 and 10), inclination of principal axes (θ= 0°, 45° and 90°), ratio of Forchheimer constants (F* = 1, 10 and 100), Prandtl number (Pr = 0.1,1 and 10) and thermal conductivity ratio (k* = 0.1, 1 and 10) on the heat and fluid flow behavior. The Rayleigh number (Ra) is varied from10^3 to 10^6, Darcy number is varied from 10^{-5} to 10^{-2} and porosities of 0.3 and 0.6 have been considered. The results are described in terms of streamlines, isotherms, heatlines and average Nusselt number. In the subsequent sections, initially, the effect of Ra, Da and ε are discussed and later the influence of anisotropic properties (K*, F*, k* and θ) on thermal transport has been addressed.

7.6.1. Effect of Rayleigh number (Ra)

Fig.7.4 provides the streamlines, isotherms and heatlines for Rayleigh numbers 10^3 and 10^6. It was observed that for Ra ≥10^7, the flow instability is observed due to which the code got diverged. Hence, the study is restricted to Ra ≤ 10^6. Other parameters are kept constant and are equal to Da = 10^{-3}, θ = 0º, K* = 1, k* = 1, F* = 1, Pr = 1, ε = 0.3 (solid line) and ε = 0.6 (dotted line). At Ra = 10^3, viscous force prevail over buoyancy force and hence circulation of the fluid is not observed to be effective. With the increase in Rayleigh number (Ra = 10^6), the intensity of the circulation inside the enclosure increased. Because of this, higher vortex strength is attained for higher Rayleigh number (Ra = 10^6), while the vortex strength is less for lower Ra (Ra=10^3). The increase in vortex strength lead to proper mixing of the fluid which enhanced the heat transfer and hence increase in average Nusselt number is observed as shown in Table 7.3. At Ra=10^3, the circulation is very weak and hence it can be regarded as conduction dominant

phenomenon. Hence, the isotherms are parallel to each other just like in the case of pure conduction. On the other hand, for Ra = 10^6, because of the circulation of fluid, the isotherms tend to move from left bottom corner to top right corner of the enclosure.

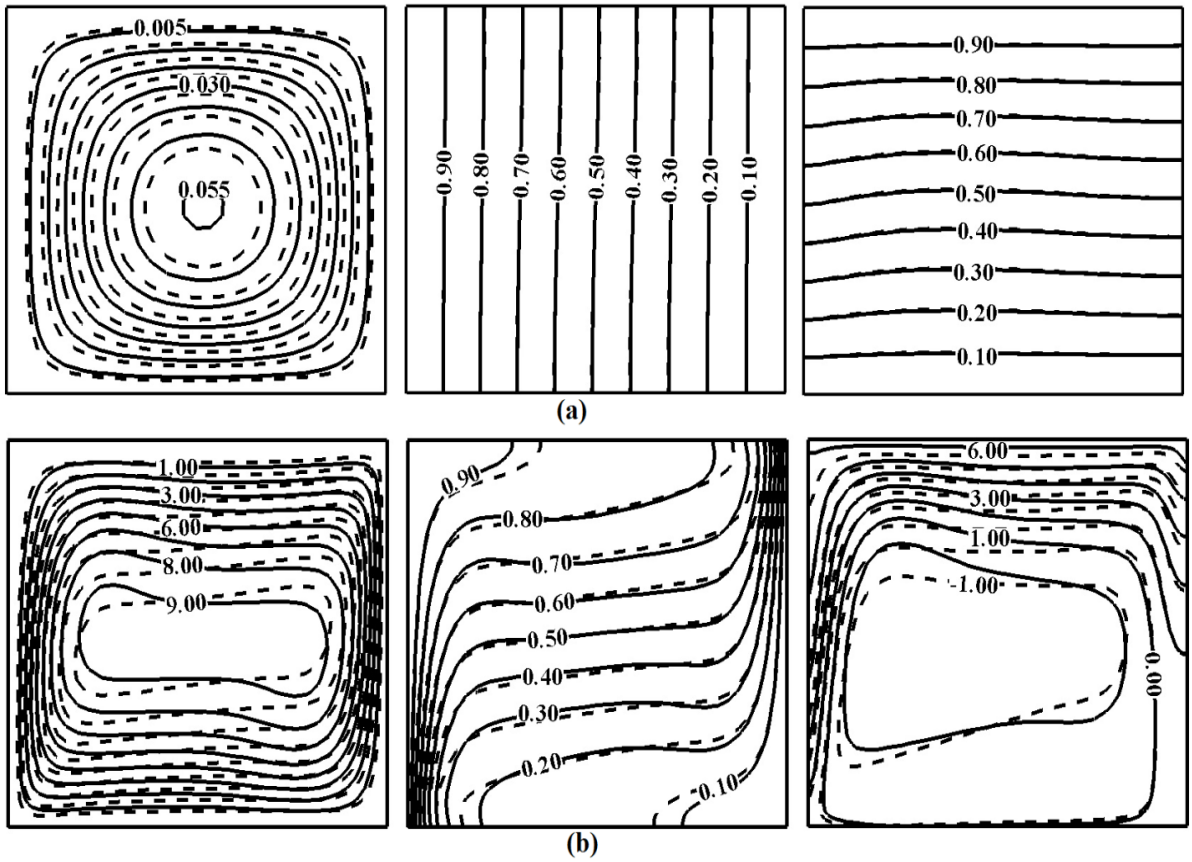

Fig. 7. 4. Streamline (left), isotherm (center), heatline (right),(a) Ra = 10^3 and (b) Ra = 10^6 when Da = 10^{-3}, θ = 0°,K* = 1, k* = 1,F* = 1, Pr = 1, ε = 0.3 (solid line) and ε = 0.6 (dotted line).

The magnitude of heat function increased with the increase in Rayleigh number as can be seen from heatline contours. This indicates the enhancement in heat transfer with the increase in Rayleigh number. The heatline show the path of heat flow from hot to cold region. As can be observed from the heatline contours, at lower Rayleigh number as there is no strong circulation, heatlines are perpendicular to isotherms. At Ra=10^6, the closed loop heatlines at the center of the cavity represents the thermal mixing at the center of the cavity.

Table 7.3. Variation of Average Nusselt number (Nu_{avg}) with Ra, Da, ε, K*, Pr and k* for F* =1, θ = 0°

Figure	Ra	Da	Pr	K*	k*	Average Nusselt number(Nu_{avg})	
						ε = 0.3	ε = 0.6
7.4	10^3	10^{-3}	1	1	1	1.003	1.003
	10^6					4.878	5.541
7.5	10^5	10^{-2}	1	1	1	2.759	3.322
		10^{-6}				1.014	1.014
7.6	10^4	10^{-2}	0.1	1	1	1.162	1.226
			1			1.291	1.460
			10			1.320	1.529
7.7	10^5	10^{-4}	1	0.1	1	1.168	1.185
				1		1.062	1.066
				10		1.004	1.004
7.10	10^5	10^{-3}	1	1	0.1	2.265	2.478
					1	1.956	2.121
					10	1.344	1.407

7.6.2. Effect of Darcy number (Da)

Darcy number is the non-dimensional form of permeability. The increase in Da, enhance the vortex strength and heat transfer rate. The effect of Darcy number on the flow behavior, isotherms and heat flow is depicted in Fig. 7.5. Two Darcy numbers 10^{-2} and 10^{-6} are considered and other parameters are kept constant at Ra = 10^5, θ = 0^o, K* = 1, k* = 1, F* = 1 and Pr = 1. The variation of average Nusselt number with Darcy number is given in Table 7.3.

It is observed that the fluid circulations are strongly dependent on Darcy number (Da). At higher Da =10^{-2}, the ability of the fluid to flow through solid matrix increases because of the higher permeability. This is depicted in Fig. 7.5 (a) in which the denser streamlines can be observed. The maximum value of stream function $|\psi|_{max}$ is observed as 5.0. The features of the

heat flow behavior are explained with the help of heatlines. From Fig. 7.5(a) it can be observed that the heatlines are denser at the left wall which represents the higher heat transfer

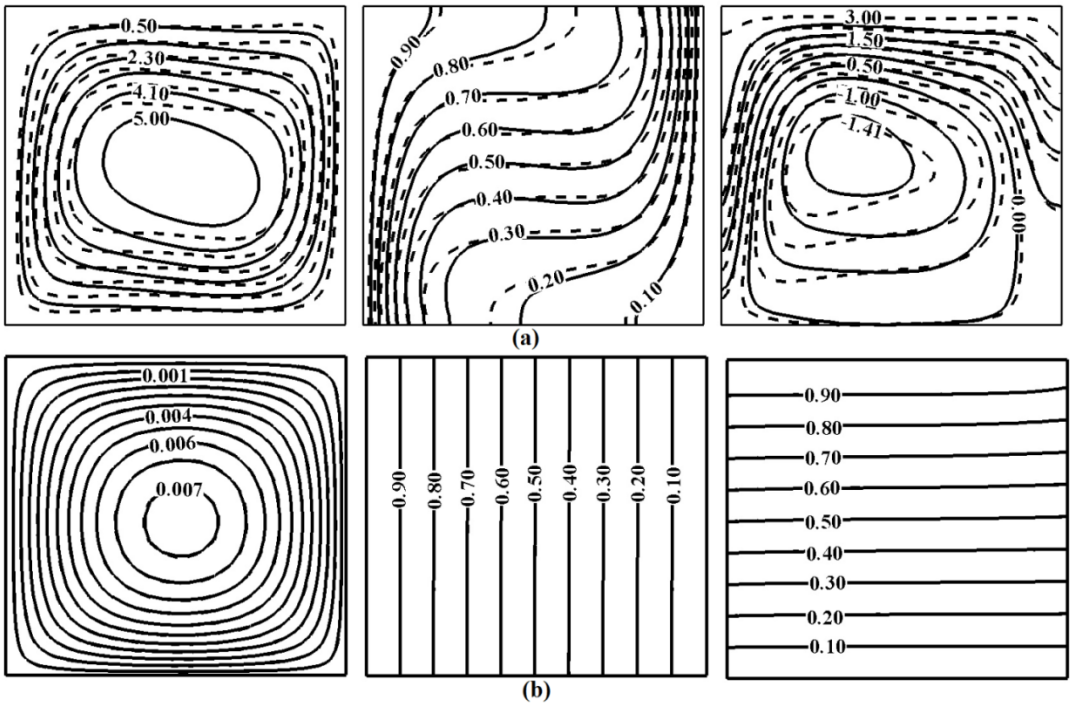

Fig. 7.5. Streamline (left), isotherm (center) and heatline (right) (a) Da = 10^{-2}; (b) Da = 10^{-6} when Ra = 10^5, θ = 0°,K* = 1, k* = 1,F* = 1, Pr = 1, ε = 0.3 (solid line) and ε = 0.6 (dotted line)

rate. End to end heatlines are formed at the top portion of the cavity, whereas closed loop heatlines can be observed at the center of the cavity. These closed loop heatlines represent effective thermal mixing.

From the Fig. 7.5 (b) it can be observed that the magnitude of stream function values for Da=10^{-6} are relatively small when compared to the stream function values for Da=10^{-2}. For Da=10^{-6}, the maximum value of stream function $|\psi|_{max}$ is found to be 0.007. This denotes that the circulation of fluid is considerably weaker at low Darcy numbers and hence rate of heat transfer is observed to be less. Heat flow template inside the cavity is explained by heatlines. Because of the conduction dominant phenomenon at low Darcy number, the heatlines are observed to be orthogonal to the isotherms Fig. 7.5(b). Uniform heat function gradients are observed due to uniform temperature gradients.

7.6.3. Effect of Porosity (ε)

The porosity for most of the materials used for engineering applications varies from 0.2 (tightly packed sand) to 0.93 (loosely packed metal foam). However, in the present study the influence of porosity on thermal-hydraulics has been investigated by varying Rayleigh number, Darcy number, permeability ratio, Forchheimer constants ratio, inclination of principal axes, and thermal conductivities ratio. The applications with porosities of 0.3 and 0.6 include sand (0.37-0.5), rod bundle (0.214-0.9), heat sink (≈0.6), etc. due to which the porosities of 0.3 and 0.6 have been considered. The details pertaining to variation of average Nusselt number with porosity is given in Table 7.3. Porosity is defined as ratio of void volume to total volume. With the increase in porosity, flow area increases which leads to higher convective strength of fluid. Hence, the heat transfer rate got increased with the increase in porosity. However, it is observed that for the flows which are conduction dominant i.e. lower Rayleigh number and lower Darcy number, the effect of porosity becomes less predominant. Same can be observed from Fig. 7.4 (a) and Fig.7.5 (b) in which effect of porosity is depicted. At $Ra=10^3$, an average Nusselt number of 1.003 is obtained for porosities 0.3 and 0.6. On the other hand, an increase in Nusselt number of 13.58% is observed by changing the porosity from 0.3 to 0.6 at $Ra=10^6$. Similar kind of results are obtained for variation in Darcy number also. Hence, it can be concluded that the effect of porosity is not significant for conduction dominant flows.

7.6.4. Effect of Prandtl number (Pr)

Prandtl number is defined as the ratio of momentum diffusivity to thermal diffusivity of the fluid. The effect of Prandtl number is studied by varying 'Pr' from 0.1 to 10. The Prandtl number for air is 0.6 and for water it is about 7. As most of the thermal equipment deals with the above fluids the Prandtl number of 0.1 (near to 0.6) and 10 (near to 7) has been considered. The influence of 'Pr' on flow behavior and Nu_{avg} is shown in Fig. 7.6 and given in Table 7.3. Increase in the 'Pr' increases the flow circulation and hence the convective strength increased. Enhanced convective strength lead to enhanced thermal mixing and hence increase in the Nusselt number is observed. From Fig. 7.6 it can be observed that the maximum stream function value increased with the increase in Pr. Maximum heat function value increased from 0.97 to 1.4 which indicates

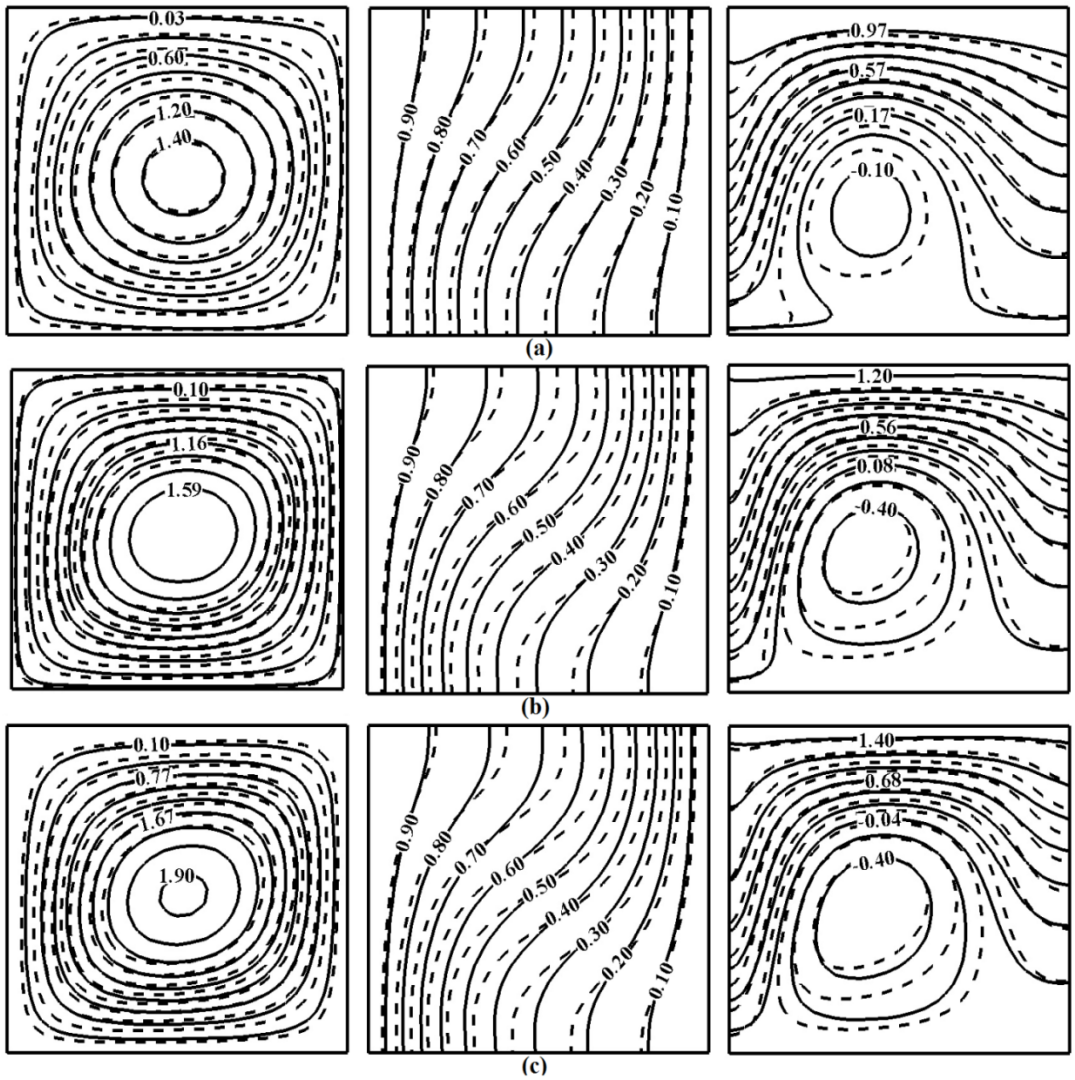

Fig. 7.6. Streamline (left), isotherm (center), heatline (right) (a) Pr = 0.1 (b) Pr = 1 and (c) Pr = 10 for Ra = 10^4, Da = 10^{-2} , θ = 0°,K* = 1, k* = 1,F* = 1, ε = 0.3 (solid line) and ε = 0.6 (dotted line).

the increase in heat transfer rate with the increase in 'Pr'. Same can be observed from the heatlines plot. At higher Pr, the maximum heat function value is 1.4, whereas at Pr = 0.1 maximum heat function value is observed to be 0.97. Heatlines are observed to be compressed at top and left walls of the cavity at Pr=10 when compared to heatlines at Pr=0.1.

7.6.5. Effect of Permeability Ratio (K*)

The influence of permeability ratio (K*) on thermal hydraulics is shown in Fig.7.7 and the variation of average Nusselt number with K* is given in Table 7.3. Permeability ratio is defined

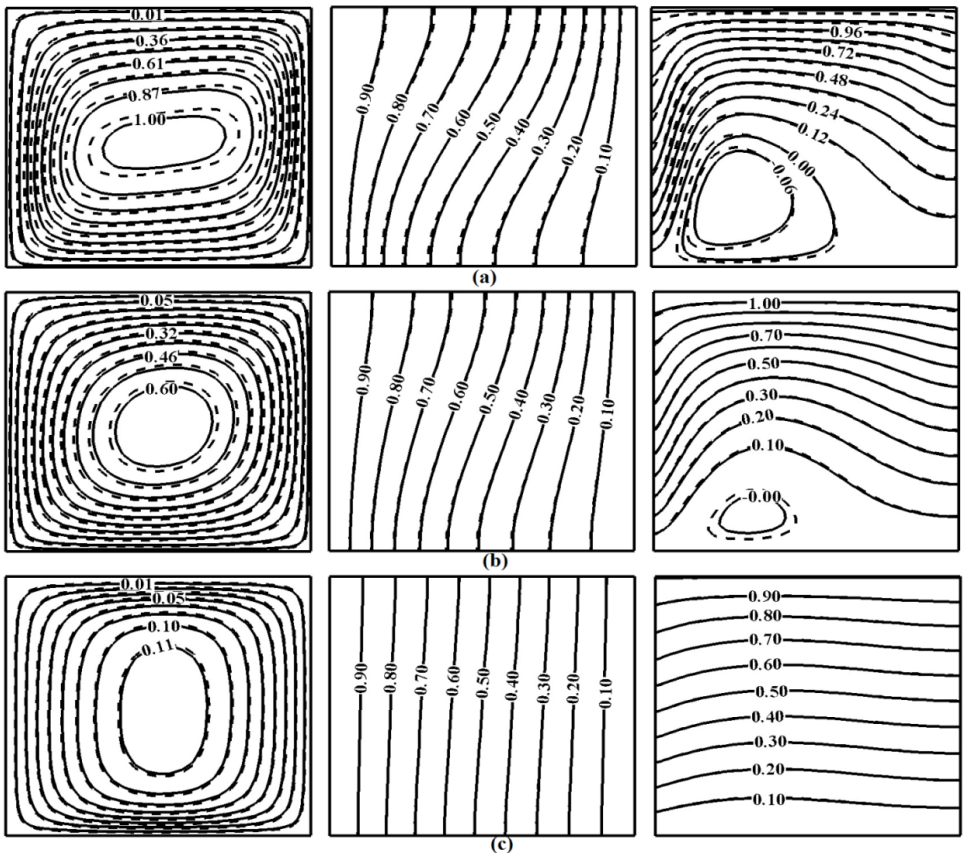

Fig. 7.7. Streamline (left), isotherm (center), heatline (right) (a) K* = 0.1 (b) K* = 1 and (c) K* = 10 for Ra = 10^5, Da = 10^{-4} , θ = 0º,Pr = 1, k* = 1,F* = 1, ε = 0.3 (solid line) and ε = 0.6 (dotted line).

as the ratio of permeabilities in principal axes directions (K_1/K_2). Here, positive-x and positive-y axes are taken as principal axes i.e. inclination of principal axes is zero. It may be noted that K* = K_1/K_2 and Da = K_1/L^2. For a given Darcy number, K_1 remains fixed and with the variation of K*, the magnitude in the direction of K_2 changes. For K* = 0.1, the permeability in vertical direction (K_2) is 10 times more than horizontal direction (K_1). Hence, for lower permeability ratio, the resistance to the flow in vertical direction is less when compared to the resistance in horizontal direction due to which Nu_{avg} is more. It can be observed that the streamlines are closely spaced near left and right walls for lower permeability ratio (K*=0.1). With the increase in permeability ratio the resistance to flow in vertical direction increases with no change in resistance in horizontal direction. This leads the flow to be dominant in horizontal direction and hence the streamlines are closely spaced at top and bottom walls which can be observed in Fig. 7.7 (c) and makes the phenomenon to be conduction dominant. For higher permeability ratio, heat lines and

isotherms are nearly perpendicular which confirmed the flow as conduction dominant. As discussed in the previous section (7.6.3), effect of porosity is negligible for conduction dominant flow for K*=10.

With the increase in permeability ratio closed loop heatlines tend to vanish which represents the reduction in thermal mixing. This means that at higher permeability ratio i.e. at K*=10, convective heat transfer gets nullified and hence heatlines become perpendicular to isotherms. At lower permeability ratio the heatlines are observed to be denser which shows the higher heat transfer rate. On the other hand, for higher permeability ratio, the heatlines are widely spaced which means that the heat transfer rate is less.

7.6.6. Effect of Forchheimer constants ratio (F^*)

Fig. 7.8 describes the effect of Darcy number (Da) on the average Nusselt number with different Forchheimer constants ratio (F*). The highest permeability (Da = 10^{-2}) and lowest non-linear drag (F* = 10 and 100) cause minimum obstruction for the flow field and result in higher average Nusselt number. Therefore, maximum vortex strength occurred for Da = 10^{-2} and F*=100. As Da decreased from 10^{-2} to 10^{-5} the obstruction for the flow field increased. The effect of porosity and non-linear drag of solid matrix is nullified, which can be observed from Fig. 7.8.

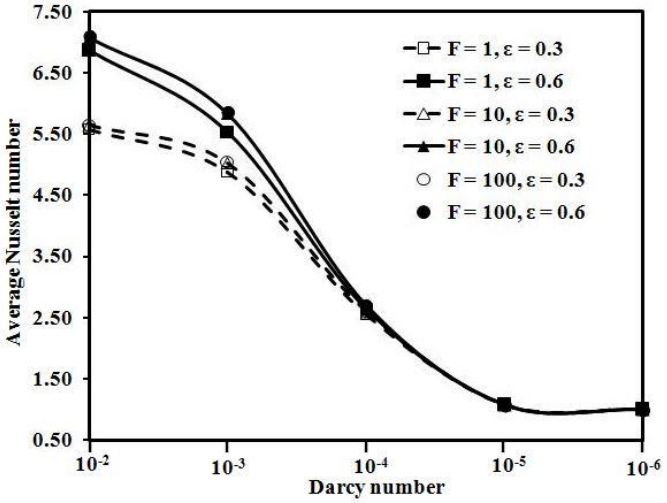

Fig. 7.8. Effect of Darcy number (Da) on the average Nusselt number (Nu_{avg}) with the variation of Forchhemier constants ratio (F*) for Ra = 10^6, θ = 45°, K* = 1, Pr=1, F* = 1, k*=1.

Darcy number can be given as the non-dimensional form of permeability. The permeability can be inferred to the hydraulic conductivity of the medium. With the decrease of Darcy number, the obstruction for the flow increases. For Da $\leq 10^{-5}$ the porous media can be classified in non-Darcy regime where the thermal transport is conduction dominant. As the circulation of fluid is observed to be weaker at low Darcy numbers (Da = 10^{-5} and 10^{-6}) the heat transfer is noted to be by conduction. Because of the conduction dominant phenomenon at Da = 10^{-5} and 10^{-6} the average Nusselt number is observed to be minimum.

7.6.7. Effect of principal axes inclination (θ)

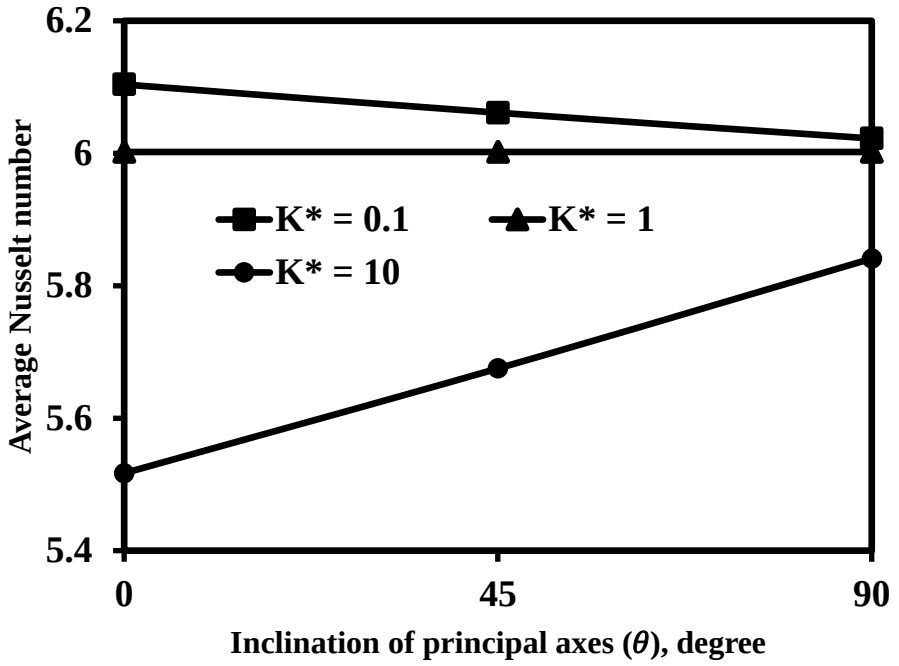

Fig. 7. 9. Effect of inclination of principal axes (θ) on the average Nusselt number (Nu_{avg}) with the variation of permeability ratio (K*) for Ra = 10^6, Da = 10^{-2}, Pr = 1, k* = 0.1, F* = 1, ε = 0.3.

The orientation of principal axis influences the permeability in horizontal and vertical directions. The variation of average Nusselt number with change in 'θ' for different K* values is given in Fig. 7.9. For the same permeability ratio, permeabilities in horizontal and vertical directions vary for different inclinations of principal axes. If permeability ratio is less than 1 as $K^* = K_1/K_2$ with the increase in inclination, permeability in vertical direction decreases

(Fig. 7.1). This leads to conduction dominant flow and hence decrease in average Nusselt number is observed. If K*>1, with the increase in inclination of principal axes, permeability in vertical direction increases. Therefore, the convective strength and hence heat transfer rate increases. Because of this an increase in average Nusselt number is observed for K*=10. If K*=1 as K_1 = K_2 irrespective of the inclination of principal axes, Nusselt number remains same which can be observed in Fig. 7.9.

7.6.8. Effect of thermal conductivity ratio (k*)

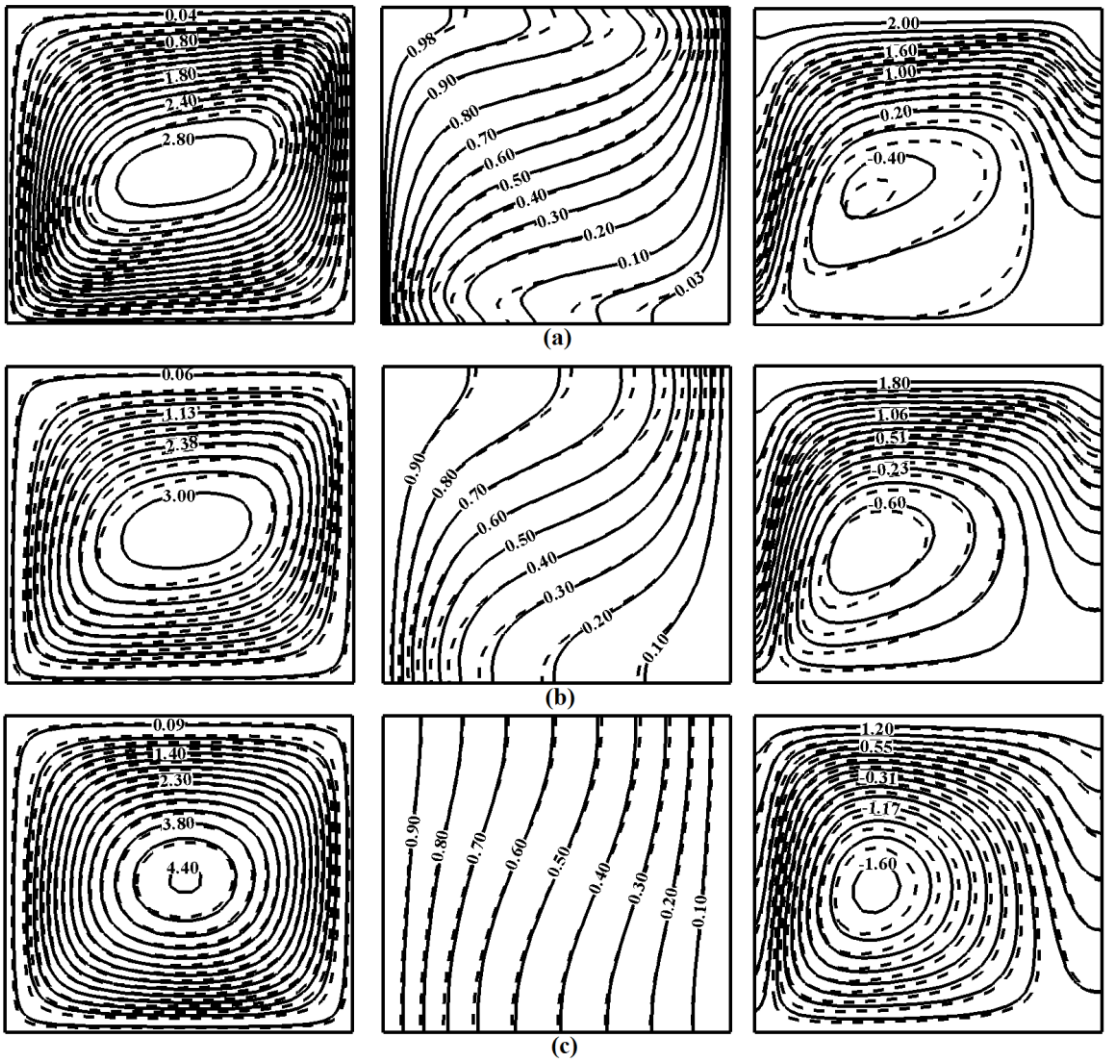

Fig. 7.10. Streamline (left), isotherm (center), heatline (right) (a) k* = 0.1, (b) k* = 1 and (c) k* = 10 for Ra = 10^5, Da = 10^{-3}, θ = 0°, Pr = 1, K* = 1, F* = 1, ε = 0.3 (solid line) and ε = 0.6 (dotted line).

Thermal conductivity ratio is defined as the ratio of thermal conductivities in y and x directions (k_y/k_x). For k* = 0.1, the thermal conductivity in horizontal direction is 10 times more than that of thermal conductivity in vertical direction. The higher thermal conductivity in horizontal direction contributes to effective thermal transport. This leads to faster rise in temperature of the fluid and because of density variation, the fluid tends to move upwards. This ensures effective circulation of the fluid. Fig. 7.10 and Table 7.3 provides the variation of flow behavior and Nu_{avg} with 'k*'.

It can be noted that due to effective circulation the streamlines shown in Fig. 7.10 (a) can be observed to be much closer representing larger magnitude for velocity near the walls due to which the Nu_{avg} is more for k* = 0.1. With the increase in k*, thermal conductivity in vertical direction increases. Hence, the thermal transport becomes effective in vertical direction. For k* = 10 the velocity magnitude near the vertical walls is observed to be less when compared to that of k* = 0.1 due to which lower Nu_{avg} is observed. Based on heatline contours shown in Fig. 7.10 the maximum magnitude for heat function for k* = 0.1 can be noted to be 2.00 and with k* = 10 is 1.2. As the heat function value provides the magnitude of heat flow the thermal transport with k* = 0.1 can be considered to be more when compared with k* = 1 and 10.

7.7. CONCLUSIONS

An in-house code is developed to analyze the thermal transport for a square cavity filled with anisotropic porous medium. The solution methodology is based on SIMPLE algorithm and finite volume approach is employed. Parametric analysis is carried out by varying different anisotropic parameters and the following conclusions are drawn.

- Increase in Rayleigh number lead to enhanced vortex strength which resulted in higher average Nusselt number. The closed loop heatlines are observed at higher Ra which represents the enhanced heat transfer.
- Heat transfer rate is increased by increasing the Darcy number. Denser heatlines are observed at left and top walls which resulted in enhanced thermal transport.
- Increase in permeability ratio resulted in flow to be dominant in horizontal direction which is the case of poor mixing of fluid. Hence, average Nusselt number decreased. Closed loop heatlines have diminished with the increase in permeability ratio.

- Increase in Prandtl number leads to enhanced heat transfer rate. Same conclusion can be drawn from the contours of heatlines which are compressed at higher Pr.
- Increase in thermal conductivity ratio caused reduction in average Nusselt number
- Inclination of principal axes also has influence on the heat transfer rate depending upon permeability ratio.
- The effect of porosity is observed to be negligible for scenarios which are conduction dominant.

7.8 CLOSURE

In this chapter the numerical analysis of steady-state natural convection inside a square cavity filled with anisotropic porous media using generalized non-Darcy model is presented. The results are presented in terms of streamlines, isotherms, heatlines and average Nusselt number. The heatlines are plotted to visualize the path of the thermal transport. The anisotropic behavior of the porous matrix is observed to significantly influence the thermal hydraulics.

CHAPTER 8
CONCLUSIONS AND SUGGESTIONS FOR FUTURE WORK

8.1. INTRODUCTION

In this study, a numerical code has been developed for the visualization of thermal transport in various solid domains and anisotropic porous media. Pertaining to modeling of flow through anisotropic porous media generalized non – Darcy formulation has been employed. A finite volume method based in – house code is developed to analyze the flow and heat transport characteristics. The previous chapters have been devoted to the description of research problems and the work carried out, to fulfill the objectives set for the present study.

Discussions of results obtained for each problem were presented in the respective chapters. However, for the sake of completeness, the overall conclusions that resulted from the study are presented next. The scope of future work is also identified at the end of the chapter.

8.2. OVERALL CONCLUSIONS FROM THE PRESENT STUDY

- Non – orthogonal solid domains with and without discrete heat sources:
  - A numerical code in C^{++} has been developed to read the mesh from GAMBIT and linked to the in – house finite volume method code for the visualization of thermal transport.
  - The study pertaining to thermal transport in various shapes could reveal that for a domain with lower thermal conductivity the magnitude of temperature increases with the increase in size.
  - Visualization of heatlines provide a better insight of energy transport in various solid domains with discrete heat sources.
- Anisotropic porous media:
  - An in house numerical code for anisotropic porous media based on generalized non – Darcy formulation has been satisfactorily validated for wide range of porous media i.e. Darcy and non – Darcy regimes.

- At higher Darcy numbers a decrease of maximum stream function value is noticed with the increase of Reynolds number due to the influence of non-linear drag forces.
- For a given Darcy number (permeability) in non – Darcy regime, the decrease in porosity leads to the increase in maximum stream function value due to the increase in pore velocity.
- The influence of the permeability ratio (K*) and principal axes inclination (θ) are observed to play a significant role on thermal hydraulics at higher Darcy number (loosely packed porous media). But observed to decrease with the reduction of Darcy number.
- Increase in Rayleigh number leads to enhanced vortex strength which resulted in higher average Nusselt number.
- Heat transfer rate is increased by increasing the Darcy number as denser heatlines are observed at left and top walls which resulted in enhanced thermal transport.
- The average Nusselt number is observed to increase with the increase in Prandtl number due to the enhancement of convective strength.
- Analysis of heat transport for anisotropic porous media in terms of isotherms, streamlines and heatlines provide a better insight.

8.3. SUGGESTION FOR FUTURE WORK

- The study can be extended to natural convective heat transfer problems for non-orthogonal geometries with anisotropic non-Darcy porous media through heatline visualization.
- It would be interesting to analyze the thermal transport via heatline visualization for buoyancy induced flows with heat generating anisotropic porous media.
- Heatline visualization for anisotropic porous media using a non – thermal equilibrium approach can be studied.
- The analysis of thermal-hydraulics with nanofluids in anisotropic porous media will be a potential topic to study.

REFERENCES

1. Ahmed, Sameh E.,Mixed Convection in Thermally Anisotropic Non-Darcy Porous Medium in Double Lid-Driven Cavity Using Bejan's Heatlines, *Alexandria Eng. J.*, vol. **55**, no. 1, pp. 299–309, 2016. https://doi.org/10.1016/j.aej.2015.07.016
2. Ahmed, Sameh Elsayed and Rashad, A. M., Natural Convection of Micropolar Nanofluids in A Rectangular Enclosure Saturated with Anisotropic Porous Media, *J. Porous Media*, vol. **19**, no. 8, pp. 737–750, 2016. https://doi.org/10.1615/JPorMedia. v19.i8.60
3. Ajmera, S. K. and Mathur, A. N., Effect of Transverse Aspect Ratio and Distinct Ventilation Techniques on Convective Heat Transfer from a Rectangular Enclosure: Experimental and Numerical Study, *Arab. J. Sci. Eng.*, vol. **41**, no. 5, pp. 1617–1633, 2016. https://doi.org/10.1007/s13369-015-1880-x
4. Al-Amiri, A. M., Analysis of Momentum and Energy Transfer in a Lid-Driven Cavity Filled with a Porous Medium, *Int. J. Heat Mass Transf.*, vol. **43**, pp. 3513–3527, 2000. https://doi.org/10.1016/S0017-9310(99)00391-9
5. Alam, M., Rahman, M., Parvin, S. and Vajravelu, K., Finite Element Simulation for Heatline Visualization of Natural Convective Flow and Heat Transfer inside a Prismatic Enclosure, *Int. J. Heat Technol.*, vol. **34**, no. 3, pp. 391–400, 2016. https://doi.org/10.18280/ijht.340307
6. Alsabery, A. I., Chamkha, A. J., Saleh, H. and Hashim, I., Heatline Visualization of Conjugate Natural Convection in a Square Cavity Filled with Nanofluid with Sinusoidal Temperature Variations on Both Horizontal Walls, *Int. J. Heat Mass Transf.*, vol. **100**, pp. 835–850, 2016. https://doi.org/10.1016/j.ijheatmasstransfer.2016.05.031
7. Aly, A. M. and Ahmed, S. E., An Incompressible Smoothed Particle Hydrodynamics Method for Natural/Mixed Convection in a Non-Darcy Anisotropic Porous Medium, *Int. J. Heat Mass Transf.*, vol. **77**, pp. 1155–1168, 2014. https://doi.org/10.1016/j. ijheatmass transfer.2014.06.044
8. Anandalakshmi, R., Basak, T. and Lukose, L.,Numerical Visualization via Heatlines for Natural Convection in Porous Bodies of Rhombic Shapes Subjected to Thermal Aspect

Ratio-Based Heating of Walls, *Numer. Heat Transf. Part A Appl.*, vol. **76**, no. 9, pp. 687–711, 2019. https://doi.org/10.1080/10407782.2019.1647734

9. Banerjee, S., Mukhopadhyay, A., Sen, S. and Ganguly, R., Natural Convection in a Bi-Heater Configuration of Passive Electronic Cooling, *Int. J. Therm. Sci.*, vol. **47**, no. 11, pp. 1516–1527, 2008. https://doi.org/10.1016/j.ijthermalsci.2007.12.004
10. Basak, T., Anandalakshmi, R. and Singh, A. K., Heatline Analysis on Thermal Management with Conjugate Natural Convection in a Square Cavity, *Chem. Eng. Sci.*, vol. **93**, pp. 67–90, 2013. https://doi.org/10.1016/j.ces.2013.01.033
11. Basak, T., Aravind, G. and Roy, S., Visualization of Heat Flow Due to Natural Convection within Triangular Cavities Using Bejan's Heatline Concept, *Int. J. Heat Mass Transf.*, vol. **52**, no. 11–12, pp. 2824–2833, 2009. https://doi.org/10.1016/ j.ijheatmass transfer.2008.10.034
12. Basak, T., Ramakrishna, D., Roy, S., Matta, A. and Pop, I., A Comprehensive Heatline Based Approach for Natural Convection Flows in Trapezoidal Enclosures: Effect of Various Walls Heating, *Int. J. Therm. Sci.*, vol. **50**, pp. 1385–1404, 2011. https://doi.org /10.1016/j.ijthermalsci.2011.03.006
13. Basak, T. and Roy, S., Role of 'Bejan's Heatlines' in Heat Flow Visualization and Optimal Thermal Mixing for Differentially Heated Square Enclosures, *Int. J. Heat Mass Transf.*, vol. **51**, pp. 3486–3503, 2008. https://doi.org/10.1016/ j.ijheatmasstransfer. 2007.10.033
14. Basak, T., Roy, S., Babu, S. K. and Pop, I., Finite Element Simulations of Natural Convection Flow in an Isosceles Triangular Enclosure Filled with a Porous Medium : Effects of Various Thermal Boundary Conditions, *Int. J. Heat Mass Transf.*, vol. **51**, pp. 2733–2741, 2008. https://doi.org/10.1016/j.ijheatmasstransfer.2007.10.009
15. Basak, T., Roy, S., Paul, T. and Pop, I., Natural Convection in a Square Cavity Filled with a Porous Medium: Effects of Various Thermal Boundary Conditions, *Int. J. Heat Mass Transf.*, vol. **49**, pp. 1430–1441, 2006. https://doi.org/10.1016/j.ijheatmasstransfer. 2005.09.018
16. Basak, T., Roy, S. and Pop, I., Heat Flow Analysis for Natural Convection within Trapezoidal Enclosures Based on Heatline Concept, *Int. J. Heat Mass Transf.*, vol. **52**, no. 11–12, pp. 2471–2483, 2009. https://doi.org/10.1016/j.ijheatmasstransfer.2009.01.020

17. Basak, T., Roy, S., Singh, A. and Balakrishnan, A. R., Natural Convection Flows in Porous Trapezoidal Enclosures with Various Inclination Angles, *Int. J. Heat Mass Transf.*, vol. **52**, pp. 4612–4623, 2009. https://doi.org/10.1016/j.ijheatmasstransfer.2009.01.050
18. Basak, T., Roy, S., Singh, S. K. and Pop, I., Analysis of Mixed Convection in a Lid-Driven Porous Square Cavity with Linearly Heated Side Wall (S), *Int. J. Heat Mass Transf.*, vol. **53**, pp. 1819–1840, 2010. https://doi.org/10.1016/j.ijheatmasstransfer.2010.01.007
19. Baytas, A. C. and Pop, I., Free Convection in Oblique Enclosures Filled with a Porous Medium, *Int. J. Heat Mass Transf.*, vol. **42**, pp. 1047–1057, 1999. https://doi.org/10.1016/S0017-9310(98)00208-7
20. Beckermann, C., Ramadhyani, S. and Viskanta, R., Natural Convection Flow and Heat Transfer Between a Fluid Layer and a Porous Layer Inside a Rectangular Enclosure, *ASME J. Heat Transf.*, vol. **109**, pp. 363–370, 1987. https://doi.org/10.1115/1.3248089
21. Bejan, A. and Tien, C. L., Natural Convection in a Horizontal Porous Medium Subjected to an End-to-End Temperature Difference, *J. Heat Transfer*, vol. **100**, pp. 191–198, 1978. https://doi.org/10.1115/1.3450780
22. Bejan, A., On The Boundary Layer Regime in A Vertical Enclosure Filled With a Porous Medium, *Lett. Heat Mass Transf.*, vol. **6**, pp. 93–102, 1979.
23. Biswal, P. and Basak, T., Sensitivity of Heatfunction Boundary Conditions on Invariance of Bejan's Heatlines for Natural Convection in Enclosures with Various Wall Heatings, *Int. J. Heat Mass Transf.*, vol. **89**, pp. 1342–1368, 2015. https://doi.org/10.1016/j.ijheatmasstransfer.2015.05.030
24. Biswal, P., Nag, A. and Basak, T., Analysis of Thermal Management during Natural Convection within Porous Tilted Square Cavities via Heatline and Entropy Generation, *Int. J. Mech. Sci.*, 2016. https://doi.org/10.1016/j.ijmecsci.2016.07.011
25. Blythe, P. A. and Simpkins, P. G., Convection in a Porous Layer for a Temperature Dependent Viscosity, *Int. J. Heat Mass Transf.*, vol. **24**, pp. 497–506, 1981.
26. Bondarenko, D. S., Sheremet, M. A., Oztop, H. F. and Ali, M. E., Natural Convection of Al2O3/H2O Nanofluid in a Cavity with a Heat-Generating Element. Heatline Visualization, *Int. J. Heat Mass Transf.*, vol. **130**, pp. 564–574, 2019. https://doi.org/

10.1016/j.ijheatmasstransfer.2018.10.091

27. Bourchtein, A., Bourchtein, L. and Lukaszczyk, J. P., Numerical Simulation of Incompressible Flows through Granular Porous Media, *Appl. Numer. Math.*, vol. **40**, pp. 291–306, 2002. https://doi.org/10.1016/S0168-9274(01)00072-1
28. Brinkman, H. C., A Calculation of the Viscous Force Exerted By a Flowing Fluid on a Dense Swarm of Particles, *Appl. Scienific Res.*, vol. **A1**, pp. 27–34, 1947.
29. Burns, P. J., Chow, L. C. and Tien, C. L., Convection in a Vertical Slot Filled with Porous Insulation, *Int. J. Heat Mass Transf.*, vol. **20**, pp. 919–926, 1977. https://doi.org/10.1016/0017-9310(77)90062-X
30. Chan, B. K. C., Ivey, C. M. and Barry, J. M., Natural Convection in Enclosed Porous Media With Rectangular Boundaries, *ASME J. Heat Transf.*, vol. **92**, pp. 21–27, 1970. https://doi.org/10.1115/1.3449641
31. Chandra, P. and Satyamurty, V. V., Non-Darcian and Anisotropic Effects on Free Convection in a Porous Enclosure, *Transp. Porous Media*, vol. **90**, pp. 301–320, 2011. https://doi.org/10.1007/s11242-011-9785-y
32. Chandran, P., Sacheti, N. C., Bhadauria, B. S. and Singh, A. K., Natural Convection in a Hydrodynamically and Thermally Anisotropic Non-Rectangular Porous Cavity: Effect of Internal Heat Generation/Absorption, *Int. J. Appl. Mech. Eng.*, vol. **23**, no. 3, pp. 595–609, 2018. https://doi.org/10.2478/ijame-2018-0032
33. Chandran, P., Sacheti, N. C., Singh, A. K. and Bhadauria, B. S.,A Comparative Analysis of Isotropic and Anisotropic Features on Natural Convection in a Permeable Cavity, *Int. J. Eng. Res. Technol.*, vol. **12**, no. 6, pp. 873–878, 2019.
34. Chang, W.-J. and Hsiao, C.-F., Natural Convection in a Vertical Cylinder Filled with Anisotropic Porous Media, *Int. J. Heat Mass Transf.*, vol. **36**, no. 13, pp. 3361–3367, 1993. https://doi.org/10.1016/0017-9310(93)90017-Z
35. Chang, W.-J. and Lin, H.-C., Natural Convection in a Finite Wall Rectangular Cavity Filled with an Anisotropic Porous Medium, *Int. J. Heat Mass Transf.*, vol. **37**, no. 2, pp. 303–312, 1994. https://doi.org/10.1016/0017-9310(94)90101-5
36. Chevalier, S., Bernard, D. and Joly, N., Natural Convection in a Porous Layer Bounded by Impervious Domains: From Numerical Approaches to Experimental Realization, *Int. J. Heat Mass Transf.*, vol. **42**, pp. 581–597, 1999. https://doi.org/10.1016/S0017-

9310(98)00222-1

37. Choi, S. K., Nam, H. Y. and Cho, M., (a) Systematic Comparison of Finite-Volume Calculation Methods with Staggered and Nonstaggered Grid Arrangements, *Numer. Heat Transf. Part B*, vol. **25**, no. 2, pp. 205–221, 1994.
38. Choi, S. K., Nam, H. Y. and Cho, M., (b) Use of Staggered and Nonstaggered Grid Arrangements for Incompressible Flow Calculations on Nonorthogonal Grids, *Numer. Heat Transf. Part B*, vol. **25**, pp. 193–204, 1994. https://doi.org/10.1080/10407799408955917
39. Costa, V. A. F., Heatline and Massline Visualization of Laminar Natural Convection Boundary Layers near a Vertical Wall, *Int. J. Heat Mass Transf.*, vol. **43**, pp. 3765–3774, 2000.
40. Costa, V. A. F., Bejan's Heatlines and Masslines for Convection Visualization and Analysis, *Trans. ASME*, vol. **59**, pp. 126–145, 2006. https://doi.org/10.1115/1.2177684
41. Dalal, A. and Das, M. K., Heatline Method for the Visualization of Natural Convection in a Complicated Cavity, *Int. J. Heat Mass Transf.*, vol. **51**, pp. 263–272, 2008. https://doi.org/10.1016/j.ijheatmasstransfer.2007.04.005
42. Das, D. and Basak, T., Role of Distributed/Discrete Solar Heaters during Natural Convection in the Square and Triangular Cavities: CFD and Heatline Simulations, *Sol. Energy*, vol. **135**, pp. 130–153, 2016. https://doi.org/10.1016/j.solener.2016.04.045
43. Das, D., Lukose, L. and Basak, T.,Analysis of Efficiency of Convection in Porous Geometries (Square vs Triangular) with Multiple Discrete Heaters on Walls: A Heatline Perspective, *Int. J. Numer. Methods Heat Fluid Flow*, vol. **29**, no. 9, pp. 3305–3346, 2019. https://doi.org/10.1108/HFF-11-2018-0675
44. Davis, G. D. E. V. and Jones, I. P., Natural Convection in A Square Cavity: A Comparison Exercise, *Int. J. Numer. Methods Fluids*, vol. **3**, pp. 227–248, 1983.
45. Degan, G. and Vasseur, P., Boundary-Layer Regime in a Vertical Porous Layer with Anisotropic Permeability and Boundary Effects, *Int. J. Heat Fluid Flow*, vol. **18**, pp. 334–343, 1997. https://doi.org/10.1016/S0142-727X(97)00011-8
46. Degan, G., Vasseur, P. and Bilgen, E., Convective Heat Transfer in a Vertical Anisotropic Porous Layer, *Int. J. Heat Mass Transf.*, vol. **38**, no. 11, pp. 1975–1987, 1995. https://doi.org/10.1016/0017-9310(94)00330-X

47. Deng, Q. H., Fluid Flow and Heat Transfer Characteristics of Natural Convection in Square Cavities Due to Discrete Source-Sink Pairs, *Int. J. Heat Mass Transf.*, vol. **51**, pp. 5949–5957, 2008. https://doi.org/10.1016/j.ijheatmasstransfer.2008.04.062
48. Deng, Q. H. and Tang, G. F., Numerical Visualization of Mass and Heat Transport for Mixed Convective Heat Transfer by Streamline and Heatline, *Int. J. Heat Mass Transf.*, vol. **45**, pp. 2373–2385, 2002. https://doi.org/10.1016/S0017-9310(01)00317-9
49. Durlofsky, L. and Brady, J. F., Analysis of the Brinkman Equation as a Model for Flow in Porous Media., *Phys. Fluids*, vol. **30**, no. 11, pp. 3329–3341, 1987. https://doi.org/10.1063/1.866465
50. Elsharkawy, A. A. and Guedouar, L. H., Hydrodynamic Lubrication of Porous Journal Bearings Using a Modified Brinkman-Extended Darcy Model, *Tribol. Int.*, vol. **34**, pp. 767–777, 2001.
51. Ergun, S., Fluid Flow through Packed Columns, *Chem. Eng. Prog.*, 1952.
52. Ettefagh, J., Vafai, K. and Kim, S. J., Non-Darcian Effects in Open- Ended Cavities Filled With a Porous Medium, *J. Heat Transfer*, vol. **113**, pp. 747–756, 1991. https://doi.org/10.1083/jcb.146.6.1227
53. Forchheimer, P., Wasserbewegung Durch Boden, *Zeit Ver Deut Ing*, vol. **45**, pp. 1782–1788, 1901. https://doi.org/10.1371/journal.pone.0083536
54. Gaikwad, S. . N. and Dhanraj, M., Onset of Double Diffusive Convection in a Maxwell Fluid Saturated Anisotropic Porous Layer with Internal Heat Source, *Spec. Top. Rev. Porous Media - An Int. J.*, vol. **4**, no. 4, pp. 359–374, 2013. https://doi.org/10.1615/SpecialTopicsRevPorousMedia.v4.i4.70
55. Georgiadis, J. G. and Catton, I., Free Convective Motion in an Infinite Vertical Porous Slot: The Non-Darcian Regime, *Int. J. Heat Mass Transf.*, vol. **28**, no. 12, pp. 2389–2392, 1985. https://doi.org/10.1016/0017-9310(85)90060-2
56. Ghia, U., Ghia, K. N. and Shin, C. T., High-Re Solutions for Incompressible Flow Using the Navier-Stokes Equations and a Multigrid Method, *J. Comput. Phys.*, vol. **48**, pp. 387–411, 1982. https://doi.org/10.1016/0021-9991(82)90058-4
57. Guo, Z. and Zhao, T. S., Lattice Boltzmann Model for Incompressible Flows through Porous Media, *Am. Phys. Soc. Phys. Rev.*, vol. **66**, pp. 1–9, 2002. https://doi.org/10.1103/PhysRevE.66.036304

58. Haajizadeh, M. and Tien, C. L., Natural Convection in a Rectangular Porous Cavity With One Permeable Endwall, *ASME J. Heat Transf. Heat Transf.*, vol. **105**, pp. 803–808, 1983. https://doi.org/10.1115/1.3245665
59. Haddad, S., Thermal Convection in a Rotating Anisotropic Fluid Saturated Darcy Porous Medium, *Fluids*, vol. **2**, no. 44, pp. 1–15, 2017. https://doi.org/10.3390/fluids2030044
60. Harlow, F. H. and Welch, J. E., Numerical Calculation of Time-Dependent Viscous Incompressible Flow of Fluid with Free Surface, *Phys. Fluids*, vol. **8**, pp. 2182–2189, 1965. https://doi.org/10.1063/1.1761178
61. Havstad, M. A. and Burns, P. J., Convective Heat Transfer in Vertical Cylindrical Annuli Filled with a Porous Medium, *Int. J. Heat Mass Transf.*, vol. **25**, no. 11, pp. 1755–1766, 1982. https://doi.org/10.1016/0017-9310(82)90155-7
62. Hickox, C. E. and Gartling, D. K., A Numerical Study of Natural Convection in a Vertical, Annular, Porous Layer, *Int. J. Heat Mass Transf.*, vol. **28**, no. 3, pp. 720–723, 1985. https://doi.org/10.1016/0017-9310(85)90196-6
63. Holst, P. . and Aziz, K., (a) Transient Three-Dimensional Natural Convection in Confined Porous Media, *Int. J. Heat Mass Transf.*, vol. **15**, pp. 73–90, 1972.
64. Holst, P. H. and Aziz, K., (b) A Theoretical and Experimental Study of Natural Convection in a Confined Porous Medium, *Can. J. Chem. Eng.*, vol. **50**, pp. 232–241, 1972. https://doi.org/10.1002/cjce.5450500216
65. Hong, J. T., Tien, C. L. and Kaviany, M., Non-Darcian Effects on Vertical-Plate Natural Convection in Porous Media with High Porosities, *Int. J. Heat Mass Transf.*, vol. **28**, no. 11, pp. 2149–2157, 1985. https://doi.org/10.1016/0017-9310(85)90109-7
66. Hong, J. T., Yamada, Y. and Tien, C. L., Effects of Non-Darcian and Nonuniform Porosity on Vertical-Plate Natural Convection in Porous Media, *Trans. ASME*, vol. **109**, pp. 356–362, 1987. https://doi.org/10.1115/1.3248088
67. Hooman, K., Energy Flux Vectors as a New Tool for Convection Visualization, *Int. J. Numer. Methods Heat Fluid Flow*, vol. **20**, no. 2, pp. 240–249, 2010. https://doi.org/10.1108/09615531011016984
68. Hooman, K., Gurgenci, H. and Dincer, I., Heatline and Energy-Flux-Vector Visualization of Natural Convection in a Porous Cavity Occupied by a Fluid with Temperature-Dependent Viscosity, *J. Porous Media*, vol. **12**, no. 3, pp. 265–275, 2009. https://doi.org/

10.1615/jpormedia.v12.i3.60

69. Hsiao, S., A Numerical Study of Transient Natural Convection about a Corrugated Plate Embedded In an Enclosed Porous Medium, *Int. J. Numer. Methods Heat Fluid Flow*, vol. **5**, pp. 629–645, 1995.
70. Hu, Y., Li, D., Shu, S. and Niu, X., A Multiple-Relaxation-Time Lattice Boltzmann Model for the Flow and Heat Transfer in a Hydrodynamically and Thermally Anisotropic Porous Medium, *Int. J. Heat Mass Transf.*, vol. **104**, pp. 544–558, 2017. https://doi.org/10.1016/j.ijheatmasstransfer.2016.08.008
71. Hung, C., Chen, C. and Chen, C., Non-Darcy Free Convection along a Nonisothermal Vertical Surface in a Thermally Stratified Porous Medium, *Int. J. Eng. Sci.*, vol. **37**, pp. 477–495, 1999.
72. Hung, C. I. and Chen, C. B., Non-Darcy Free Convection in a Thermally Stratified Porous Medium along a Vertical Plate with Variable Heat Flux, *Heat Mass Transf.*, vol. **33**, pp. 101–107, 1997. https://doi.org/10.1007/s002310050166
73. Jaya Krishna, D., Basak, T. and Das, S. K., Non-Darcy Buoyancy Driven Flows in a Fluid Saturated Porous Medium: The Use of Asymptotic Computational Fluid Dynamics (ACFD) Approach, *Heat Mass Transf.*, vol. **44**, pp. 1117–1125, 2008. https://doi.org/10.1007/s00231-007-0348-2
74. Jue, T. C., Analysis of Flows Driven by a Torsionally-Oscillatory Lid in a Fluid-Saturated Porous Enclosure with Thermal Stable Stratification, *Int. J. Therm. Sci.*, vol. **41**, pp. 795–804, 2002. https://doi.org/10.1016/S1290-0729(02)01373-X
75. Kaluri, R. S., Anandalakshmi, R. and Basak, T., Bejan's Heatline Analysis of Natural Convection in Right-Angled Triangular Enclosures: Effects of Aspect-Ratio and Thermal Boundary Conditions, *Int. J. Therm. Sci.*, vol. **49**, pp. 1576–1592, 2010. https://doi.org/10.1016/j.ijthermalsci.2010.04.022
76. Kaluri, R. S. and Basak, T., Analysis of Distributed Thermal Management Policy for Energy-Efficient Processing of Materials by Natural Convection, *Energy*, vol. **35**, pp. 5093–5107, 2010. https://doi.org/10.1016/j.energy.2010.08.006
77. Keyhani, M. and Polehn, R. A., Finite Difference Modeling of Anisotropic Flows, *J. Heat Transfer*, vol. **117**, no. 2, pp. 458–464, 1995. https://doi.org/10.1115/1.2822544
78. Khanafer, K. and Vafai, K., Double-Diffusive Mixed Convection in a Lid-Driven

Enclosure Filled with a Fluid-Saturated Porous Medium, *Numer. Heat Transf. Part A Appl.*, vol. **42**, no. 5, pp. 465–486, 2002. https://doi.org/10.1080/10407780290059657

79. Kimura, S. and Bejan, A., The 'Heatline' Visualization of Convective Heat Transfer, *Trans. ASME*, vol. **105**, pp. 916–919, 1983.
80. Knupp, P. M. and Lage, J. L., Generalization of the Forchheimer-Extended Darcy Flow Model to the Tensor Permeability Case via a Variational Principle, *J. Fluid Mech.*, vol. **299**, pp. 97–104, 1995. https://doi.org/10.1017/S0022112095003430
81. Kozelkov, A. S., Lashkin, S. V., Efremov, V. R., Volkov, K. N., Tsibereva, Y. A. and Tarasova, N. V., An Implicit Algorithm of Solving Navier–Stokes Equations to Simulate Flows in Anisotropic Porous Media, *Comput. Fluids*, vol. **160**, pp. 164–174, 2018. https://doi.org/10.1016/j.compfluid.2017.10.029
82. Krishna, D. J., Basak, T. and Das, S. K., (a) Natural Convection in a Heat Generating Hydrodynamically and Thermally Anisotropic Non-Darcy Porous Medium, *Int. J. Heat Mass Transf.*, vol. **51**, pp. 4691–4703, 2008. https://doi.org/10.1016/j.ijheatmasstransfer.2008.02.019
83. Krishna, D. J., Basak, T. and Das, S. K., (b) Numerical Study of Lid-Driven Flow in Orthogonal and Skewed Porous Cavity, *Commun. Numer. Methods Eng.*, vol. **24**, pp. 815–831, 2008. https://doi.org/10.1002/cnm.993
84. Krishna, D. J., Basak, T. and Das, S. K., Natural Convection in a Non-Darcy Anisotropic Porous Cavity with a Finite Heat Source at the Bottom Wall, *Int. J. Therm. Sci.*, vol. **48**, pp. 1279–1293, 2009. https://doi.org/10.1016/j.ijthermalsci.2008.11.022
85. Krishna, D. J., Thansekhar, M. R., Venkateshan, S. P., Basak, T. and Das, S. K., Natural Convection in a Partially Heat Generating Rod Bundle Inside an Enclosure, *J. Heat Transfer*, vol. **132**, pp. 1–11, 2010. https://doi.org/10.1115/1.4001610
86. Kumari, M. and Nath, G., Steady Mixed Convection Flow in a Lid-Driven Square Enclosure Filled With a Non-Darcy Fluid-Saturated Porous Medium With Internal Heat Generation, *J. Porous Media*, vol. **14**, no. 10, pp. 893–905, 2011. https://doi.org/10.1615/JPorMedia.v14.i10.50
87. Lage, J. L., Effect of the Convective Inertia Term on Bénard Convection in a Porous Medium, *Numer. Heat Transf. Part A Appl.*, vol. **22**, pp. 469–485, 1992. https://doi.org/10.1080/10407789208944778

88. Lage, J. L., Natural Convection within a Porous Medium Cavity: Predicting Tools for Flow Regime and Heat Transfer, *Int. Commun. Heat Mass Transf.*, vol. **20**, pp. 501–513, 1993.
89. Lauriat, G. and Prasad, V., Natural Convection in a Vertical Porous Cavity: A Numerical Study for Brinkman-Extended Darcy Formulation, *Trans. ASME*, vol. **109**, pp. 688–696, 1987. https://doi.org/10.1115/1.3248143
90. Lauriat, G. and Prasad, V., Non-Darcian Effects on Natural Convection in a Vertical Porous Enclosure, *Int. J. Heat Mass Transf.*, vol. **32**, no. 11, pp. 2135–2148, 1989. https://doi.org/10.1016/0017-9310(89)90120-8
91. Lee, S. L. and Yang, J. H., Modeling of Darcy-Forchheimer Drag for Fluid Flow across a Bank of Circular Cylinders, *Int. J. Heat Mass Transf.*, vol. **40**, no. 13, pp. 3149–3155, 1997. https://doi.org/10.1016/S0017-9310(96)00347-X
92. *Les fontaines publiques de la ville de Dijon*, 1856.
93. Lima, T. P. and Ganzarolli, M. M., A Heatline Approach on the Analysis of the Heat Transfer Enhancement in a Square Enclosure with an Internal Conducting Solid Body, *Int. J. Therm. Sci.*, vol. **105**, pp. 45–56, 2016. https://doi.org/10.1016/ j.ijthermalsci. 2016.02.012
94. Lundgren, T. S., Slow Flow through Stationary Random Beds and Suspensions of Spheres, *J. Fluid Mech.*, vol. **51**, no. 2, pp. 273–299, 1972. https://doi.org/10.1017/ S002211207200120X
95. Maliska, C. R. and Raithy, G. D., A Method for Computing Three Dimensional Flows Using Non-Orthogonal Boundary-Fitted Co-Ordinates, *Int. J. Numer. Methods Fluids*, vol. **4**, pp. 519–537, 1984.
96. Mamou, M., Mahidjiba, A., Vasseur, P. and Robillard, L., Onset of Convection in an Anisotropic Porous Medium Heated from Below by a Constant Heat Flux, *Int. Commun. Heat Mass Transf.*, vol. **25**, no. 6, pp. 799–808, 1998.
97. Mbaye, M., Bilgen, E. and Vasseur, P., Natural Convection Heat Transfer in an Inclined Porous Layer Boarded By a Finite- Thickness Wall, *Int. J. Heat Fluid Flow*, vol. **14**, no. 3, pp. 284–291, 1993.
98. Melaaen, M. C., (a) Calculation of Fluid Flows with Staggered and Non Staggered Curvilinear Non Orthogonal Grids- The Theory, *Numer. Heat Transf. Part B*, vol. **21**, pp.

1–19, 1992. https://doi.org/10.1080/10407782.2013.832071

99. Melaaen, M. C., (b) Calculation of Fluid Flows with Staggered and Nonstaggered Curvilinear Nonorthogonal Grids- A Comparison, *Numer. Heat Transf. Part B*, vol. **21**, pp. 21–39, 1992. https://doi.org/10.1080/10407782.2013.832071
100. Merrikh, A. A. and Mohamad, A. A., Non-Darcy Effects in Buoyancy Driven Flows in an Enclosure Filled with Vertically Layered Porous Media, *Int. J. Heat Mass Transf.*, vol. **45**, pp. 4305–4313, 2002. https://doi.org/10.1016/S0017-9310(02)00135-7
101. Miller, T. F. and Schmidt, F. W., Use of A Pressure-Weighted Interpolation Method for the Solution of the Incompressible Navier-Stokes Equations on A Nonstaggered Grid System, *Numer. Heat Transf.*, vol. **14**, pp. 213–233, 1988.
102. Mishra, A. K., Kumar, S. and Sharma, R. V., Non-Darcy Effects on Three-Dimensional Natural Convection in A Rectangular Box Containing A Heat-Generating Porous Medium, *J. Porous Media*, vol. **19**, no. 12, pp. 1033–1043, 2016. https://doi.org/10.1615/JPorMedia.v19.i12.20
103. Misra, D. and Sarkar, A., A Comparative Study of Porous Media Models in a Differentially Heated Square Cavity Using a Finite Element Method, *Int. J. Numer. Methods Heat Fluid Flow*, vol. **5**, pp. 735–752, 1995. https://doi.org/10.1108/EUM0000000004124
104. Mobedi, M., Özkol, Ü. and Sunden, B., Visualization of Diffusion and Convection Heat Transport in a Square Cavity with Natural Convection, *Int. J. Heat Mass Transf.*, vol. **53**, pp. 99–109, 2010. https://doi.org/10.1016/j.ijheatmasstransfer.2009.09.048
105. Mohamad, A. A., Orfi, J. and Al-Ansary, H., Non-Darcy Fluid Flow and Heat Transfer in Conduits Fitted With Porous Media, *J. Porous Media*, vol. **18**, no. 4, pp. 449–453, 2015. https://doi.org/10.1615/JPorMedia.v18.i4.70
106. Mohan, C. G. and Satheesh, A., The Numerical Simulation of Double-Diffusive Mixed Convection Flow in a Lid-Driven Porous Cavity with Magnetohydrodynamic Effect, *Arab. J. Sci. Eng.*, vol. **41**, pp. 1867–1882, 2016. https://doi.org/10.1007/s13369-015-1998-x
107. Nakayama, A., Kokudai, T. and Koyama, H., Forchheimer Free Convection Over a Nonisothermal Body of Arbitrary Shape in a Saturated Porous Medium, *J. Heat Transfer*, vol. **112**, no. 2, pp. 511–515, 1990. https://doi.org/10.1115/1.2910413

108. Nakayama, A., Kuwahara, F. and Hayashi, T., Numerical Modelling for Three-Dimensional Heat and Fluid Flow through a Bank of Cylinders in Yaw, *J. Fluid Mech.*, vol. **498**, pp. 139–159, 2004. https://doi.org/10.1017/S0022112003006712

109. Nakayama, A., Kuwahara, F., Umemoto, T. and Hayashi, T., Heat and Fluid Flow Within an Anisotropic Porous Medium, *Trans. ASME*, vol. **124**, pp. 746–753, 2002. https://doi.org/10.1115/1.1481355

110. Natarajan, E., Basak, T. and Roy, S., Heatline Visualization of Natural Convection Flows within Trapezoidal Enclosures, *Iasme*, pp. 59–66, 2007.

111. Nayak, A. K., Jena, P. K. and Narayana, P. A. L., Flow Simulation and Mixed Convection in a Lid-Driven Square Cavity With Saturated Porous Media, *J. Porous Media*, vol. **17**, no. 6, pp. 537–548, 2014. https://doi.org/10.1615/JPorMedia.v17.i6.50

112. Neale, G., Degrees of Anisotropy for Fluid Flow and Diffusion (Electrical Conduction) through Anisotropic Porous Media, *AIChE J.*, vol. **23**, no. 1, pp. 56–62, 1977. https://doi.org/10.1002/aic.690230110

113. Neale, G. and Nader, W., Practical Significance of Brinkman Extension of Darcy's Law: Coupled Parallel Flows within a Channel and a Bounding Porous Medium, *Can. Chem. Eng.*, vol. **52**, pp. 475–478, 1974. https://doi.org/10.1002/cjce.5450520407

114. Ni, J. and Beckermann, C., Natural Convection in a Vertical Enclosure Filled With Anisotropic Porous Media, *ASME J. Heat Transf.*, vol. **113**, pp. 1033–1037, 1991. https://doi.org/10.1115/1.2911201

115. Nield, D. A., The Boundary Correction for the Rayleigh-Darcy Problem: Limitations of the Brinkman Equation, *J. Fluid Mech.*, vol. **128**, pp. 37–46, 1983. https://doi.org/10.1017/S0022112083000361

116. Nield, D. A. and Bejan, A., *Convection in Porous Media* (4th edition), 2013, New York, NY, USA: Springer.

117. Nithiarasu, P., Seetharamu, K. N. and Sundararajan, T., Natural Convective Heat Transfer in a Fluid Saturated Porous Medium, *Int. J. Heat Mass Transf.*, vol. **40**, no. 16, pp. 3955–3967, 1997. https://doi.org/10.1016/S0142-727X(97)10008-X

118. Nithiarasu, P., Seetharamu, K. N. and Sundararajan, T., Effect of Porosity on Natural Convective Heat Transfer in a Fluid Saturated Porous Medium, *Int. J. Heat Fluid Flow*, vol. **19**, pp. 56–58, 1998. https://doi.org/10.1016/S0142-727X(97)10008-X

119. Nithiarasu, P., Seetharamu, K. N. and Sundararajan, T., Numerical Investigation of Buoyancy Driven Flow in a Fluid Saturated Non-Darcian Porous Medium, *Int. J. Heat Mass Transf.*, vol. **42**, pp. 1205–1215, 1999. https://doi.org/10.1016/S0017-9310(98)00254-3

120. Nithiarasu, P., Sujatha, K. S., Ravindran, K., Sundararajan, T. and Seetharamu, K. N., Non-Darcy Natural Convection in a Hydrodynamically and Thermally Anisotropic Porous Medium, *Comput. Methods Appl. Mech. Eng.*, vol. **188**, pp. 413–430, 2000. https://doi.org/10.1016/S0045-7825(99)00163-2

121. Nithyadev, N., Rajarathinam, M. and Suresh, N., Density Maximum Effect of Double-Diffusive Mixed Convection Heat Transfer in A Two-Sided Lid-Driven Porous Cavity, *Spec. Top. Rev. Porous Media An Int. J.*, vol. **8**, no. 3, pp. 245–261, 2017. https://doi.org/10.1615/SpecialTopicsRevPorousMedia.v8.i3.60

122. Nithyadevi, N. and Rajarathinam, M., Double Diffusive Heat Convection of MHD Nanofluid in a Two Sided Lid-Driven Porous Cavity, *J. Nanofluids*, vol. **6**, no. 3, pp. 466–477, 2017. https://doi.org/10.1166/jon.2017.1331

123. Osinov, V. A., Cyclic Shearing and Liquefaction of Soil under Irregular Loading: An Incremental Model for the Dynamic Earthquake-Induced Deformation, *Soil Dyn. Earthq. Eng.*, vol. **23**, no. 7, pp. 535–548, 2003. https://doi.org/10.1016/S0267-7261(03)00072-1

124. Ouarhlent, F. and Soudani, A., Numerical Study of Thermal Convection in a Porous Medium, *Instrum. Mes. Metrol.*, vol. **18**, no. 1, pp. 69–74, 2019.

125. Oztop, H. F., Combined Convection Heat Transfer in a Porous Lid-Driven Enclosure Due to Heater with Finite Length, *Int. Commun. Heat Mass Transf.*, vol. **33**, pp. 772–779, 2006. https://doi.org/10.1016/j.icheatmasstransfer.2006.02.003

126. Pakdee, W. and Rattanadecho, P., Unsteady Effects on Natural Convective Heat Transfer through Porous Media in Cavity Due to Top Surface Partial Convection, *Appl. Therm. Eng.*, vol. **26**, pp. 2316–2326, 2006. https://doi.org/10.1016/j.applthermaleng.2006.03.004

127. Perić, M., Kessle, R. and Scheuerer, G., Comparison of Finite-Volume Numerical Methods with Staggered and Collocated Grids, *Comput. Fluids*, vol. **16**, no. 4, pp. 389–403, 1988.

128. Philip, J. R., (a) Axisymmetric Free Convection at Small Rayleigh Number in Porous Cavities, *Int. J. Heat Mass Transf.*, vol. **25**, no. 11, pp. 1689–1699, 1982.

https://doi.org/10.1016/0017-9310(82)90148-X

129. Philip, J. R., (b) Free Convection at Small Rayleigh Number in Porous Cavities of Rectangular, Elliptical, Triangular and Other Cross-Sections, *Int. J. Heat Mass Transf.*, vol. **25**, no. 10, pp. 1503–1509, 1982. https://doi.org/10.1016/0017-9310(82)90029-1
130. Pilkington, L. A. B., Review Lecture. The Float Glass Process, *Proc. R. Soc. A Math. Phys. Eng. Sci.*, vol. **314**, pp. 1–25, 1969. https://doi.org/10.1098/rspa.1969.0212
131. Plumb, O. A. and Huenefeld, J. C., Non-Darcy Natural Convection from Heated Surfaces in Saturated Porous Media, *Int. J. Heat Mass Transf.*, vol. **24**, no. 4, pp. 765–768, 1981. https://doi.org/10.1016/0017-9310(81)90020-X
132. Pop, I. and Na, T., Naturnal Convection of a Darcian Fluid about a Wavy Cone, *Int. Commun. Heat Mass Transf.*, vol. **21**, no. 6, pp. 891–899, 1994. https://doi.org/10.1016/0735-1933(94)90042-6
133. Pop, I. and Na, T., Natural Convection over a Frustum of a Wavy Cone in a Porous Medium, *Mech. Res. Commun.*, vol. **22**, no. 2, pp. 181–190, 1995.
134. Poulikakos, D. and Bejan, A., The Departure from Darcy Flow in Natural Convection in a Vertical Porous Layer, *Phys. Fluids*, vol. **28**, no. 12, pp. 3477–3484, 1985. https://doi.org/10.1063/1.865301
135. Prasad, V., A Numerical Study of Natural Convection in a Vertical Annulus with Constant Heat Flux on the Inner Wall, *Int. J. Heat Mass Transf.*, vol. **29**, no. 6, pp. 841–853, 1986. https://doi.org/10.1108/eb017550
136. Prasad, V. and Kulacki, F. A., (a) Convective Heat Transfer in a Rectangular Porous Cavity—Effect of Aspect Ratio on Flow Structure and Heat Transfer, *Trans. ASME*, vol. **106**, pp. 158–165, 1984. https://doi.org/10.1115/1.3246629
137. Prasad, V. and Kulacki, F. A., (b) Natural Convection in a Vertical Porous Annulus, *Int. J. Heat Mass Transf.*, vol. **27**, no. 2, pp. 207–219, 1984. https://doi.org/10.1016/0017-9310(84)90212-6
138. Prasad, V. and Kulacki, F. A., Natural Convection in Porous Media Bounded by Short Concentric Vertical Cylinders, *ASME J. Heat Transf.*, vol. **107**, pp. 147–154, 1985. https://doi.org/10.1115/1.3247371
139. Prasad, V., Kulacki, F. A. and Keyhani, M., Natural Convection in Porous Media, *J. Fluid Mech.*, vol. **150**, pp. 89–119, 1985. https://doi.org/10.1017/s0022112085000040

140. Prasad, V., Kulacki, F. A. and Kulkarni, A. V., Free Convection in a Vertical, Porous Annulus with Constant Heat Flux on the Inner Wall- Experimental Results, *Int. J. Heat Mass Transf.*, vol. **29**, no. 5, pp. 713–723, 1986. https://doi.org/10.1115/1.3245606
141. Prasad, V. and Tuntomo, A., Inertia Effects on Natural Convection in a Vertical Porous Cavity, *Numer. Heat Transf.*, vol. **11**, pp. 295–320, 1987. https://doi.org/10.1080/10407788708913556
142. Rahman, M. S., Nasrin, R. and Hoque, M. I., Mixed Convective Flow in Lid-Driven Porous Cavity : Effect of Solid Volume Fraction, *Int. J. Pure Appl. Math.*, vol. **120**, no. 6, pp. 6547–6561, 2018.
143. Rout, S. K., Thatoi, D. N., Acharya, A. K. and Mishra, D. P., CFD Supported Performance Estimation of an Internally Finned Tube Heat Exchanger under Mixed Convection Flow, *Procedia Eng.*, vol. **38**, pp. 585–597, 2012. https://doi.org/10.1016/j.proeng.2012.06.073
144. Roy, M., Roy, S. and Basak, T., Fluids Finite Element Simulations on Heatline Trajectories for Mixed Convection in Porous Square Enclosures : Effects of Various Moving Walls, *Eur. J. Mech. B/Fluids*, vol. **59**, pp. 140–160, 2016. https://doi.org/10.1016/j.euromechflu.2016.04.011
145. Roychowdhury, D. G., Das, S. K. and Sundararajan, T., An Efficient Solution Method for Incompressible N-S Equations Using Non-Orthogonal Collocated Grid, *Int. J. Numer. Methods Eng.*, vol. **45**, pp. 741–763, 1999. https://doi.org/10.1002/(SICI)1097-0207(19990630)45:6<741::AID-NME601>3.0.CO;2-5
146. Saeid, N. H., Conjugate Natural Convection in a Porous Enclosure : Effect of Conduction in One of the Vertical Walls, *Int. J. Therm. Sci.*, vol. **46**, pp. 531–539, 2007. https://doi.org/10.1016/j.ijthermalsci.2006.08.003
147. Saeid, N. H. and Pop, I., Non-Darcy Natural Convection in a Square Cavity Filled with a Porous Medium, *Fluid Dyn. Res.*, vol. **36**, pp. 35–43, 2005. https://doi.org/10.1016/j.fluiddyn.2004.10.004
148. Safi, S. and Benissaad, S., Double-Diffusive Convection in an Anisotropic Porous Layer Using the Darcy–Brinkman–Forchheimer Formulation, *Arch. Mech.*, vol. **70**, no. 1, pp. 89–102, 2018.
149. Sai, B. V. K. S., Seetharamu, K. N., Narayana, P. A. A. and Reddy, J. N., Finite Element

Analysis of the Effect of Radius Ratio on Natural Convection in an Annular Cavity, *Int. J. Numer. Methods Heat Fluid Flow*, vol. **3**, no. 4, pp. 305–318, 1993.

150. Saravanan, V., Umesh, C. K., Hithaish, D. and Seetharamu, K., Numerical Investigation of Pressure Drop and Heat Transfer in Pin Fin Heat Sink and Micro Channel Pin Fin Heat Sink, *Int. J. Heat Technol.*, vol. **36**, no. 1, pp. 267–276, 2018. https://doi.org/10.18280/ijht.360136
151. Sathiyamoorthy, M., Basak, T., Roy, S. and Pop, I., Steady Natural Convection Flow in a Square Cavity Filled with a Porous Medium for Linearly Heated Side Wall (S), *Int. J. Heat Mass Transf.*, vol. **50**, pp. 1892–1901, 2007. https://doi.org/10.1016/j.ijheatmasstransfer.2006.10.010
152. Shalini and Kumar, B. V. R., Influence of Variable Heat Flux on Natural Convection along a Corrugated Wall in Porous Media, *Commun. Nonlinear Sci. Numer. Simul.*, vol. **12**, pp. 1454–1463, 2007. https://doi.org/10.1016/j.cnsns.2006.02.003
153. Sheremet, M. A., Pop, I. and Nazar, R., Natural Convection in a Square Cavity Filled with a Porous Medium Saturated with a Nanofluid Using the Thermal Nonequilibrium Model with a Tiwari and Das Nanofluid Model, *Int. J. Mech. Sci.*, vol. **100**, pp. 312–321, 2015. https://doi.org/10.1016/j.ijmecsci.2015.07.007
154. Shyy, W., Computation Modeling for Fluid Flow and Interfacial Transport, *Eur. J. Eng. Educ.*, vol. **19**, no. 3, pp. 376, 1994. https://doi.org/10.1080/03043799408928316
155. Shyy, W., Tong, S. S. and Correa, S. M., Numerical Recirculating Flow Calculation Using a Body-Fitted Coordinate System, *Numer. Heat Transf.*, vol. **8**, pp. 99–113, 1985.
156. Simpkins, P. G. and Blythe, P. A., Convection in a Porous Layer, *Int. J. Heat Mass Transf.*, vol. **23**, pp. 881–887, 1980. https://doi.org/10.1016/0017-9310(80)90043-5
157. Singh, A. K., Basak, T., Nag, A. and Roy, S., Heatlines and Thermal Management Analysis for Natural Convection within Inclined Porous Square Cavities, *Int. J. Heat Mass Transf.*, vol. **87**, pp. 583–597, 2015. https://doi.org/10.1016/j.ijheatmasstransfer.2015.03.043
158. Slimi, K. and Nasrallah, S. Ben, Transient Natural Convection in a Vertical Cylinder Opened at the Extremities and Filled with a Fluid Saturated Porous Medium : Validity of Darcy Flow Model and Thermal Boundary Lay ... Transient Natural Convection in a Vertical Cylinder Opened at the Ext, *Int. J. Heat Mass Transf.*, vol. **41**, pp. 1113–1125,

1998. https://doi.org/10.1016/S0017-9310(97)00155-5

159. Srivastava, A. K., Bhadauria, B. S. and Kumar, J., Magnetoconvection in an Anisotropic Porous Layer Using Thermal Nonequilibrium Model, *Spec. Top. Rev. Porous Media - An Int. J.*, vol. **2**, no. 1, pp. 1–10, 2011. https://doi.org/10.1615/SpecialTopicsRevPorousMedia.v2.i1.10
160. Srivastava, A. and Singh, A. K., Linear and Weak Nonlinear Double Diffusive Convection in a Viscoelastic Fluid Saturated Anisotropic Porous Medium with Internal Heat Source, *J. Appl. Fluid Mech.*, vol. **11**, no. 1, pp. 65–77, 2018. https://doi.org/10.18869/acadpub.jafm.73.244.27519
161. Swamy, M. S., Shivakumara, I. S. and Sidram, W., The Onset of Convection in a Gravity-Modulated Viscoelastic Fluid-Saturated Anisotropic Porous Layer, *Spec. Top. Rev. Porous Media - An Int. J.*, vol. **4**, no. 1, pp. 69–80, 2013. https://doi.org/10.1615/specialtopicsrevporousmedia.v4.i1.70
162. Tao, W. Q., He, Y. L. and Chen, L.,A comprehensive review and comparison on heatline concept and field synergy principle, *Int. J. Heat Mass Transf.*, vol. **135**, pp. 436–459, 2019. DOI: 10.1016/j.ijheatmasstransfer.2019.01.143.
163. Thompson, J. F., Warsi, Z. U. A. and Mastin, C. W., Boundary-Fitted Coordinate Systems for Numerical Solution of Partial Differential Equations-A Review, *J. Comput. Phys.*, vol. **47**, pp. 1–108, 1982.
164. Tien, C. and Hong, J., Natural Convection in Porous Media under Non-Darcian and Non-Uniform Permeability Conditions, *Nat. Convect. Fundam. Appl.*, vol. **17**, no. 21, pp. 573–587, 1985. Retrieved from https://inis.iaea.org/search/search.aspx?orig_q=RN:17074167
165. Tong, T. W. and Subramanian, E., A Boundary-Layer Analysis for Natural Convection in Vertical Porous Enclosures-Use of the Brinkman-Extended Darcy Model, *Int. J. Heat Mass Transf.*, vol. **28**, no. 3, pp. 563–571, 1985. https://doi.org/10.1016/0017-9310(85)90179-6
166. Triveni, Manoj K and Panua, R., Numerical Analysis of Natural Convection in a Triangular Cavity with Different Configurations of Hot Wall, *Int. J. Heat Technol.*, vol. **35**, no. 1, pp. 11–18, 2017. https://doi.org/10.18280/ijht.350102
167. Triveni, Manoj Kr, Panua, R. and Sen, D., Natural Convection in a Partially Heated Triangular Cavity with Different Configurations of Cold Walls, *Arab. J. Sci. Eng.*, vol.

40, pp. 3285–3297, 2015. https://doi.org/10.1007/s13369-015-1778-7

168. Tsybulin, V. G., Karasözen, B. and Ergenç, T., Selection of Steady States in Planar Darcy Convection, *Phys. Lett. A*, vol. **356**, pp. 189–194, 2006. https://doi.org/10.1016/j.physleta.2006.03.043
169. Vafai, K. and Kim, S. J., On the Limitations of the Brinkman-Forchheimer-Extended Darcy Equation, *Int. J. Heat Fluid Flow*, vol. **16**, no. 1, pp. 11–15, 1995. https://doi.org/10.1016/0142-727X(94)00002-T
170. Vafai, K and Kim, S. J., On The Limitations of the Brinkman – Forchheimer – Extended Darcy Equation, *Int. J. Heat Fluid Flow*, vol. **16**, pp. 11–15, 1995.
171. Vafai, K and Tien, C. L., Boundary and Inertia Effects on Flow and Heat Transfer in Porous Media, *Int. J. Heat Mass Transf.*, vol. **24**, pp. 195–203, 1981.
172. Vafai, Kambiz, Convective Flow and Heat Transfer in Variable-Porosity Media, *J. Fluid Mech.*, vol. **147**, pp. 233–259, 1984. https://doi.org/10.1017/S002211208400207X
173. Vafai, Kambiz and Tien, C. L., Boundary and Inertia Effects on Flow and Heat Transfer in Porous Media, *Int. J. Heat Mass Transf.*, vol. **24**, pp. 195–203, 1981.
174. Varol, Y., Oztop, H. F. and Varol, A., Free Convection in Porous Media Filled Right-Angle Triangular Enclosures, *Int. Commun. Heat Mass Transf.*, vol. **33**, pp. 1190–1197, 2006. https://doi.org/10.1016/j.icheatmasstransfer.2006.08.008
175. Vasseur, P. and Degan, G., Free Convection along a Vertical Heated Plate in a Porous Medium with Anisotropic Permeability, *Int. J. Numer. Methods Heat Fluid Flow*, vol. **8**, no. 1, pp. 43–63, 1998. https://doi.org/10.1108/09615539810197925
176. Vasseur, P. and Robillard, L., The Brinkman Model for Boundary Layer Regime in a Rectangular Cavity with Uniform Heat Flux from the Side, *Int. J. Heat Mass Transf.*, vol. **30**, no. 4, pp. 717–727, 1987. https://doi.org/10.1016/0017-9310(87)90202-X
177. Vasseur, P., Wang, C. H. and Sen, M., The Brinkman Model for Natural Convection in a Shallow Porous Cavity with Uniform Heat Flux, *Numer. Heat Transf. Part A Appl.*, vol. **15**, pp. 221–242, 1989. https://doi.org/10.1080/10407788908944686
178. Vasseur, P., Wang, C. H. and Sen, M., Natural Convection in an Inclined Rectangular Porous Slot: The Brinkman-Extended Darcy Model, *ASME J. Heat Transf.*, vol. **112**, pp. 507–511, 1990.
179. Vinokur, M., An Analysis of Finite-Difference and Finite-Volume Formulations of

Conservation Laws, *J. Comput. Phys.*, vol. **81**, pp. 1–52, 1989. https://doi.org/10.1016/0021-9991(89)90063-6

180. Vishnuvardhanarao, E. and Das, M. K., Laminar Mixed Convection in a Parallel Two-Sided Lid-Driven Differentially Heated Square Cavity Filled with a Fluid-Saturated Porous Medium, *Numer. Heat Transf. Part A*, vol. **53**, pp. 88–110, 2008. https://doi.org/10.1080/10407780701454006
181. Waheed, M. A., Heat function Formulation of Thermal Convection in Rectangular Enclosures Filled with Porous Media, *Numer. Heat Transf. , Part A*, vol. **55**, pp. 185–204, 2009. https://doi.org/10.1080/10407780802603246
182. Walker, K. L. and Homsy, G. M., Convection in a Porous Cavity, *J. Fluid Mech.*, vol. **87**, no. 3, pp. 449–474, 1978. https://doi.org/10.1017/S0022112078001718
183. Ward, J. C., Turbulent Flow in Porous Media, *J. Hydraul. Div.*, vol. **90**, no. 5, pp. 1–12, 1964.
184. Weber, J. E., The Boundary-Layer Regime for Convection in a Vertical Porous Layer, *Int. J. Heat Mass Transf.*, vol. **18**, pp. 569–573, 1975. https://doi.org/10.1016/0017-9310(75)90298-7
185. Wooding, R. A., Steady State Free Thermal Convection of Liquid in a Saturated Permeable Medium, *J. Fluid Mech.*, vol. **2**, no. 3, pp. 273–285, 1957. https://doi.org/10.1017/S0022112057000129
186. Yang, J. H. and Lee, S. L., Effect of Anisotropy on Transport Phenomena in Anisotropic Porous Media, *Int. J. Heat Mass Transf.*, vol. **42**, pp. 2673–2681, 1999.

PUBLICATIONS BASED ON THE PRESENT WORK

International Journals:

1. **Narasimha Suri Tinnaluri** and D. Jaya Krishna, A Collocated Grid Based Finite Volume Approach for the Visualization of Heat Transport in 2D Complex geometries, Procedia Engineering, 127, pp. 79-86, 2015.
2. **Narasimha Suri Tinnaluri** and D. Jaya Krishna, Heatline Visualization for Thermal Transport in Complex Solid Domains with Discrete Heat Sources at the Bottom Wall, International Journal of Heat and Technology, 37 (1), pp. 100-108, 2019.
3. **Narasimha Suri Tinnaluri** and D. Jaya Krishna, Numerical Investigation of Hydrodynamics for a Lid Driven Non-Darcy Anisotropic Porous Cavity, Special Topics & Reviews in Porous Media: An International Journal, 10 (4), pp. 339-355, 2019.
4. **Narasimha Suri Tinnaluri**, K. Lokesh and D. Jaya Krishna, Heatline Visualization of Buoyancy Induced Flows for Non-Darcy Anisotropic Porous Media, Special Topics & Reviews in Porous Media: An International Journal. (Under review: second revised draft submitted).

Book chapter

1. **Narasimha Suri Tinnaluri** and Jaya Krishna Devanuri, Visualization of Thermal Transport in Complex Geometries with Discrete Heat Sources at Bottom and Left Walls, Mechanical Engineering for Sustainable Development State-of-the-Art Research, published in Apple Academic Press (AAP), pp. 537 – 549, 2019.

International Conferences

1. **Narasimha Suri Tinnaluri** and D. Jaya Krishna, Visualization of Energy Transport in 2-D Complex Solid Geometries, IEEE International Conference on Energy Efficient Technologies for Sustainability (ICEETS'16), St. Xavier's Catholic College of Engineering, Nagercoil, Tamilnadu, India, April 7^{th} –8^{th}, 2016, Published in IEEE Conference Publications, pp. 922 – 926.

2. **Narasimha Suri Tinnaluri** and D. Jaya Krishna, Visualization of Thermal Transport in discretely Heated 2-D Complex Solid Geometries, Sixth International Congress on Computational Mechanics and Simulation (ICCMS2016) Proceedings, Indian Institute of Technology Bombay (IITB), Mumbai, India, 27th June – 1st July, 2016, pp. 605-608.
3. **Narasimha Suri Tinnaluri** and D. Jaya Krishna, Heatline Approach for Visualization of Heat Transport in 2D Complex Geometries with Discrete Heat Sources, 6th International and 43rd National Conference on Fluid Mechanics and Fluid Power (FMFP 2016), Motilal Nehru National Institute of Technology, Allahabad (MNNITA), India, December 15th -17th, 2016.
4. **Narasimha Suri Tinnaluri** and D. Jaya Krishna, Visualization of Thermal Transport in Complex Geometries with Discrete Heat Sources at Bottom and Left Walls, 1st International and 18th ISME Conference (ISME18), National Institute of Technology Warangal (NITW), India, February 23rd – 25th, 2017.
5. **Narasimha Suri Tinnaluri** and D. Jaya Krishna, Visualization of Thermal Transport in 2-D Complex Solid Geometries with Discretely Heated Bottom Wall (CJ7015), International Conference on Advanced Technology Innovation (ICATI 2017), Samui, Thailand, June 25th – 28th, 2017.

National Conferences

1. **Narasimha Suri Tinnaluri** and D. Jaya Krishna, A Novel Algorithm for Bejan's Heatline Visualization in Complex Geometries, National Symposium of Mechanical Engineering Research Scholars (NSMERS 2016), National Institute of Technology Warangal (NITW), India, October 7th, 2016.
2. **Narasimha Suri Tinnaluri** and Jaya Krishna Devanuri, Influence of Shear Driven Velocity and Porous Matrix Orientation on Flow Behavior, National Conference on Emerging Trends in Mechanical Engineering (ETME 2019), National Institute of Technology Warangal (NITW), India, January 9th - 10th, 2019.